GKSS FORSCHUNGSZENTRUM

Characterisation of Ductile Tearing Resistance by the Energy Dissipation Rate: Effects of Material, Specimen Shape and Size

Autoren:
P. Anuschewski,
W. Brocks,
D. Hellmann

GKSS 2002/xx

Abstract

The *J* integral, which is widely used in elastic-plastic fracture mechanics, is not the true driving force any more if the crack is propagating. This leads to some inconsistencies when ductile tearing resistance is characterised in terms of *J*, especially for large crack extensions. Instead, TURNER has proposed the energy dissipation rate as a physically more meaningful quantity. His concept is discussed and more evidence is given, which will provide a better understanding of ductile tearing. It is shown how this quantity can be re-evaluated from experimental J_R-cuvves of bend and tensile specimens. The energy dissipation rate is decreasing with crack extension in gross plasticity and approaches a stationary state. The analysis of numerous experimental data revealed, that the $R(\Delta a)$-curves can be described by an exponential function with three parameters, namely the initial value, $R_0 = R(\Delta a=0)$, the final stationary value, R_∞, and a "length of decay", $1/\lambda$, from the initial to the stationary value. The shapes of the cumulative J_R-curves can be derived for different specimen geometries by integration. The three parameters, R_0, R_∞, λ, together with an integration constant, the initiation value, J_i, characterise ductile fracture resistance both quantitatively and physically interpretable, and hence constraint effects on R-curves can be quantified in terms of these parameters. Geometry functions derived from plastic limit load expressions are defined for normalisation of $R(\Delta a)$-curves, which cover some of the geometry effects. The concept of the dissipation rate does not give a final answer to the problem of geometry dependence of R-curves, but it provides some approaches to a better physical understanding, what J_R-curves actually are, how they can be characterised and parametrised, which are the reasons for "geometry effects" and how the latter can be quantified under certain conditions.

Acknowledgement

The authors gratefully acknowlegde financial support for the analysis and intepretation of R-curve data by the Deutsche Forschungsgemeinschaft under contract number **Br 521/7-1**.

Zusammenfassung

Das in der elastisch-plastischen Bruchmechanik verwendete *J*-Integral stellt nicht mehr die risstreibende Kraft dar, sobald der Riss wächst. Dies führt zu einigen Widersprüchen, wenn der duktile Risswiderstand mit Hilfe von *J* beschrieben wird, und zwar insbesondere bei großem Risswachstum. Stattdessen hat Turner die Energiedissipationsrate als physikalisch bedeutsame Größe vorgeschlagen. Sein Konzept wird im vorliegenden Bericht diskutiert und untermauert, um damit zu einem besseren Verständnis duktiler Rissausbreitung zu kommen. Es wird gezeigt, wie diese Größe aus experimentell ermittelten J_R-Kuvven rückgerechnet werden kann. Die Energiedissipationsrate nimmt bei starker Plastizierung mit wachsendem Riss ab und nähert sich einem stationären Wert. Die Analyse zahlreicher experimenteller Daten hat gezeigt, dass die $R(\Delta a)$-Kurven durch eine Exponential-Funktion mit drei Parametern beschreiben werden kann, nämlich dem Anfangswert R_0, dem stationären Endwert R_∞ und einer Abklinglänge $1/\lambda$. Die Formen der kumulativen J_R-Kurven für unterschiedliche Probenformen können durch Integration bestimmt werden. Die drei Parameter R_0, R_∞ und λ beschreiben zusammen mit dem Rissinitiierungswert J_i als Integrationskonstante das duktile Risswiderstandsverhalten sowohl quantitativ als auch physikalisch interpretierbar. Deshalb können "Constraint"-Effekte auf das Risswiderstandsverhalten mit Hilfe dieser Parameter quantifiziert werden. Aus Grenzlastformeln hergeleitete Geometriefunktionen werden zur Normierung von $R(\Delta a)$-Kurven benutzt, wodurch einige der Geometrieeffekte erfasst werden können. Das Konzept der Dissipationsrate gibt keine endgültige Antwort auf Probleme der Geometrieabhängigkeit von R-Kurven, aber es stellt einige Ansätze für ein besseres physikalisches Verständnis zur Verfügung, was J_R-Kuvven tatsächlich sind, wie sie beschrieben und parametrisiert werden können, was die Ursachen von "Geometrie-Effekten" sind, und wie letztere unter bestimmten Bedingungen quantifiziert werden können.

Contents

Appendices

0. Nomenclature

a	actual crack length for C(T) and SE(B), half of actual crack length for M(T)
a_0	initial crack length for C(T) and SE(B), half of initial crack length for M(T)
A	actual crack surface, $A = B\ a$ for specimens of constant thickness, B, and straight crack front
B	specimen thickness
B_n	net thickness of side-grooved specimens
E	YOUNG's modulus
E'	$E / (1- \nu^2)$ for plane strain
F	load, force
F_Y	plastic limit load (yield load)
F_0	net section yield load
f_Y	normalised plastic limit load, constraint factor, limit load factor
J	J integral
J_{el}	elastic part of J integral
J_i	value of J integral at physical crack initiation, $J(\Delta a = 0)$
J_{pl}	plastic part of J integral
J_R	crack extension resistance measured as J integral in dependence on crack extension
R	dissipation rate [TUR 90]
R_{ref}	reference dissipation rate
R_0	value of dissipation rate at physical crack initiation $R(\Delta a = 0)$
R_∞	stationary limit of dissipation rate, crack propagation energy [KLE86]
$\overline{R}$	normalised dissipation rate
R_{eL}	lower yield strength
R_m	ultimate tensile strength
$R_{p0.2}$	0.2% proof strength
S	span of SE(B) specimens
U_{dis}	total dissipated work by plastic deformation and crack extension
U_{el}	elastic (internal) energy
U_{pl}	work of plastic deformation
U_{sep}	(local) work of separation
v	displacement, e.g. crack opening or specimen elongation
v_{el}	elastic part of displacement
v_{pl}	plastic part of displacement
V	volume
W_{ext}	work of external forces

W	specimen width for C(T) and SE(B), half of specimen width for M(T)
α	parameter of exponential fit function for $R(\Delta a)$ determining R_0
$\Delta a = a - a_0$	crack extension
Γ_c	specific work of separation
Σ_Y	plastic constrain factor
γ, η	geometry functions for J evaluation of C(T) and SE(B) specimens
λ	parameter of exponential fit function for $R(\Delta a)$ determining the intensity of decay
ν	POISSON's ratio
σ_Y	yield strength (lower yield strength R_{eL} or proof strength R_p)
σ_∞	remote nominal stress

Specimen designations

C(T)	compact specimen (tension)
M(T)	middle (centre) cracked (tension)
SE(B)	single edge cracked (bending)

Subscripts

dis	dissipated
e	effective
el	elastic
ext	external
c	critical
pl	plastic
sep	separation
Y	yield, plastic limit
3D	threedimensional, accounting for finite specimen thickness
∞	infinite, remote

1. Introduction

The prediction of failure by unstable crack extension is one of the main issues in the assessment of safety and reliability of components for industrial applications. For ductile materials, crack instability may be preceded by some amount of stable crack extension. The ductile tearing resistance of a material is conventionally characterised by a *J*-resistance curve which is obtained from bend-type specimens, i.e. C(T) or SE(B), by standard procedures [ASTM1737, ASTM1820] It characterises, within certain limits set forth in the standards, the resistance against slow stable crack extension. These limits are severe. First of all, J-R curves refer to bending configurations only, and it is well known, e.g. [GAR79, BRO89, LIN91], that they generally depend on the specimen geometry and loading configuration. Second, the standards require that the permitted crack extension does not exceed 10% [ASTM1737] or 25% [ASTM1820] of the remaining ligament. These requirements may inhibit the application to structural components which in general will not meet the "validity" conditions.

The cumulative quantity *J*, which rises with increasing crack length, is not the true driving force for ductile tearing as TURNER [TUR90] has pointed out in a basic discussion on the necessity of defining an alternative measure of tearing toughness. He proposed to define tearing resistance in terms of energy dissipation rate[1]

$$R = \frac{\mathrm{d}U_{\mathrm{dis}}}{\mathrm{d}A_{\mathrm{cr}}} = \frac{\mathrm{d}W_{\mathrm{ext}}}{\mathrm{d}A_{\mathrm{cr}}} - \frac{\mathrm{d}U_{\mathrm{el}}}{\mathrm{d}A_{\mathrm{cr}}}, \tag{1-1}$$

where W_{ext} is external work, U_{el} the (recoverable) elastic strain energy, and A_{cr} is the crack area. For specimens with constant thickness B and straight crack front ("plane" problems) the increment of crack area is $\mathrm{d}A_{\mathrm{cr}} = B\,\mathrm{d}a$. This definition of eq. (1-1) is a straight transfer of GRIFFITH's elastic energy release rate [GRI20] to plastic processes which is consistent with the incremental theory of plasticity. The dissipation rate has the same dimension as J and charcterises the increment of irreversible work per crack extension increment. It falls with increasing crack length in gross plasticity and consists of two contributions, namely work of remote plastic deformation and local work of separation,

$$R = \frac{\mathrm{d}U_{\mathrm{pl}}}{\mathrm{d}A_{\mathrm{cr}}} + \frac{\mathrm{d}U_{\mathrm{sep}}}{\mathrm{d}A_{\mathrm{cr}}} \tag{1-2}$$

When introducing R, TURNER generally doubted that splitting it into local and global contributions will ever be possible. Thus, every measured ductile crack extension resistance will necessarily contain remote plastic work which in general is much larger than the local work of separation. In fact, only external work and elastic energy can be measured. Models of damage mechanics, however, provide ideas how to perform this separation.

---

[1] The term "dissipated energy" means "non-recoverable mechanical work".

The dissipation rate, R, is more appropriate for characterizing crack extension in plastically deformed structures than the conventionally used J integral [MEM93, TUR94a, KOL97, SUM99]. It is, in fact, the true "driving force" which has to equalise the structural resistance in order to propagate the crack by some amount, Δa, whereas J accumulates the plastic work done along a given loading path. It is, however, not a material but a structural property as it contains the work of remote plastic deformation.

The present report is a treatise on fundamentals and applications of this new concept of characterising ductile tearing resistance. Procedures to calculate $R(\Delta a)$ curves from existing J_R-curves and a simple curve fit are described and discussed in chapter 2. A normalisation of $R(\Delta a)$-curves is proposed which allows to transfer the data from one specimen geometry to another under certin conditions. The concept is verified in chapter 3 by re-analysing numerous J_R test data for quasi-static large ductile crack extension obtained for various materials and specimen geometries in terms of the dissipation rate. Geometry effects are quantitatively characterised by the parameters of the $R(\Delta a)$ curve fits. Examples on the transfer of R-curves between different specimen geometries are given, finally.

2. Evaluation and analysis of data

2.1 Determination from experimental R-curve testing

For quasi-static processes, the dissipation rate can be simply evaluated from the area under the measured load vs. displacement curve, see [ASTM1737, ASTM1820] for C(T) and [GAR75, SCH84] for M(T), by

$$R = \lim_{\Delta a \to 0} \frac{\Delta U_{\mathrm{dis}}}{B_{\mathrm{n}} \Delta a} = \lim_{\Delta a \to 0} \frac{F \Delta v_{\mathrm{pl}}}{B_{\mathrm{n}} \Delta a}, \tag{2-1}$$

if R is supposed to include the whole irreversible part of the work done and, hence, may also include dissipated energy in zones far remote from the crack tip, e.g. around load points or supports. As no splitting into local and global contributions according to eq (1-2) is possible, "dissipated" work equals total "plastic" work as determined from the area under the experimental load vs. displacement record. If the respective information is not available any more, R can be simply re-evaluted from existing J_{R}-curves by inverting the procedure of calculating J from test data. The respective formulas are [MEM92, BRO92, MEM93]

$$R = \left(\frac{W - a}{\eta} \right) \frac{\mathrm{d}J_{\mathrm{pl}}}{\mathrm{d}a} + J_{\mathrm{pl}} \frac{\gamma}{\eta} \tag{2-2}$$

for *bend type specimens*, **C(T)** and **SE(B)**, with the well-known geometry factors

$$\eta = \begin{Bmatrix} 2.0 + 0.522\,(1 - a / W) & \text{for C(T)} \\ 2.0 & \text{for SE(B)} \end{Bmatrix}, \tag{2-3}$$

$$\gamma = \begin{Bmatrix} 1.0 + 0.76\,(1 - a / W) & \text{for C(T)} \\ 1.0 & \text{for SE(B)} \end{Bmatrix}, \tag{2-4}$$

and

$$R = (W - a) \frac{\mathrm{d}J_{\mathrm{pl}}}{\mathrm{d}a} \tag{2-5}$$

for *tension type specimens*, **M(T)** and **DE(T)**. The derivation of these formulas is given in Appendix A1. The conversion formula given by KOLEDNIK [KOL93, STA00] for bend type specimens, misses the second term of eq. (2-2).

The evaluation of $R(\Delta a)$ curves by eqs. (2-2) and (2-5), respectively, reqires a numerical differentiation, which may result in oscillating data. A bevel procedure has been developed to avoid this problem and obtain smoother curves, see Appendix A2.

R versus Δa curves are obtained as crack extension resistance curves for the respective specimens and materials, see Fig. 2.1 [MEM93]. The dots represent the test data [AUR90], and the solid lines represent the exponential fit curves of eq. (2-9) for $R(\Delta a)$, see section 2.3 and **Table 2.1**, and their integration, see section 2.5, respectively.

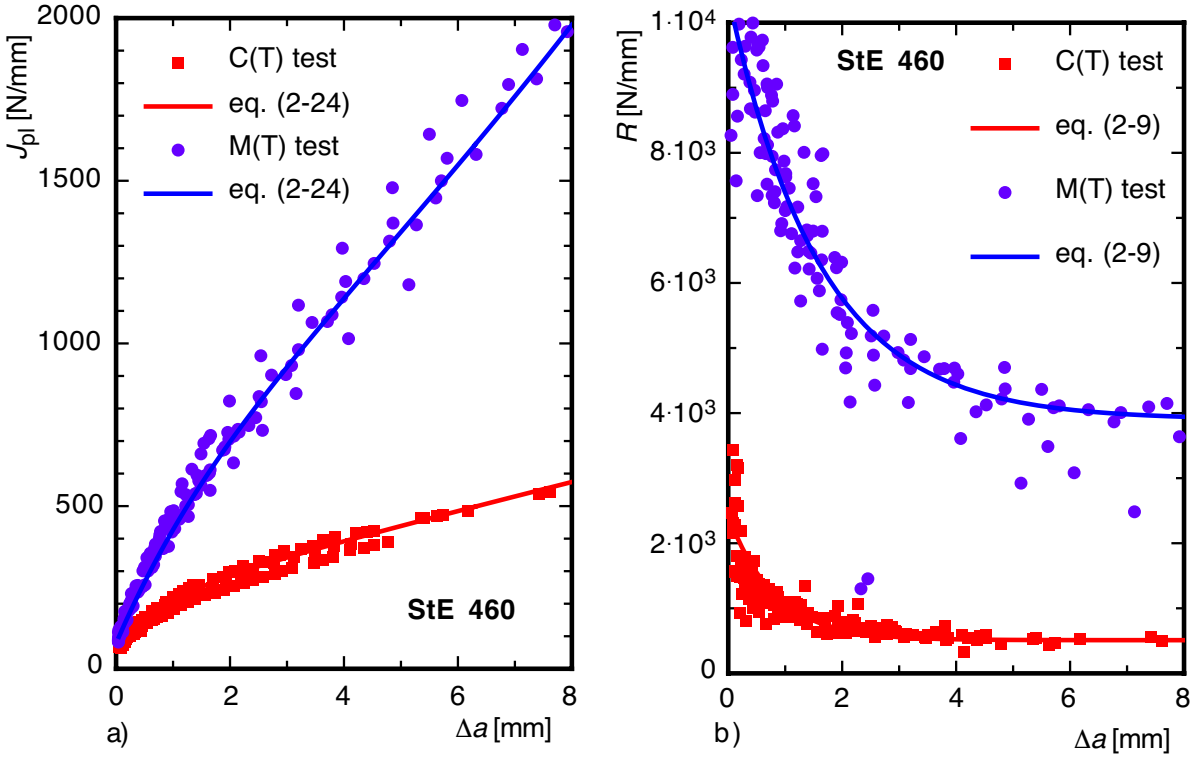

Fig. 2.1: Evaluation of dissipation rate from J_R-curve test data: a
a) J_{pl} versus Δa side-grooved C(T) and M(T) specimens of steel DIN StE 460, test data [AUR90]) and integrated curves of dissipation rate,
b) $R(\Delta a)$ test data and exponential fit curves [MEM93].

2.2 Numerical calculation

In an elastic-plastic finite element (FE) analysis of crack extension the dissipation rate can be calculated directly from stresses and strains [MEM93, SIE99]

$$\mathcal{D}_{pl} = \int_{V_{pl}} \sigma_{ij}\, \dot{\varepsilon}^{p}_{ij}\, dV = \int_{V_{pl}} \sigma_{e}\, \dot{\varepsilon}^{p}_{e}\, dV \qquad (2\text{-}6)$$

σ_e and ε_e^p being VON MISES effective stress and effective plastic strain, respectively. The volume integral may either be performed over the whole body, thus yielding the result of eqn. (2-1), or just over the plastic zone at the crack tip, how large it may be. If the FE simulation reflects plastic processes only, i.e. it is simply based on the MISES-PRANDTL-REUSS constitutive equations and follows experimental data of either $J(\Delta a)$ or $V_L(\Delta a)$ as, e.g., in [SIG83], and dissipated work equals total plastic work as in the experimental procedure.

Recent approaches to modeling of ductile rupture [YUA96, LIN97, SIE98, SIE99, SIE00a] refer to BARENBLATT's idea [BAR62] of introducing a "process zone" ahead of the crack tip where material degradation and separation occur. This approach requires a constitutive description of

the material behaviour in the process zone which can mirror the local loss of stress carrying capacitiy. In general, two alternatives are applied:

- models based on the micromechanisms of ductile failure, namely the nucleation, growth and coalescence of voids, as e.g. the most commonly used model of GURSON, TVERGAARD and NEEDLEMAN (GTN-model) [GUR77, TVE82, NEE87, XIA95], and
- phenomenological "cohesive zone models" describing the decohesion process by a tractiuon strength and the work of separation per unit area, e.g. [NEE90, YUA96, LIN97, SIE98]

For the GTN-model the energy needed for material separation, U_{sep}, in an incremental crack advance, ΔA, is given by:

$$U_{sep} = \int_V (1 - f)\sigma_e \varepsilon_e^p \, dV . \tag{2-7}$$

Here, the volume integral is performed over the single row of elements in front of the crack tip being described by the GTN-model. For the cohesive zone model U_{sep} is calculated from

$$U_{sep} = \Gamma_c \Delta A = \int_0^{\delta_c} \sigma_n \, d\delta_n \cdot \Delta A. \tag{2-8}$$

This approach allows for splitting the total dissipated work into the (local) work of separation in the process zone and the (global) plastic work in the embedding material and, thus, solves a classical problem of elastic-plastic fracture mechanics [SIE99, SIE00a, b], see Fig. 2.2. It demonstrates that the actual separation energy is only 1 to 5 % of the plastic work, or in other words: 95 to 99 % of what is measured in R-curve testing is remote plastic deformation work but no "fracture energy".

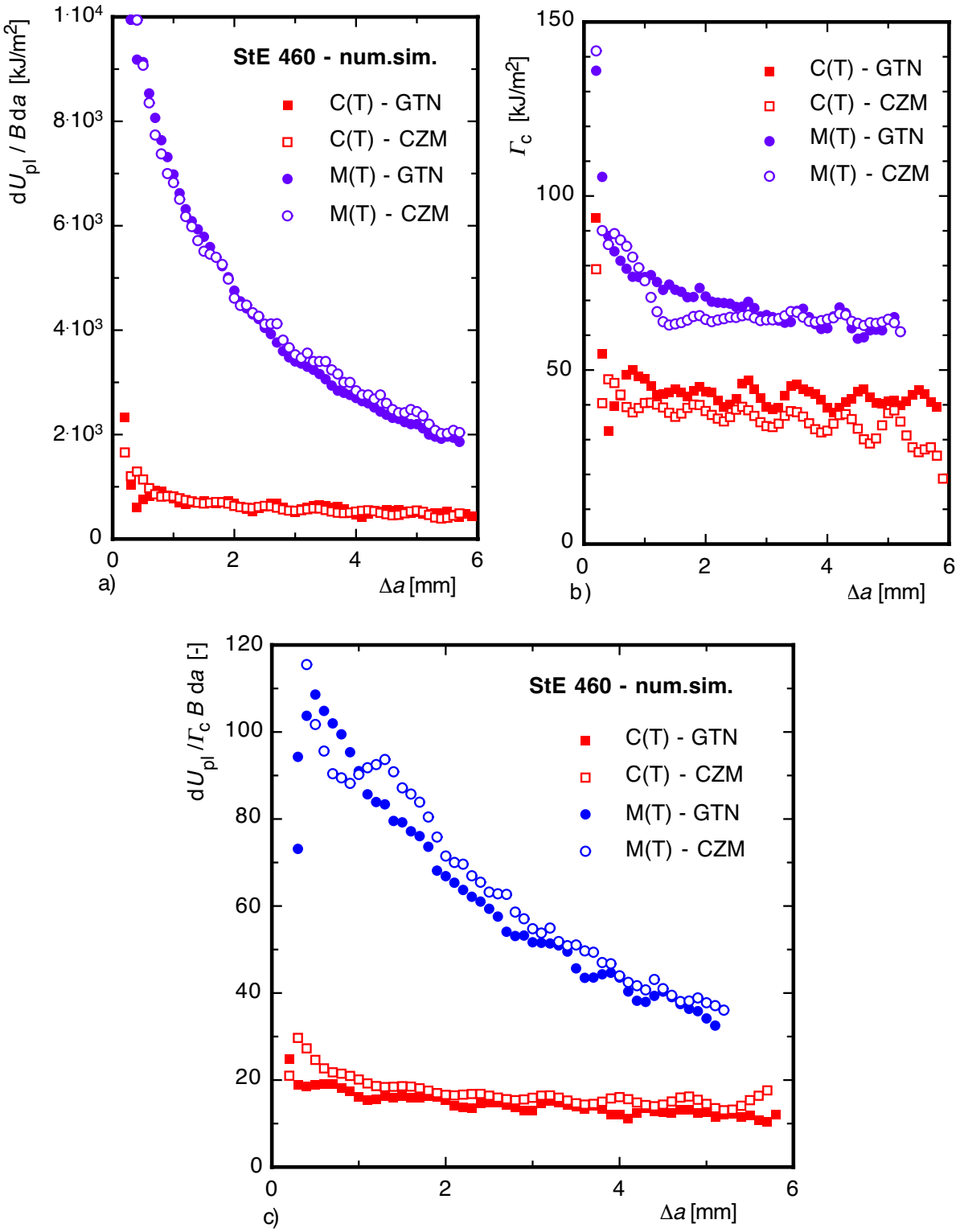

Fig. 2.2: Numerical simulations of fracture tests with GURSON-TVERGAARD-NEEDLEMAN (GTN) model and triaxiality dependent cohesive zone model (CZM) [SIE00a, b]: splitting of total dissipation rate;
a): rate of global plastic work, b): local work of separation,
c): ratio of plastic work and work of separation.

2.3 Fitting of *R*(Δa) curves

Evaluation of experimental records, e.g. presented by TURNER [TUR90] or MEMHARD et al. [MEM93], showed a general tendency that *R*(Δa) curves decreased monotonically from an initial value, R_0, and, after a nonstationary transition, approached a stationary value, R_∞, see Fig. 2.1. TURNER & KOLEDNIK [TUR94a] presented a schematic of this *R*(Δa)-curve behaviour as typical for initiation occuring close to or at maximum load. A similar behaviour is observed for the crack tip opening angle, CTOA, and relations between the two quantities have been derived by TURNER & KOLEDNIK [TUR94b] This kind of curve shape can be fitted by a decreasing exponential function [MEM93]

$$R = R_\infty \left(1 + \alpha \exp\left[-\lambda \frac{\Delta a}{W}\right]\right), \tag{2-9}$$

see Fig. 2.2b, with three free parameters R_∞, α, λ,. The parameter α determines the *initial value* $R_0 = R(\Delta a{=}0)$ according to

$$\alpha = \frac{R_0}{R_\infty} - 1. \tag{2-10}$$

The final *stationary value* R_∞ is the so-called "*crack propagation energy*" as introduced by KLEMM & KALTHOFF [KLE86] and measured from the heat production due to crack extension. The parameter λ describes the *rate of decay* from the inital value, R_0 , to the final value, R_∞,

$$\lambda = \frac{W}{R_\infty - R_0} \left.\frac{dR}{da}\right|_{\Delta a = 0}. \tag{2-11}$$

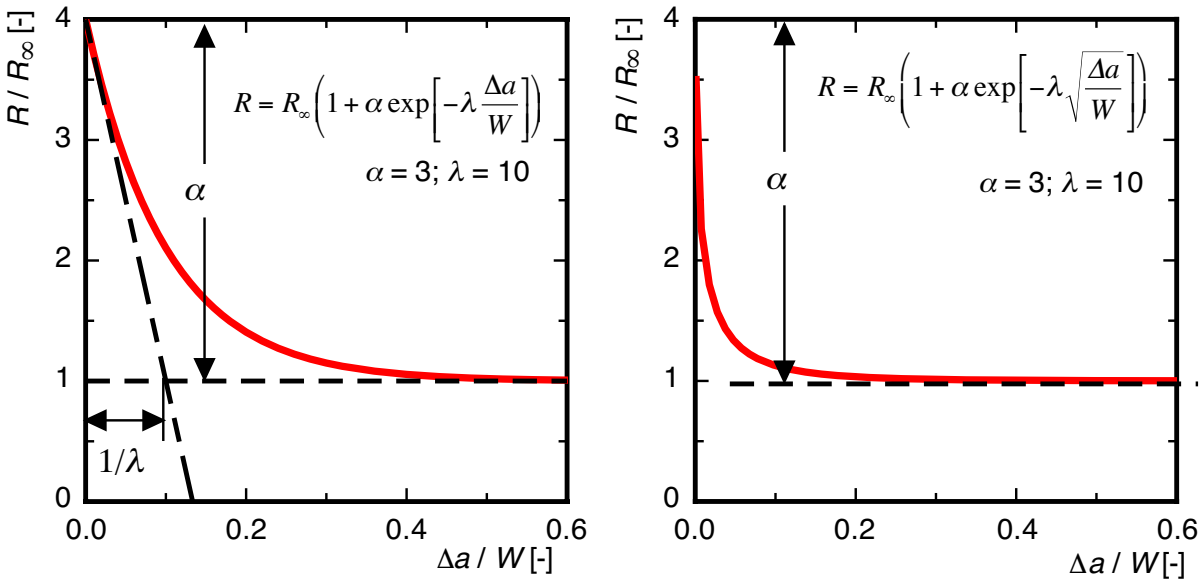

Fig 2.3: Curve fitting of *R*(Δa) curve by eqs. (2-9) and (2-12), respectively, visualizations of the parameters.

The parameters of the fit curves of eq. (2-9) for the ferritic steel DIN StE 460 are given in **Table 2.1** [MEM93, BRO98], and the respective curves are plotted in Fig. 2.1. The decreasing shape has also been verified in numerical studies based on test data, see Fig 2.2 [SIE99, SIE00a,b]. The fit curve, eq. (2-9), is applied to the analysis of all specimens in the present investigations.

Table 2.1: Analysis of R-curve test data for ferritic steel DIN StE 460 [MEM93, BRO98]; yield strength R_{eL} = 460 MPa, ultimate tensile strength R_m = 623 MPa

specimen	W [mm]	a_0 / W [-]	R_∞ [N/mm]	α [-]	λ [-]	$f_{\text{y-plstrain}}$ [-]	R_{ref} [N/mm]
C(T)	50	0.59	510.	3.77	61.97	0.1921	3.97
M(T)	50	0.49	3900.	1.67	31.30	1.1547	29.66

Further analysing J_R-curves by SCHWALBE & HELLMANN [SCH84] of aluminium alloys with a low initiation toughness showed that a better fitting could be obtained in some cases by using

$$R = R_\infty \left(1 + \alpha \exp\left[-\lambda \sqrt{\frac{\Delta a}{W}} \right] \right), \tag{2-12}$$

instead of eq. (2-9), see Fig. 2.3 (right). The parameters R_∞, and α keep the same meaning as before, whereas no simple physical interpretation exists for λ in this case, as the initial slope of the function (2-12) is infinite. The descent of the curve is much steeper, meaning that the transition regime ist much smaller, which is essential for its better fitting properties in the respective cases.

The determination of the initial value, R_0, is subject to the general uncertainty of determining the point of physical crack initiation after crack tip blunting. The latter may cause a first peak of R(Δa), see [STA00]. As the emphasis is put upon large ductile crack extension and its simple phenomenological description, this effect is neglected in the following, however.

Assuming a stationary value of the dissipation rate, R_∞, allows for a physically founded extrapolation of resistance curves beyond the measured range for long crack extensions. This has also been the intention of KLEMM & KALTHOFF [KLE86] when they introduced their parameter of "*crack propagation energy*".

STAMPFL & KOLEDNIK [STA00] present and discuss $R(\Delta a)$ curves for C(T) specimens ($W = 2B = 50$mm, $a_0/W = 0.56$) of a solution annealed maraging steel V 720 and a nitrogen alloyed ferritic-austenitic duplex steel A 905, revealing second peak values of R at $\Delta a = 2.5$ and

6.3mm, respectively, which result in a local increase of the slopes of the correspondent J_R-curves at this point. The authors explain the occurence of these peaks by splitting R into the contributions to form flat-fracture surfaces under plane strain conditions and slant shear lip surfaces, which contribute additional plastic work. This effect may have played a role for some $R(\Delta a)$ curves of the aluminium specimens in the present study, see Figs. 3.3 and 3.4, as well, but could not be verified, as the respective specimens were not available for fractographic investigations any more.

A basically different shape of $R(\Delta a)$ curves was found for thin but large aluminium panels from numerical analyses of test data [BRO00, SIE00c], see Fig. 2.4. The curves start increasing, run through a maximum and decrease again. No stationary value was obtained within 50mm of crack extension. TURNER & KOLEDNIK [TUR94a] characterise this R-curve behaviour as typical for initiation occuring well before maximum load.

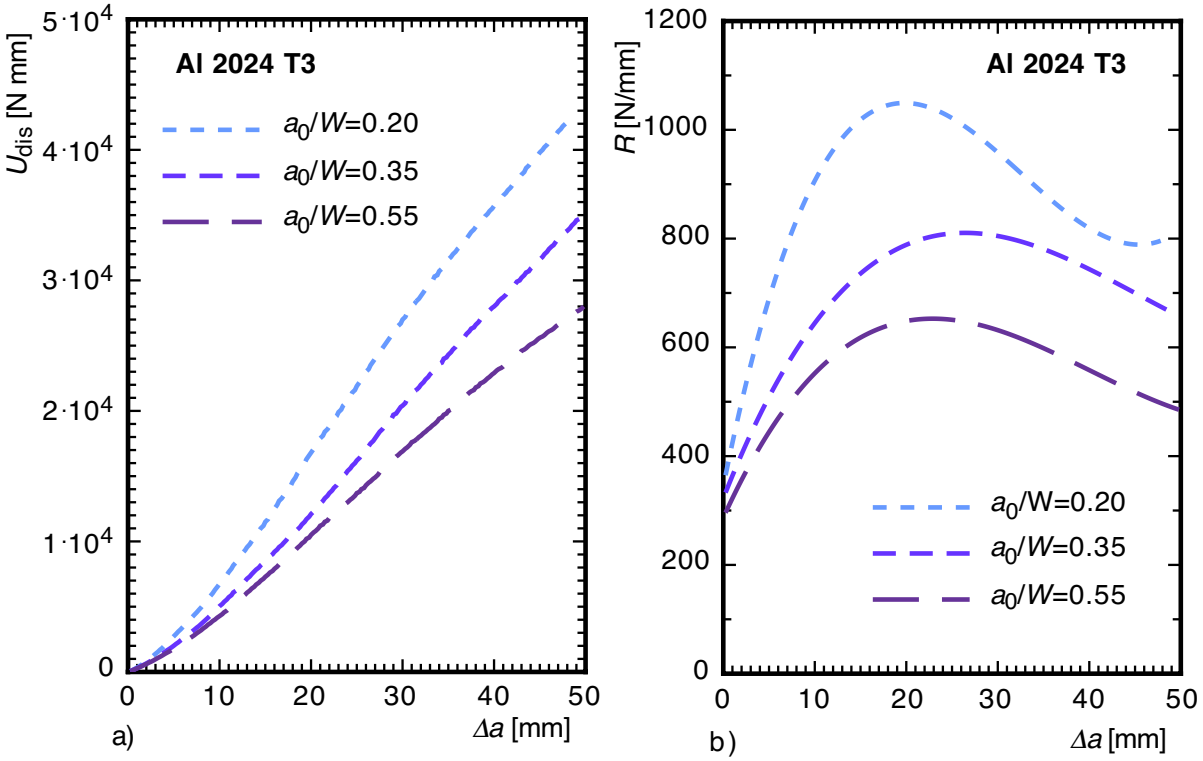

Fig. 2.4: Numerical simulations of crack extension in thin and wide centre cracked panels, $B = 1$mm, $2W = 508$mm, of Al 2024 T3 with cohesive zone model [BRO00, SIE00c];
a) total dissipated energy b) dissipation rate

2.4 Normalisation of $R(\Delta a)$ curves

As the dissipation rate - like J - contains all irreversible contributions of the external work necessary to propagate the crack by an increment Δa, i.e. not only the local work of separation but also the work of stresses on the plastic strain increment in the whole structure, eq. (1-2), it is no material property but a structural one which depends on the amount of plastification, namely the size of the plastic zone and the average magnitude of plastic strain. A scaling of $R(\Delta a)$ curves by some appropriately defined normalisation factor,

$$\overline{R}(\Delta a) = \frac{R(\Delta a)}{R_{\text{ref}}}, \tag{2-13}$$

may eliminate the geometry dependence. At least for fully yielded specimens a normalisation by a plastic limit load factor,

$$R_{\text{ref}} = \sigma_{\text{Y}}(W - a_0)\frac{\sigma_{\text{Y}}}{E} \cdot f_{\text{Y}}\left(\frac{a_0}{W}\right), \tag{2-14}$$

will have this scaling effect, as was shown in [MEM94] for M(T) and C(T) specimens of a DIN StE 460 steel, see Fig 2.7a in the next section. The "geometry function" f_{Y} is the ratio of the plastic limit load of the cracked structure, F_{Y}, to the yield load of an uncracked structure with same net section, F_0,

$$f_{\text{Y}} = \frac{F_{\text{Y}}}{F_0} = \left\{ \begin{array}{ll} \dfrac{F_{\text{Y}}}{2\sigma_{\text{Y}} B(W - a_0)} & \text{for M(T)} \\ \dfrac{F_{\text{Y}}}{\sigma_{\text{Y}} B(W - a_0)} & \text{for C(T) and SE(B)} \end{array} \right\}. \tag{2-15}$$

where σ_{Y} equals R_{eL} or $R_{\text{p0.2}}$, respectively. Plastic limit loads of plane specimen geometries can be determined from slip line solutions for the limiting cases of plane stress and plane strain. Numerous limit load solutions are summarised in the EFAM handbook ETM97 [SCH98].

For **M(T)** specimens, loaded in tension,

$$f_{\text{Y-MT}} = \left\{ \begin{array}{ll} 1 & \text{plane stress} \\ \dfrac{2}{\sqrt{3}} & \text{plane strain} \end{array} \right\}, \tag{2-16}$$

is obtained [MIL88, SCH98]. For **C(T)** specimens, solutions for single edge cracked, SE, specimens under combined bending and tension can be taken [EWI72, MIL88]:

$$f_{\text{Y-CT}} = \left\{ \begin{array}{ll} \dfrac{-\left(\dfrac{2}{\sqrt{3}}\dfrac{a_0}{W}+1\right)+\left[\left(\dfrac{2+\sqrt{3}}{\sqrt{3}}\right)\left(\dfrac{2}{\sqrt{3}}\left(\dfrac{a_0}{W}\right)^2+1\right)\right]^{1/2}}{1-\dfrac{a_0}{W}} & \text{plane stress} \\ \dfrac{2}{\sqrt{3}}\cdot\dfrac{-\left(1+1.702\dfrac{a_0}{W}\right)+\left[2.702+4.599\left(\dfrac{a_0}{W}\right)^2\right]^{1/2}}{1-\dfrac{a_0}{W}} & \text{plane strain} \end{array} \right\}. \qquad (2\text{-}17)$$

The functions in eq. (2-17) can be approximated by polynomials for an easier handling [KIM96]:

$$f_{\text{Y}} = \left\{ \begin{array}{ll} 0.47-0.70\left(\dfrac{a_0}{W}\right)+0.23\left(\dfrac{a_0}{W}\right)^2 & \text{plane stress} \\ 0.74-1.20\left(\dfrac{a_0}{W}\right)+0.46\left(\dfrac{a_0}{W}\right)^2 & \text{plane strain} \end{array} \right\}. \qquad (2\text{-}18)$$

The error lies within 0.5 % for all a_0/W ratios between 0.2 and 0.8, see Fig. 2-5, where also comparisons to the EPRI handbook [KUM81] and some FE results are displayed.

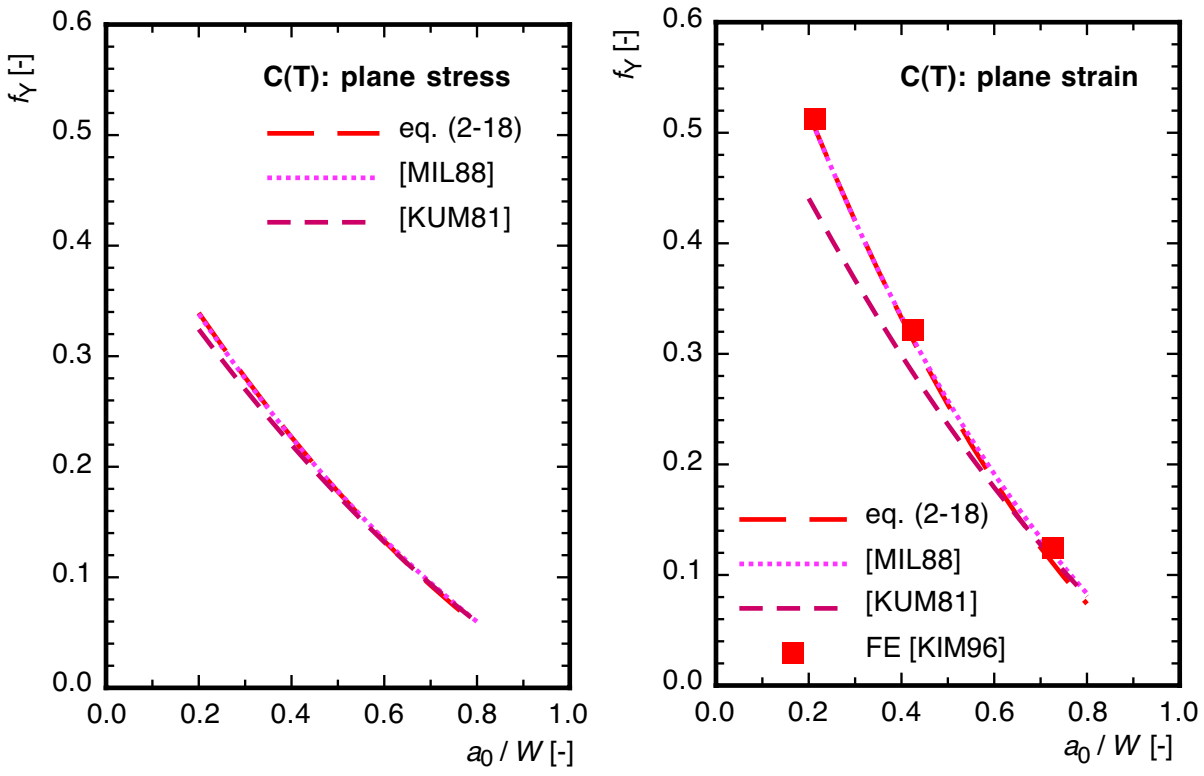

Fig. 2.5: Limit load factors in dependence on relative crack length for C(T) specimens, comparison of 2D solutions

Plane stress and plane strain solutions for deeply cracked **SE(B)** specimens have been derived by KACHANOV [KAC71] and WU et al. [WU88], respectively, which yield

$$f_{\text{Y-SEB}} = \begin{Bmatrix} 0.277\left(1-\dfrac{a_0}{W}\right) & \text{plane stress} \\ 0.358\left(1-\dfrac{a_0}{W}\right) & \text{plane strain} \end{Bmatrix} \tag{2-19}$$

for a span of $S = 4\ W$.

The plane strain solution gives an upper, the plane stress solution a lower bound for the plastic limit load of a real three-dimensional structure. The difference between the plane strain and the plane stress solution is 15% for M(T) specimens, 44% for C(T) specimens (at $a/W = 0.5$) and 29% for SE(B) specimens. Hence, the specimen thickness has a significant influence on the actual limit load of a real structure. Three-imensional FE calculations for varying B/W ratios have been performed for perfectly plastic material and the FE results have been fitted by functions

$$f_{\text{Y-3D}} = \begin{Bmatrix} \left[\dfrac{2}{\sqrt{3}} + \dfrac{\left(\sqrt{3}-2\right)}{2}\cdot\exp\left(-1.77\dfrac{B}{W}\right)\right] \\ \left[1.44 - 0.44\left(1+4.76\dfrac{B}{W}\right)\cdot\exp\left(-4.76\dfrac{B}{W}\right)\right] \\ \left[1.29 - 0.29\left(1+4.76\dfrac{B}{W}\right)\exp\left(-4.76\dfrac{B}{W}\right)\right] \end{Bmatrix} \cdot f_{\text{Y-pl.stress}} \quad \text{for} \begin{Bmatrix} \text{M(T)} \\ \text{C(T)} \\ \text{SE(B)} \end{Bmatrix}, \tag{2-20}$$

which approach the plane stress solution for $B/W \to 0$ and the plane strain solution for $B/W \to \infty$, respectively, see Fig 2.6 (unpublished results by Y-J. KIM).

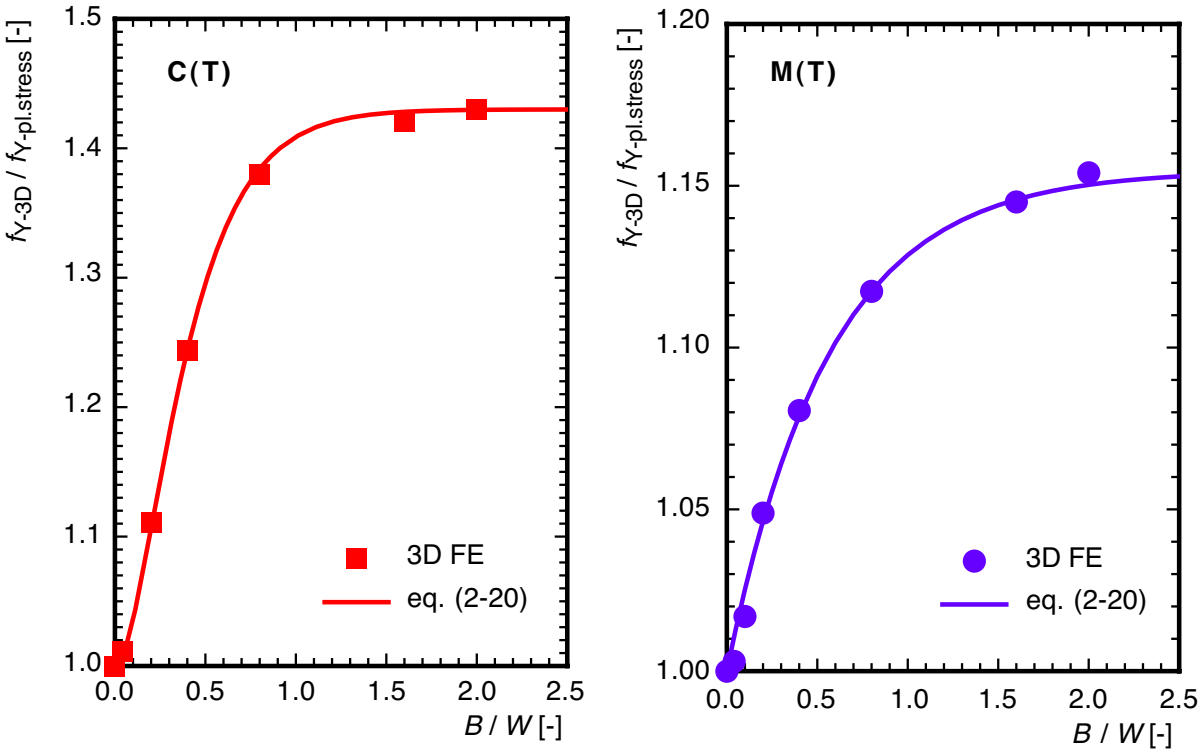

Fig. 2.6: Finite thickness corrections of limit load functions for C(T) and M/T) specimens, derived from 3D FE solutions (unpublished results by Y-J. KIM).

The respective normalisation factors, R_{ref}, obtained from eqs. (2-14) and (2-15) for the StE 460 specimens are given in **Table 2.1**, and the result of the normalisation is plotted in Fig. 2.7a. The test data of C(T) and M(T) specimens fall into one scatter band, the normalised propagation energy, R_∞ / R_{ref} is nearly identical, namely 128.6 and 131.5, respectively, but the transition regime characterised by the parameters α and λ is of course different. A prediction of the $R(\Delta a)$ curve of the M(T) specimens based on the C(T) test data can be obtained by

$$R_\infty^{MT} = R_\infty^{CT} \frac{R_{ref}^{MT}}{R_{ref}^{CT}} \quad . \tag{2-21}$$

The result is plotted in Fig. 2.7b showing that the limit load normalisation factor, R_{ref}, actually allows for a transfer of R-curve data from C(T) to M(T) specimens in this case [MEM94]. The resulting J_R-curve will be derived in the following section.

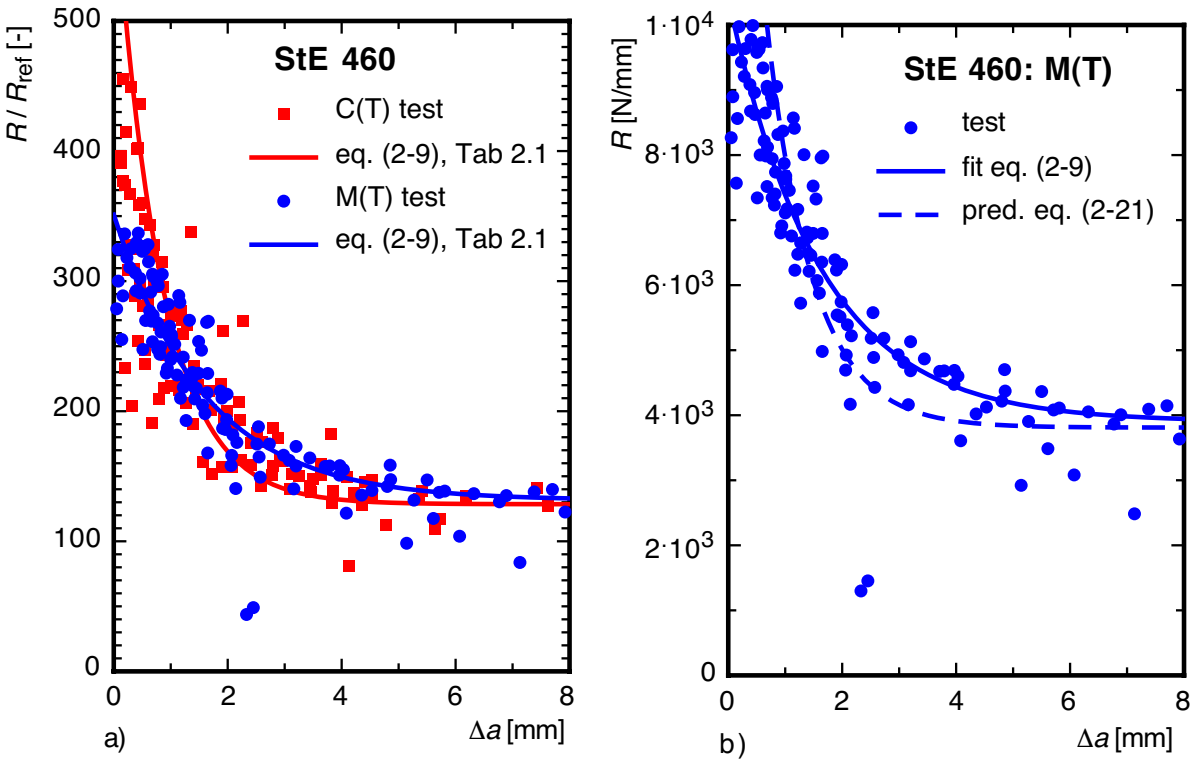

Fig. 2.7: Dissipation rate for side-grooved C(T) and M(T) specimens;
a) normalisation by R_{ref}, eq. (2-14),
b) dissipation rate of M(T) predicted from C(T) data by eq. (2-21).

2.5 Integration of *R*(Δa) curves

If an $R(\Delta a)$ curve is given, the cumulative J_R-curve is obtained by integrating eqs. (2-2) or (2-5). Introducing the normalisations

$$x = \frac{a}{W} = \frac{a_0}{W} + \frac{\Delta a}{W} = x_0 + \frac{\Delta a}{W} \quad , \quad y = \frac{J_{pl}}{R_\infty} \quad , \quad r = \frac{R}{R_\infty} \, , \tag{2-22}$$

and $$p(x) = \frac{\gamma(x)}{1-x} \quad , \quad q_b(x) = \frac{\eta(x) r(x)}{1-x} \quad , \quad q_t(x) = \frac{r(x)}{1-x} \, , \tag{2-23}$$

the differential equations take the simple forms

$$\left.\begin{array}{ll} y' + p(x)y = q_b(x) & \text{for C(T) and SE(B)} \\ y' = q_t(x) & \text{for M(T) and DE(T)} \end{array}\right\} , \tag{2-24}$$

having the general solutions

$$y = \left\{\begin{array}{ll} \exp\left(-\int p(x)dx\right)\left[\int q_b(x)\exp\left(\int p(x)dx\right)dx + C_0\right] & \text{for C(T) and SE(B)} \\ \int q_t(x)dx + C_0 & \text{for M(T) and DE(T)} \end{array}\right\} . \tag{2-25}$$

The integration constant, C_0, is determined from the initial conditions at physical or technical crack initiation, $J_0^{\mathrm{pl}} = J_{\mathrm{i}}^{\mathrm{pl}}$ at $\Delta a = 0$ or $J_0^{\mathrm{pl}} = J_{0.2}^{\mathrm{pl}}$ at $\Delta a = 0.2\,\mathrm{mm}$, respectively. The function $J_{\mathrm{pl}}(\Delta a)$ depends on the right hand sides of eqs. (2-24), i.e. the function $R(\Delta a)$. The integration has do be performed numerically, in general. However, a few closed form solutions can be found [MEM93]. The simplest case is pure *stationary crack extension*, i.e. a constant release rate, $r = R/R_\infty = 1$. The respective solutions, see Appendix A3, are a logarithmic[2] function for an M(T) specimen

$$y = y_0 + \ln\left(\frac{1 - x_0}{1 - x}\right), \tag{2-26}$$

a straight line for an SE(B) specimen,

$$y = y_0 \frac{1 - x}{1 - x_0} + 2\frac{x - x_0}{1 - x_0}, \tag{2-27}$$

and some lengthy expression containing exponential functions for a C(T) specimen[3],

$$y = \frac{1 - x}{1 - x_0} \mathrm{e}^{-\gamma_1 (x - x_0)} \left[\left(\frac{2(1 - x_0)\, \mathrm{e}^{\gamma_1 (x - x_0)}}{1 - x} - 2 \right) + (1 - x_0)(\eta_1 - 2\gamma_1) \mathrm{e}^{-\gamma_1 x_0} \int_{x_0}^{x} \frac{\mathrm{e}^{\gamma_1 \xi}}{1 - \xi}\, \mathrm{d}\xi + y_0 \right]. \tag{2-28}$$

The *transient, decaying shape of $R(\Delta a)$ curves* can be fitted by the exponential function eq. (2-9), so that $r(x) = 1 + \alpha\, \mathrm{e}^{-\lambda (x - x_0)}$. This function also allows for a partly closed form integration of eq. (2-24), see Appendix A3,

$$y = \begin{cases} y_0 + \ln\left(\dfrac{1 - x_0}{1 - x}\right) - \alpha \mathrm{e}^{\lambda x_0} \displaystyle\int_{x_0}^{x} \frac{\mathrm{e}^{-\lambda \xi}}{1 - \xi}\, \mathrm{d}\xi & \text{for M(T)} \\ y_0 \dfrac{1 - x}{1 - x_0} + 2\dfrac{x - x_0}{1 - x_0} + 2(1 - x_0)\alpha \left(\dfrac{\mathrm{e}^{-\lambda (x - x_0)}}{1 - x} - \dfrac{1}{1 - x_0} + \lambda \displaystyle\int_{x_0}^{x} \frac{\mathrm{e}^{-\lambda \xi}}{1 - \xi}\, \mathrm{d}\xi \right) & \text{for SE(B)} \end{cases}. \tag{2-29}$$

The respective J_{R}-curves under the assumption of stationary crack extension and in the transition regime, respectively, are shown in Fig. 2.8. The diagrams represent a qualitative comparison of J_R-curves, only, normalised by R_∞; the latter is however geometry dependent as shown in Fig. 2.1. They illustrate, nevertheless, that the shapes of cumulative J_R-curves are inherently geometry dependent and a unique power-law curve fit as, e.g., in [ASTM1820] is not physically based.

---

2 "ln" is the natural (NAPIERian) logarithm.

3 $\eta_1 = 0.522$, $\gamma_1 = 0.76$

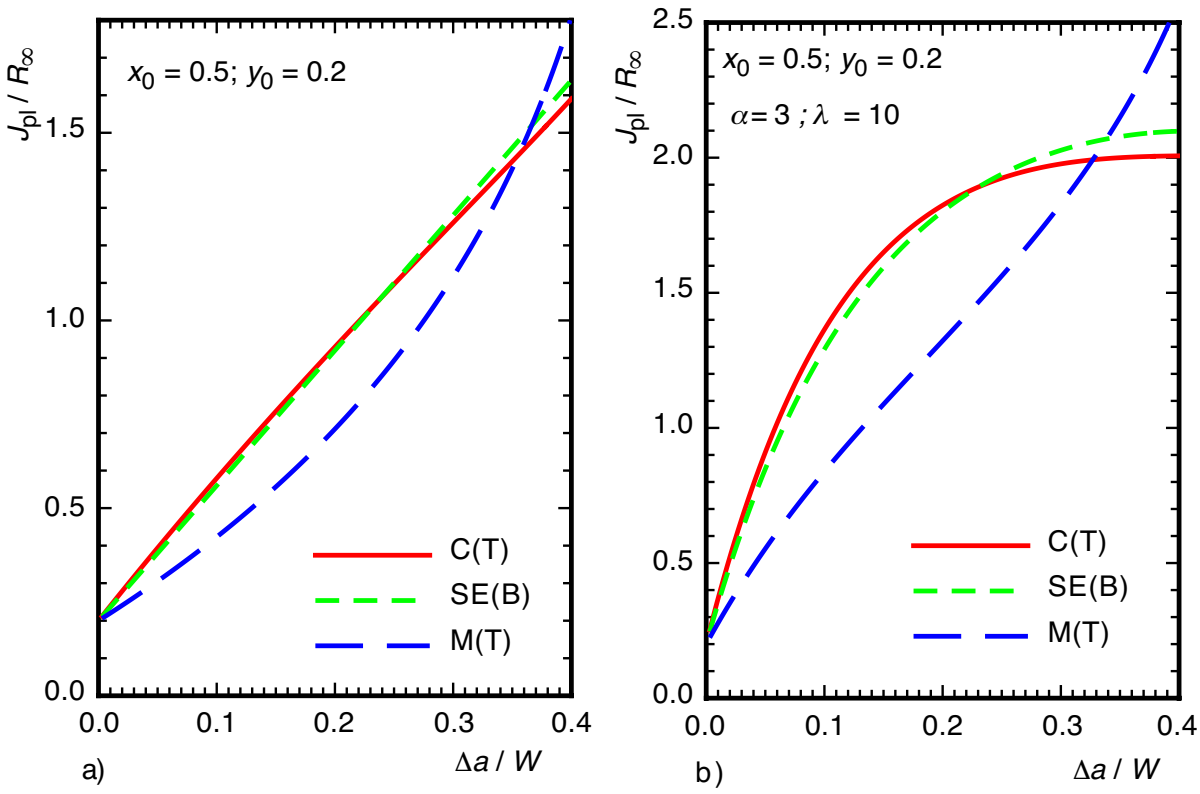

Fig. 2.8: Shapes of of J_R-curves;
a) for stationary crack extension, i.e. constant dissipation rate,
b) with transition regime, i.e. exponential decay of dissipation rate.

2.6 Prediction of J_R-curves

The procedure of converting a J_R-curve to an $R(\Delta a)$ curve, normalising and re-integrating it opens a possibility for transferring a J_R-curve from one specimen geometry "A" to another "B" [MEM94].

step 1: convert $J_{pl}(\Delta a)$ curve of "A" into $R(\Delta a)$ curve by eq. (2-2),

step 2: convert $R(\Delta a)$ curve of "A" into an $R(\Delta a)$ curve "B" by multiplying it with the factor $R^{B}_{ref} / R^{A}_{ref}$ calculated from eqs. (2-14), (2-16), (2-17) for plane strain,

step 3: integrate $R_{M(T)}(\Delta a)$ curve by eq. (2-25) into a "predicted" $J_{pl}(\Delta a)$ curve for "B".

The results are displayed in Fig. 2.9, for both directions of transfer, M(T) into C(T) and C(T) into M(T) J_R-curve, respectively. Regarding the large difference between M(T) and C(T) R-curves, the predictions are excellent. This result encouraged the idea of applying the procedure to other materials and specimen sizes. It did not work as well as in the present example, however, as will be discussed in section 3.3.

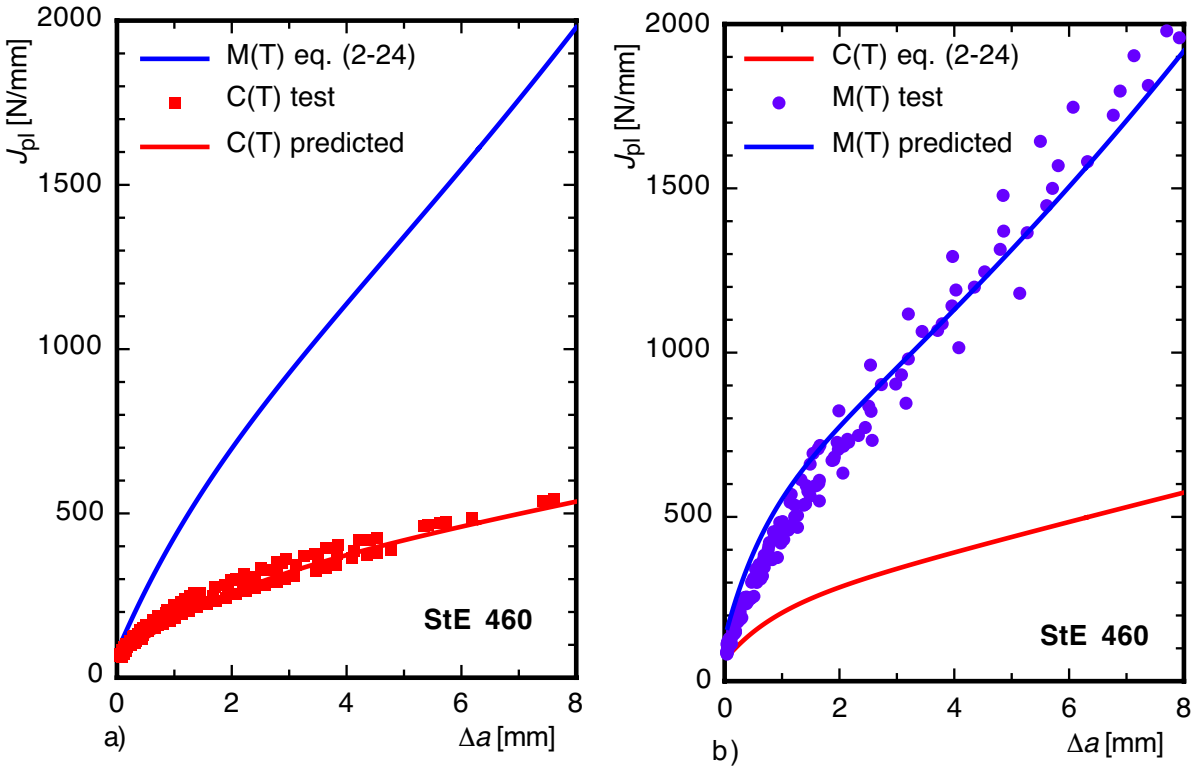

Fig. 2.9: Transferring a J_R-curve from one specimen geometry to another:
a) prediction of a C(T) R-curve from M(T) test data,
b) prediction of an M(T) R-curve from C(T) test data.

3. Experimental results

3.1 Data base

Two criteria decided over the selection of experimental J_R-curves for the evaluation of dissipation rate:

1. comparably large crack extension, even beyond the commonly accepted "validity limits" of "*J*-controlled" crack extension according to [ASTM1820] to include the transition to stationary crack extension, and
2. varying specimen geometries as well as varying a/W and B/W ratios for the same material, to investigate the dependence on loading mode and specimen geometry.

The respective data were available for the materials 20 Mn Mo Ni 5 5, Al 2024 T351 and Al 2024 FC, see [SCH84]. **Tables 3.1a,b** give an overview over the investigated materials and specimens, and Figs. 3.1a to 3.4a show the respective J_R-curves.

The evaluation procedure for the dissipation rate is as follows:

1. Calculate the $J_{pl}(\Delta a)$ curve by $J_{pl} = J - J_{el} = J - K^2/E'$; this requires the data $F(\Delta a)$ to calculate $K(\Delta a)$.
2. Differentiate the $J_{pl}(\Delta a)$ curve numerically and determine $R(\Delta a)$ by eqs. (2.2) or (2-5), respectively.

The $R(\Delta a)$ curves are displayed in Figs. 3.1b to 3.4b. The experimental data show a wide spectrum of values and give a rather diffuse impression of the relations between crack extension resistance and specimen geometry, which will be discussed in detail in section 3.1.

Table 3.1: Tested materials and specimen geometries
(a) ferritic steel 20 Mn Mo Ni 5 5

material R_{eL}; $R_{p0.2}$ [MPa] R_m [MPa] E [MPa]	**20 Mn Mo Ni 5 5 - smooth specimens** 450. 610. 210000.					
designation	type	W [mm]	B [mm]	B_n [mm]	a_0 [mm]	a_0 / W [-]
RCTMDA1	C(T)	50.	10.	10.	30.51	0.61
RCTMDB20	C(T)	50.	20.	20.	30.74	0.61
RCTMDA7	C(T)	100.	9.	9.	60.56	0.61
RCTMDV	C(T)	200.	10.	10.	119.98	0.60
RDENTMB3	DE(T)	50.	10.	10.	30.95	0.62
RCCT5	M(T)	100.	10.	10.	60.13	0.60
material R_{eL}; $R_{p0.2}$ [MPa] R_m [MPa] E [MPa]	**20 Mn Mo Ni 5 5 - side grooved specimens** 450. 610. 210000.					
CTR141	C(T)	25.	5.	4.	15.53	0.62
CTR111	C(T)	25.	10.	8.	16.64	0.67
CRMDB19A	C(T)	50.	5.	4.	30.40	0.61
CTR1	C(T)	50.	10.	8.	30.52	0.61
CTR15BA9	C(T)	50.	20.	16.	30.89	0.62
CTRMDC2	C(T)	100.	5.	4.	60.70	0.61
CTR21	C(T)	100.	10.	8.	60.36	0.61
CTR12BA9	C(T)	100.	20.	16.	60.77	0.61
CTR4BA9	C(T)	100.	50.	40.	61.86	0.62
CTRMDE9	C(T)	100.	50.	40.	61.44	0.61
CTR1BA9	C(T)	100.	50.	40.	81.34	0.81
CTRMDO2	C(T)	200.	5.	4.	120.00	0.60
CTR12	C(T)	200.	10.	8.	119.97	0.60
CTR7AA2	C(T)	200.	20.	16.	121.50	0.61
CTR1BA7	C(T)	200.	50.	40.	121.62	0.61

Table 3.1: Tested materials and specimen geometries
(b) aluminium alloys Al 2024-T351 and Al 2024-FC, smooth specimens

material R_{eL}; $R_{p0.2}$ [MPa] R_m [MPa] E [MPa]	**Al 2024-T351** 317. 440. 71600.				
designation	type	W [mm]	$B = B_n$ [mm]	a_0 [mm]	a_0 / W [-]
CT-50/0.5	C(T)	50.	5.	25.1	0.50
CT-50/0.8	C(T)	50.	5.	40.5	0.81
CT-100/0.7	C(T)	100.	20.	71.0	0.71
SEB-50/0.5	SE(B)	50.	5.	25.5	0.51
SEB-100/0.5	SE(B)	100.	5.	50.2	0.50
MT-50/0.5	M(T)	50.	5.	25.3	0.50
MT-100/0.5	M(T)	100.	5.	49.5	0.49
MT-100/0.7	M(T)	100.	20.	74.0	0.74
material R_{eL}; $R_{p0.2}$ [MPa] R_m [MPa] E [MPa]	**Al 2024-FC** (furnace cooled) 75. 217. 71600.				
CT-50/0.5	C(T)	50.	5.	25.5	0.51
CT-50/0.6	C(T)	50.	5.	30.0	0.60
CT-50/0.7	C(T)	50.	5.	35.5	0.71
CT-100/0.3	C(T)	100.	5.	30.0	0.30
CT-100/0.5	C(T)	100.	5.	51.0	0.51
CT-100/0.7	C(T)	100.	5.	70.0	0.70
SEB-50/0.5	SE(B)	50.	5.	25.0	0.50
SEB-100/0.5	SE(B)	100.	5.	50.0	0.50
MT-50/0.5	M(T)	50.	5.	25.1	0.50
MT-50/0.7	M(T)	50.	5.	35.0	0.70
MT-100/0.2	M(T)	100.	10.	20.0	0.20
MT-100/0.5	M(T)	100.	5.	50.0	0.50
MT-100/0.7	M(T)	100.	5.	70.0	0.70

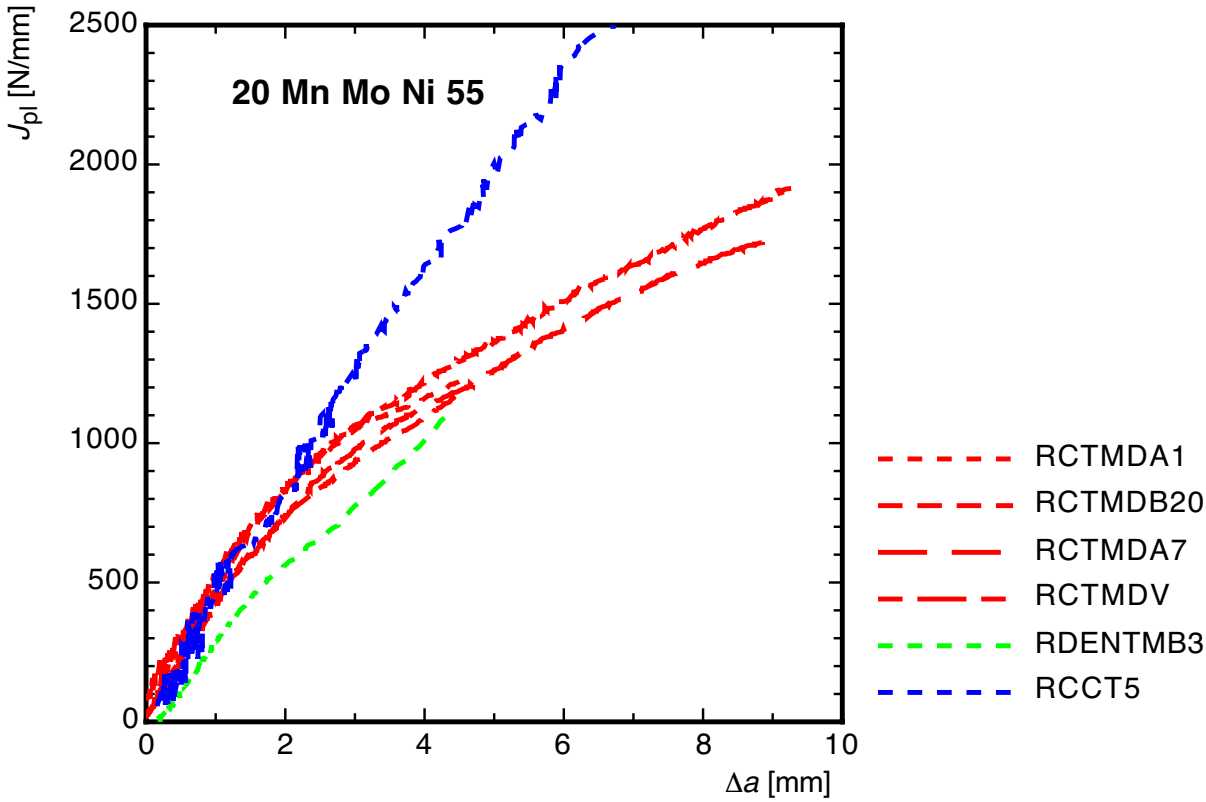

Fig. 3.1: (a) J_R-curves for 20 Mn Mi Ni 5 5 (smooth specimens)

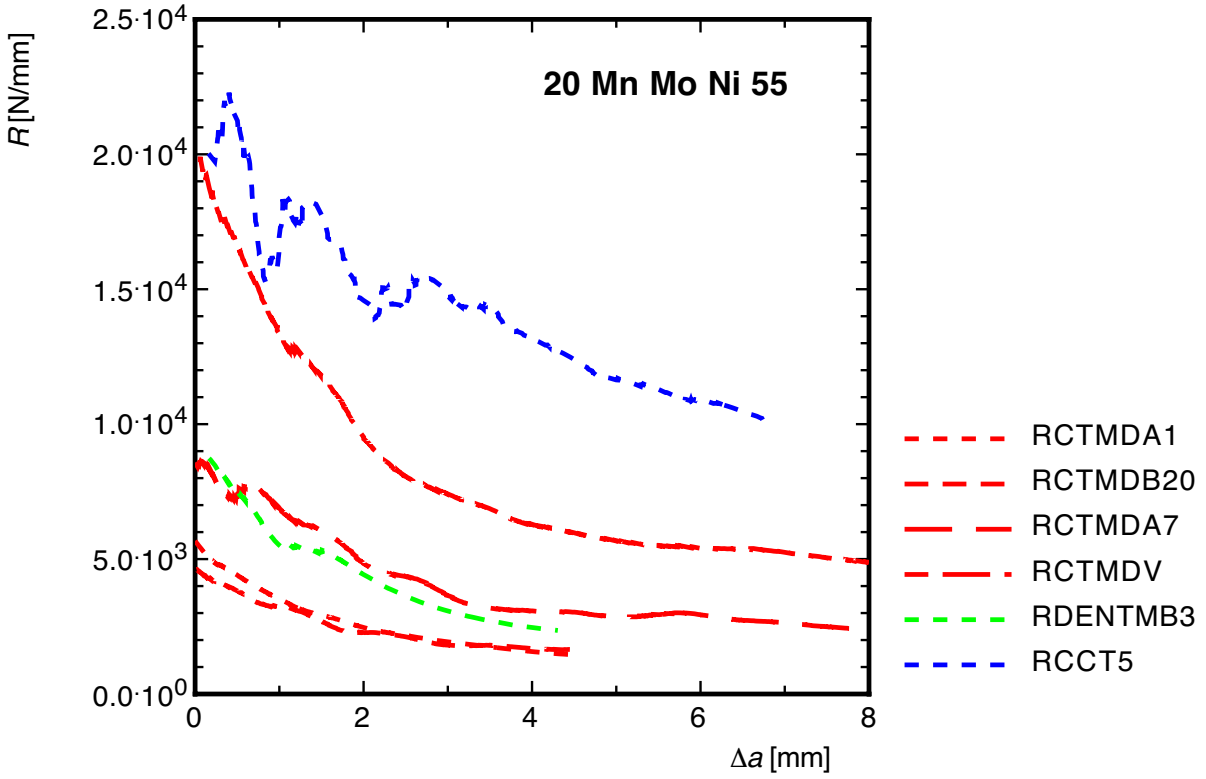

Fig. 3.1: (b) $R(\Delta a)$ curves for 20 Mn Mi Ni 5 5 (smooth specimens)

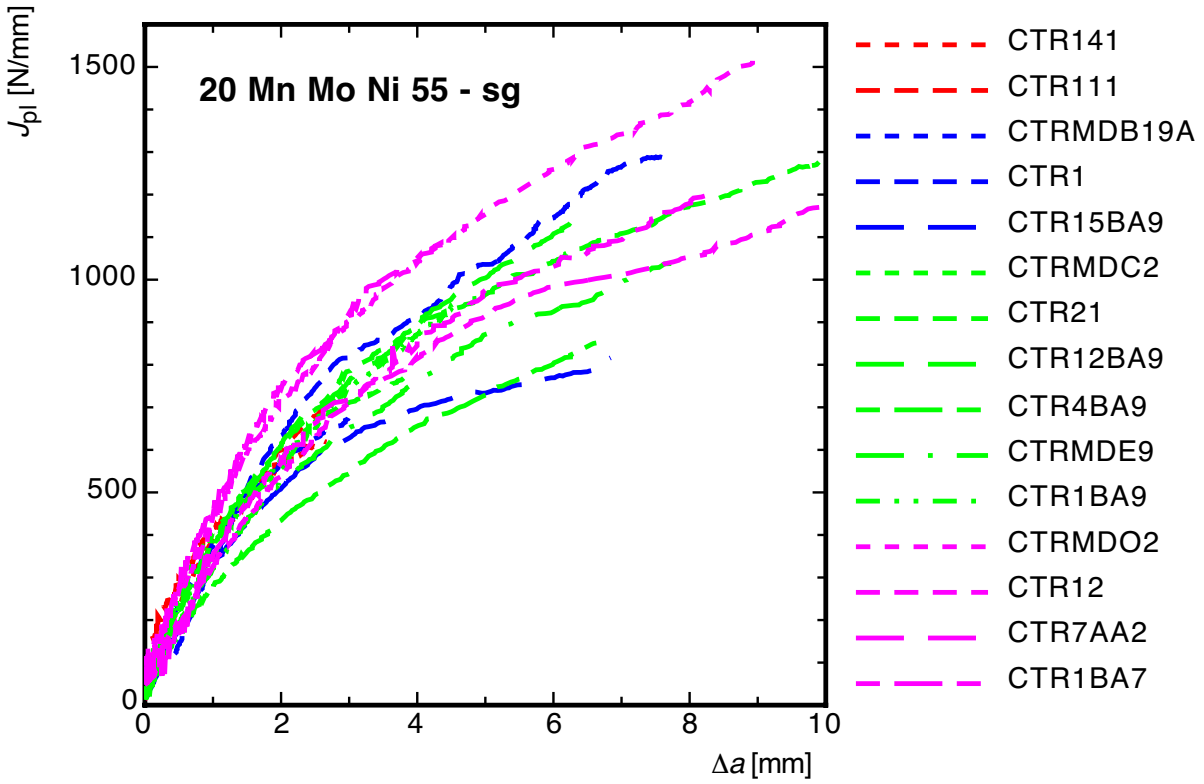

Fig. 3.2: (a) J_R-curvesfor 20 Mn Mi Ni 5 5 (side-grooved specimens)

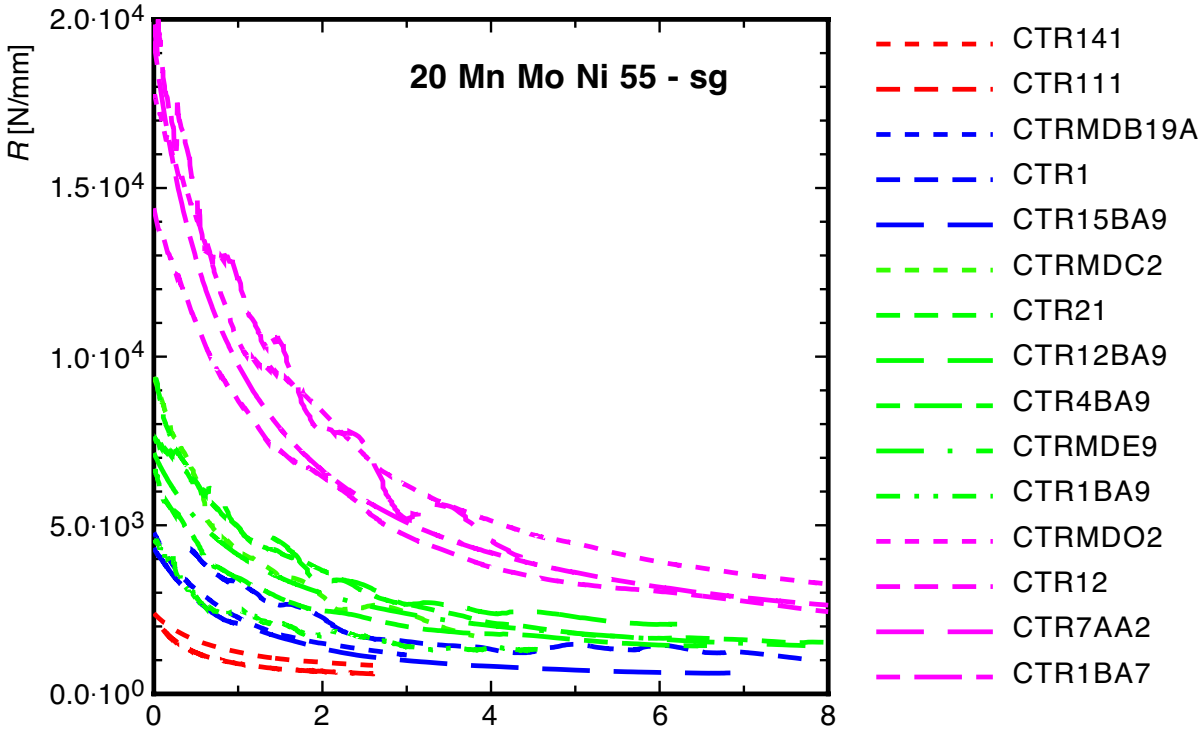

Fig. 3.2: (b) $R(\Delta a)$ curves for 20 Mn Mi Ni 5 5 (side-grooved specimens)

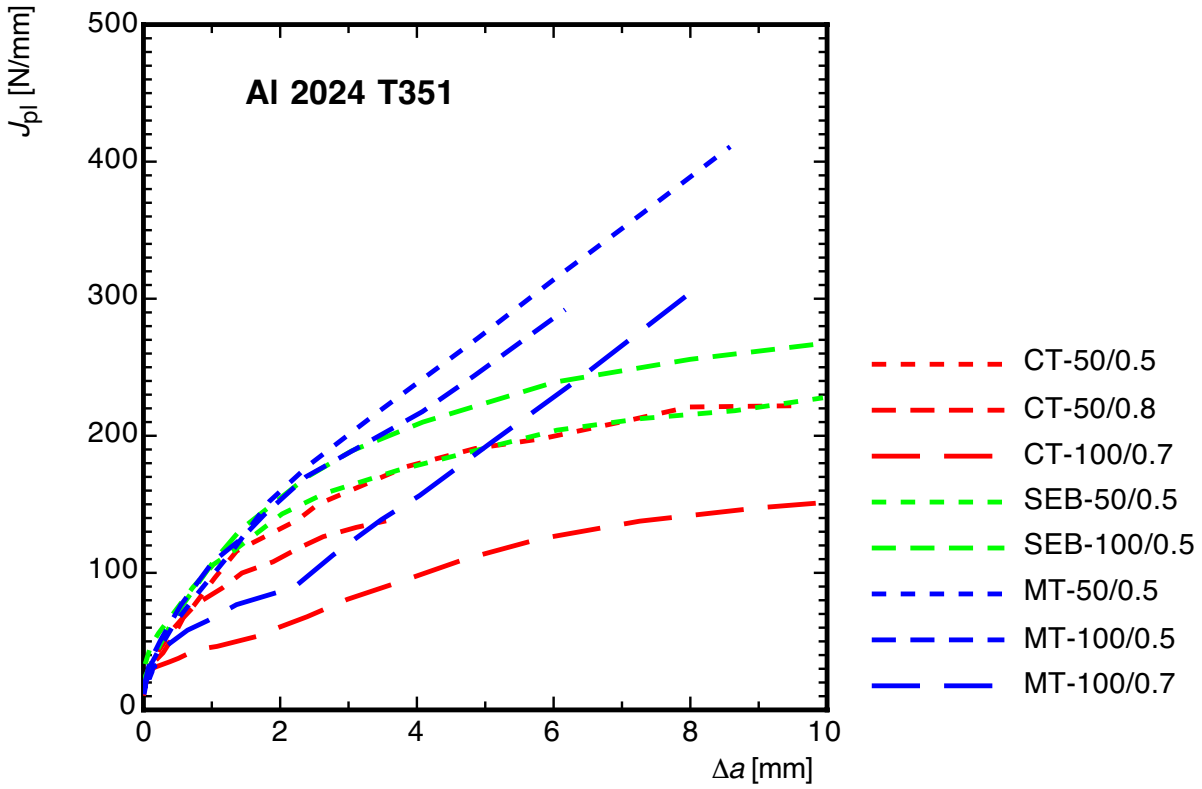

Fig. 3.3: (a) J_R-curves for Al 2024 T351

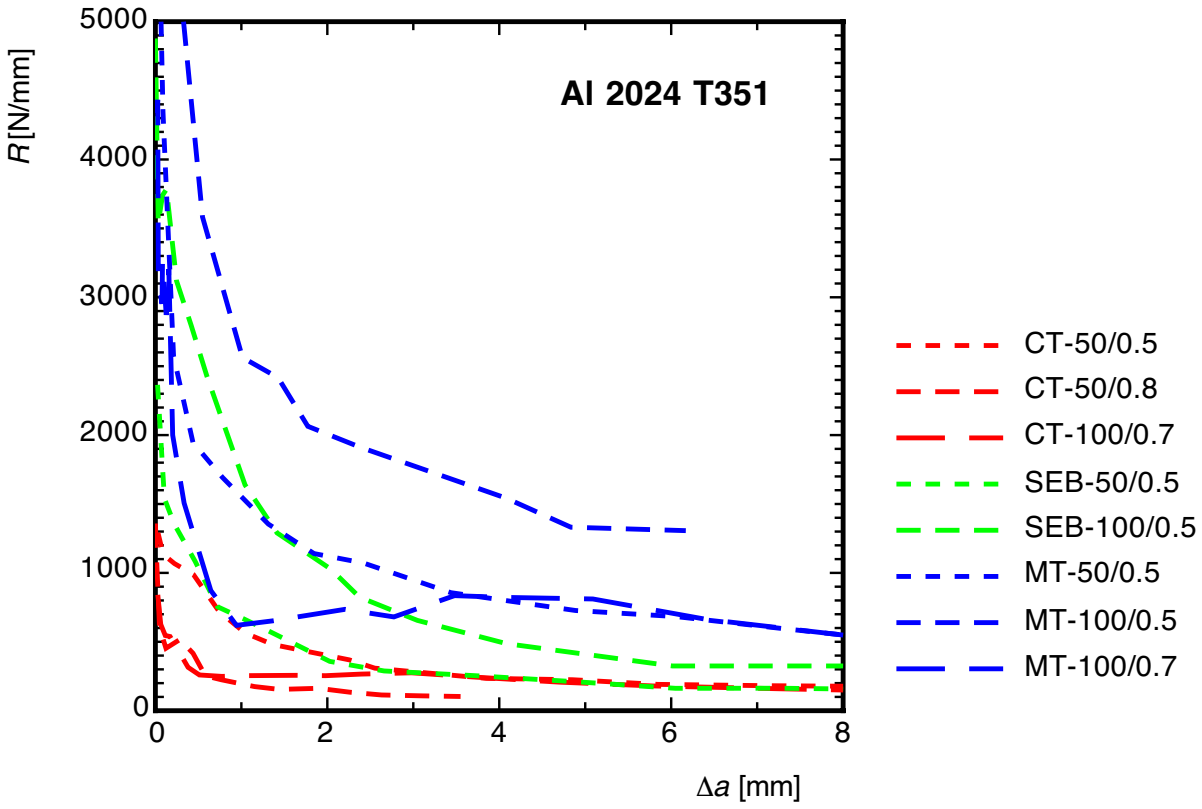

Fig. 3.3: (b) $R(\Delta a)$ curves for Al 2024 T351

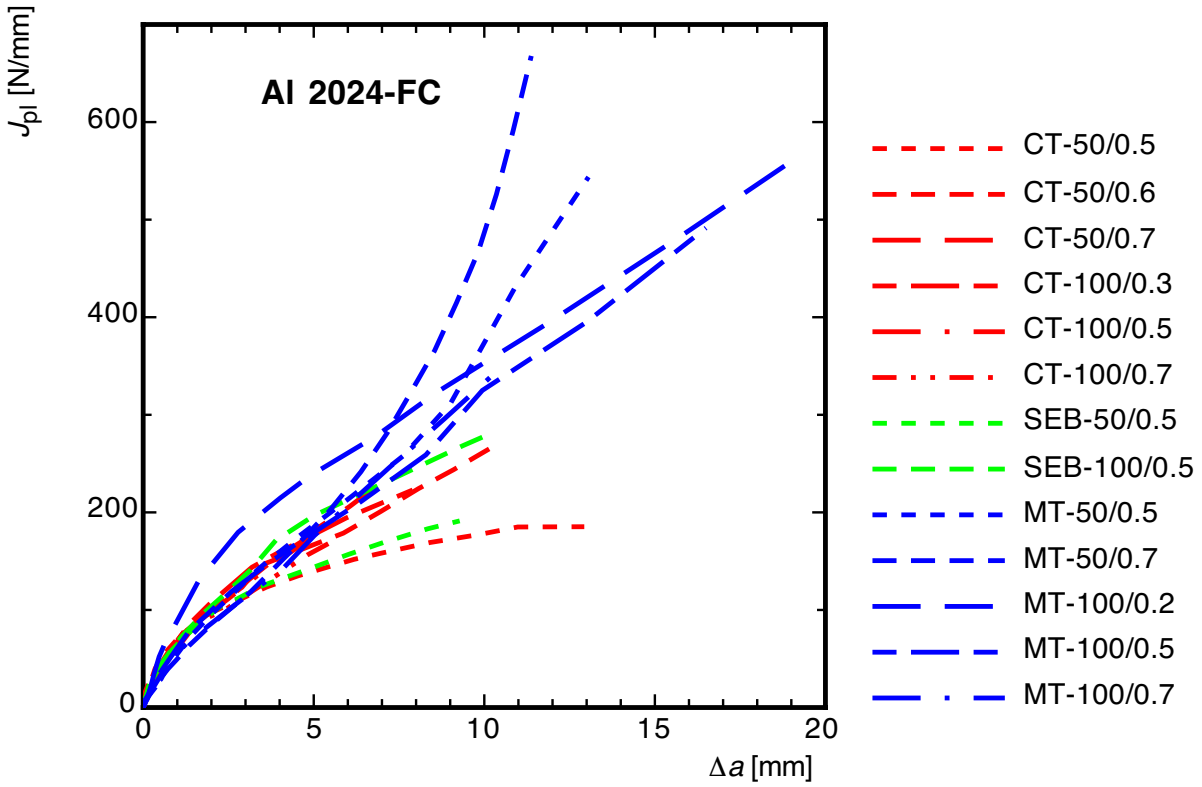

Fig. 3.4: (a) J_R-curves for Al 2024 FC

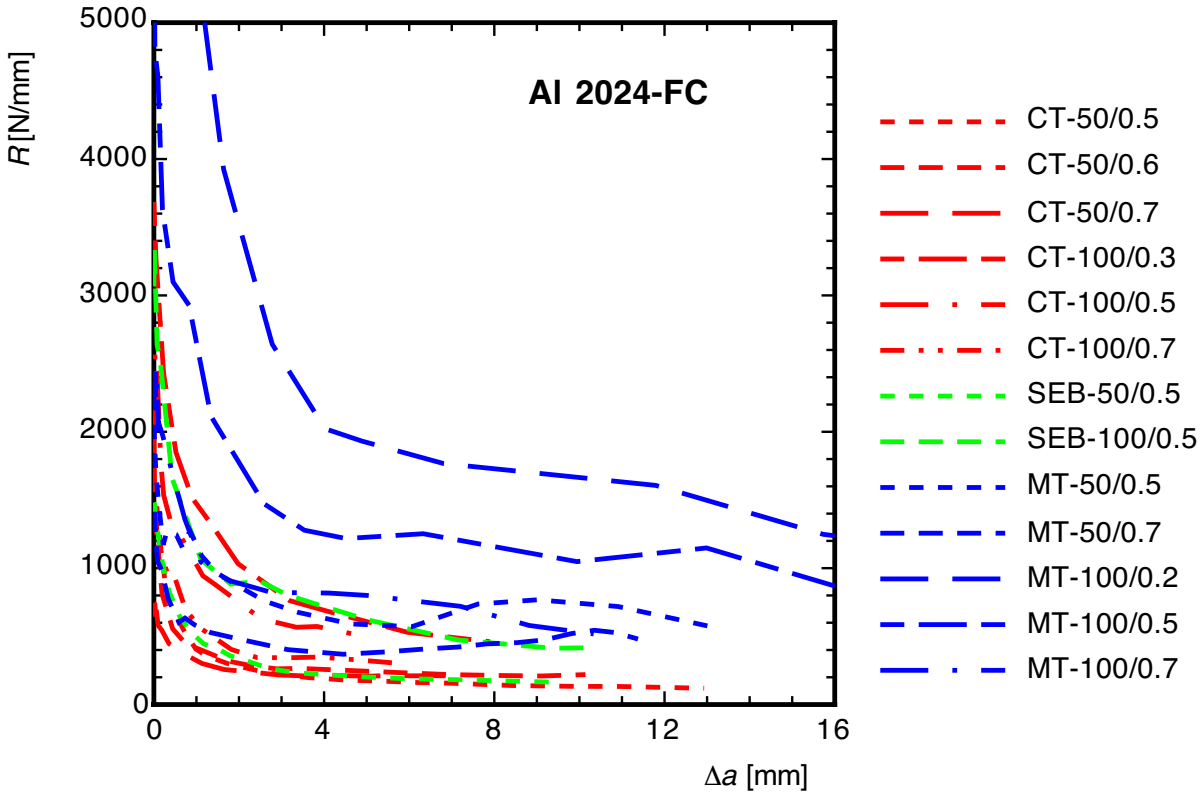

Fig. 3.4: (b) $R(\Delta a)$ curves for Al 2024 FC

Finally, the $R(\Delta a)$ data are fitted by the exponential function of eq. (2-9), see **Table 3.2**. The LEVENBERG-MARQUARDT procedure of a commercial plot software and a specially developed programme have been used for this fitting in the present investigation. The quality of the fit depends strongly of the available data. In particular, the physical significance of the crack propagation energy, R_∞, relies on the existence of data in the stationary regime. A few extreme examples are picked out of the data sets to illustrate the problems with data fitting and the reverse effects on J_R-curves.

#1: This is a "good natured" J_R-curve referring to an M(T) specimen with $W = 100$mm and $a_0/W = 0.5$ of Al 2024 T351, see Fig. 3.5. Fitting of the experimental $R(\Delta a)$ data yields in the parameters listed in **Table 3.2b**. Integrating the $R(\Delta a)$ fit curve according to eq. (2-25) results in a rather "perfect" J_R-curve.

#2: This is the J_R-curve of an M(T) specimen with $W = 100$mm and $a_0/W = 0.7$ of Al 2024 T351, which displays a change of the slope resulting in an increase of the dissipation rate after $\Delta a = 2$mm, see Fig. 3.6. Two ranges of Δa can hence be chosen for the fitting procedure, small and large crack extension, wich result in two parameter sets, R_∞ / α / λ, as described in the legend. The respective integrated curves approximate the experimental J_R-curve over $\Delta a < 3$mm (fit #1) or the whole range of data (fit #2), respectively.

#3: This is the J_R-curve of a C(T) specimen with $W = 100$mm and $a_0/W = 0.7$ of Al 2024 T351, which again, but even more pronounced, consists of two parts, see Fig. 3.7. A best fit of the experimental $R(\Delta a)$ data over the whole range seems nearly impossible. However fit #3, which pays no heed to the transition regime for small crack extension at all, appears to yield the best overall approximation of the experimental J_R-curve.

Fig. 3.6b shows that the effect of an increasing slope of J_R-curves of M(T) specimens is partly due to the integration procedure for calculating the J integral and does not necessarily indicate any "increase" of crack extension resistance, which could be concluded from Fig. 2.8, already.

Example #3 illustrates the limitations of the exponential fit and a characterization of crack extension resistance by three parameters, only. It also demonstrates that no precise fitting of the transision regime is required if only large crack extension is considered. STAMPFL & KOLEDNIK [STA00] explain the a second peak value in the $R(\Delta a)$-curve, which results in an increase of the slope of the correspondent J_R-curve, by the occurance of shear lips on the fracture surface, which contribute additional plastic work.

Figs. 3.8 to 3.11 show all fitted $R(\Delta a)$ curves with the parameters listed in.**Table 3.2.** The significant advantage of the proposed fits, eqs. (2-9) or (2-12), is that the crack extension resistance can be quantified by the three parameters, R_∞, α, λ, which allow for some physical interpretation.

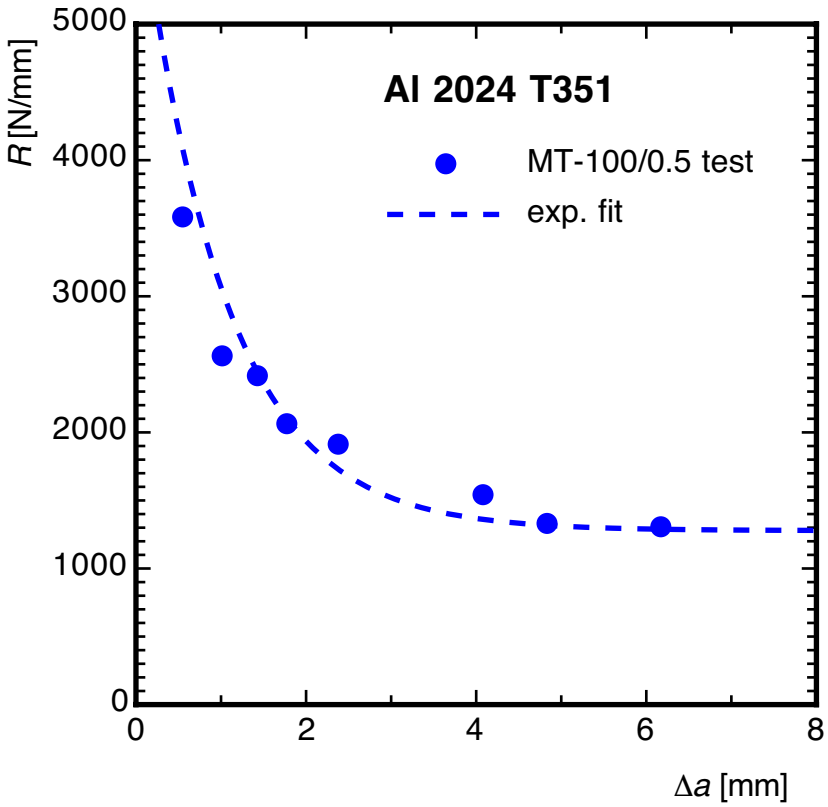

Fig. 3.5: (a) $R(\Delta a)$ curve for Al 2024 T351, M(T)-100/0.5, test data and exponential fit

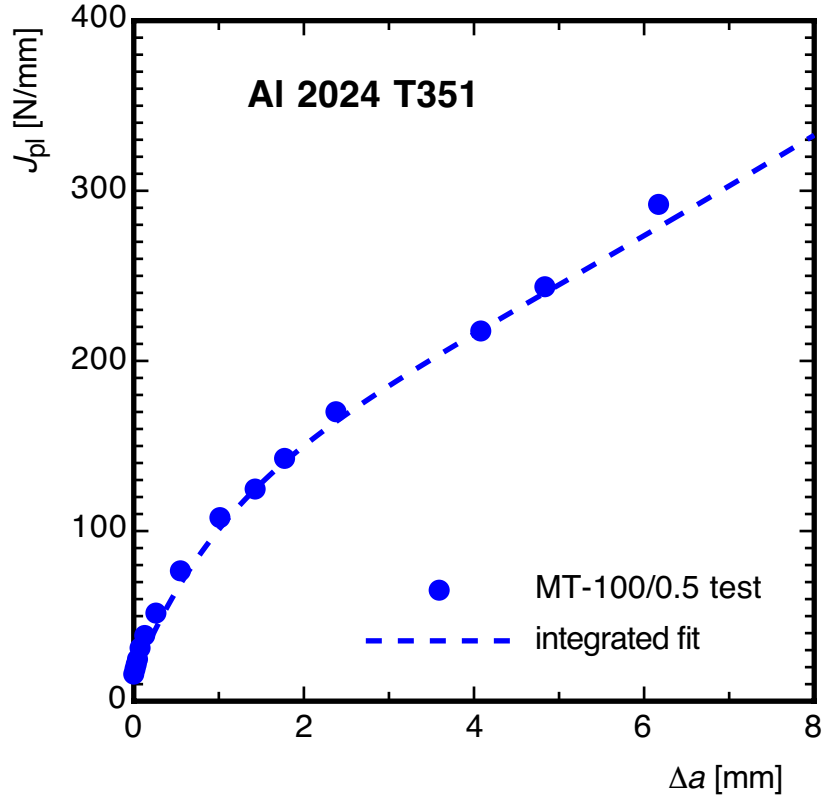

Fig. 3.5: (b) J_R- curve for Al 2024 T351, M(T)-100/0.5, test data and integrated $R(\Delta a)$ fit

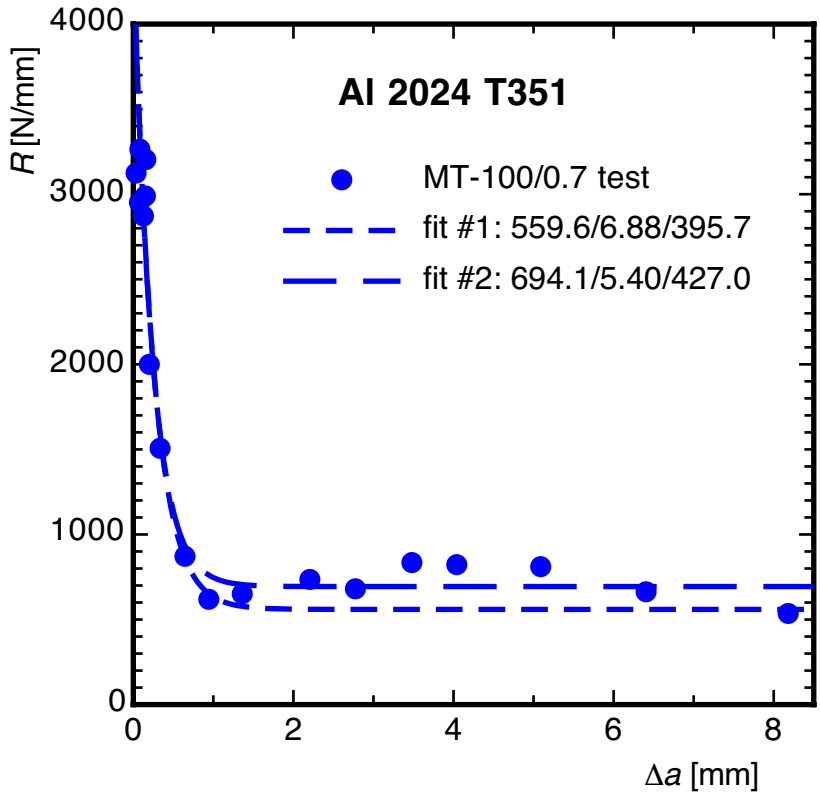

Fig. 3.6: (a) $R(\Delta a)$ curve for Al 2024 T351, M(T)-100/0.7, test data and exponential fits

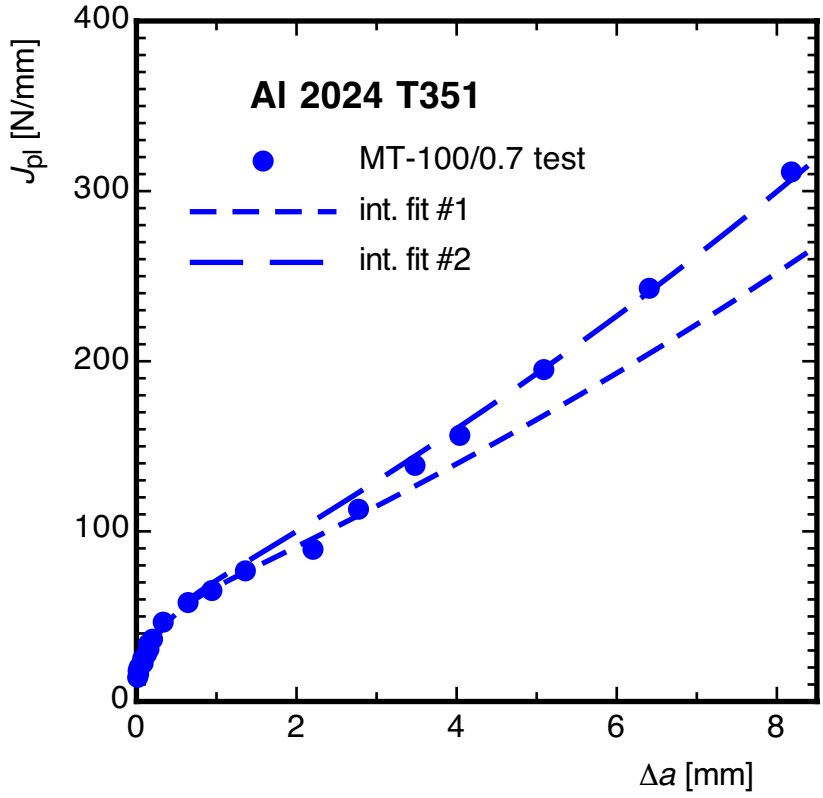

Fig. 3.6: (b) J_R- curve for Al 2024 T351, M(T)-100/0.7, test data and integrated $R(\Delta a)$ fits

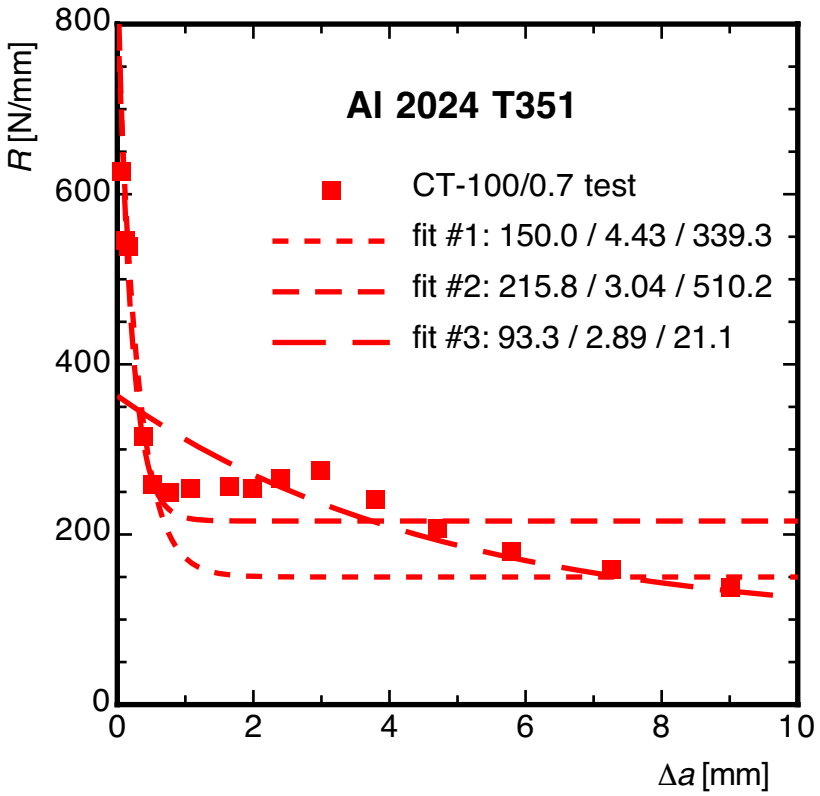

Fig. 3.7: (a) $R(\Delta a)$ curve for Al 2024 T351, C(T)-100/0.7, test data and exponential fits

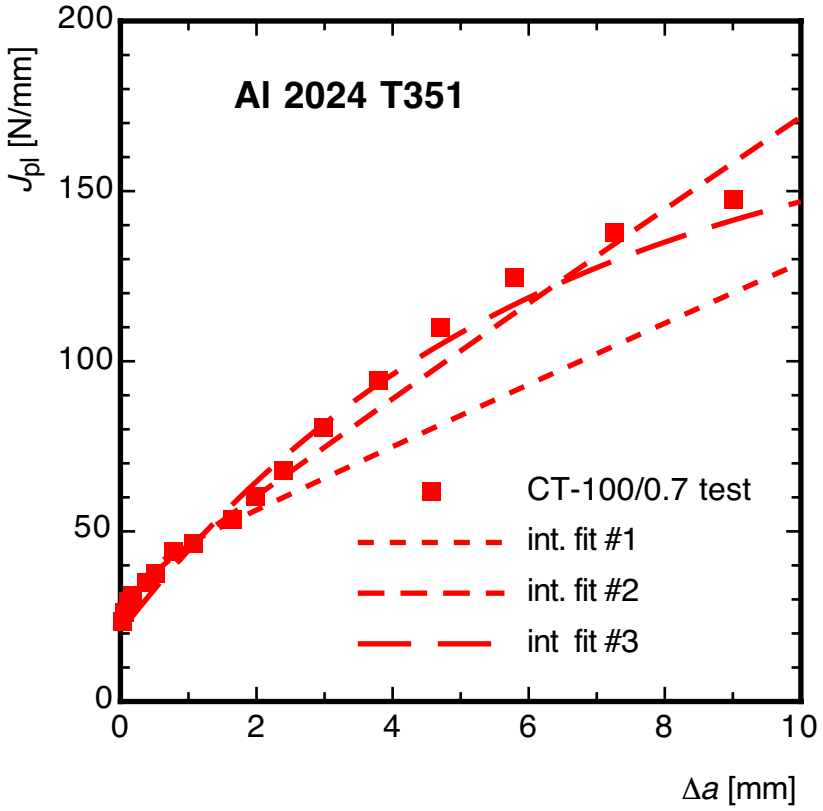

Fig. 3.7: (b) J_R- curve for Al 2024 T351, C(T)-100/0.7, test data and integrated $R(\Delta a)$ fits

Table 3.2: Parameters of $R(\Delta a)$ fit, eq. (2-9)
(a) ferritic steel 20 Mn Mo Ni 5 5

material	**20 Mn Mo Ni 5 5 - smooth specimens**			
designation	R_∞ [N/mm]	α [-]	λ [-]	λ / W [mm^{-1}]
RCTMDA1	1203.	3.575	30.52	0.610
RCTMDB20	1395.	2.334	31.05	0.621
RCTMDA7	2173.	3.107	43.52	0.435
RCTMDV	4574.	3.442	111.70	0.558
RDENTMB3	1744.	4.292	28.13	0.563
RCCT5	5530.	3.275	26.22	0.262
material	**20 Mn Mo Ni 5 5 - side grooved specimens**			
CTR141	813.	1.884	32.74	0.764
CTR111	593.	2.493	40.69	1.616
CRMDB19A	1085.	3.313	56.72	1.134
CTR1	1108.	3.812	34.68	0.694
CTR15BA9	612.	5.354	38.34	0.767
CTRMDC2	2012.	3.618	113.63	1.136
CTR21	1462.	4.824	64.45	0.644
CTR12BA9	1971.	2.955	63.59	0.636
CTR4BA9	1471.	3.330	87.32	0.873
CTRMDE9	1429.	3.783	63.86	0.639
CTR1BA9	1290.	2.433	104.89	1.049
CTRMDO2	3014.	4.707	103.88	0.519
CTR12	1812.	6.475	94.96	0.475
CTR7AA2	3142.	5.167	121.83	0.609
CTR1BA7	2740.	5.465	139.15	0.696

Table 3.2: Parameters of $R(\Delta a)$ fit, eq. (2-9)
(b) aluminium alloys Al 2024-T351 and Al 2024-FC, smooth specimens

material	**Al 2024-T351**			
designation	R_∞ [N/mm]	α [-]	λ [-]	λ / W [mm^{-1}]
CT-50/0.5	174.4	6.303	44.14	0.883
CT-50/0.8	110.0	8.949	226.30	4.526
CT-100/0.7	150.0	4.430	339.30	3.393
SEB-50/0.5	150.0	12.830	73.76	1.475
SEB-100/0.5	300.0	12.829	96.19	0.962
MT-50/0.5	641.0	3.230	41.20	0.824
MT-100/0.5	1278.3	3.800	100.00	1.000
MT-100/0.7	559.6	6.885	395.66	3.957
material	**Al 2024-FC**			
CT-50/0.5	126.8	11.349	95.87	1.917
CT-50/0.6	213.1	2.373	94.13	1.883
CT-50/0.7	230.1	5.043	119.31	2.386
CT-100/0.3	453.0	6.482	109.45	1.094
CT-100/0.5	513.0	3.714	159.21	1.592
CT-100/0.7	290.1	3.681	125.97	1.260
SEB-50/0.5	159.4	7.893	67.75	0.678
SEB-100/0.5	413.4	6.322	117.94	1.179
MT-50/0.5	576.7	2.117	47.75	0.954
MT-50/0.7	400.0	2.342	117.71	2.354
MT-100/0.2	1583.1	6.000	80.00	0.800
MT-100/0.5	1100.0	3.180	79.00	0.790
MT-100/0.7	600.0	2.886	107.05	1.070

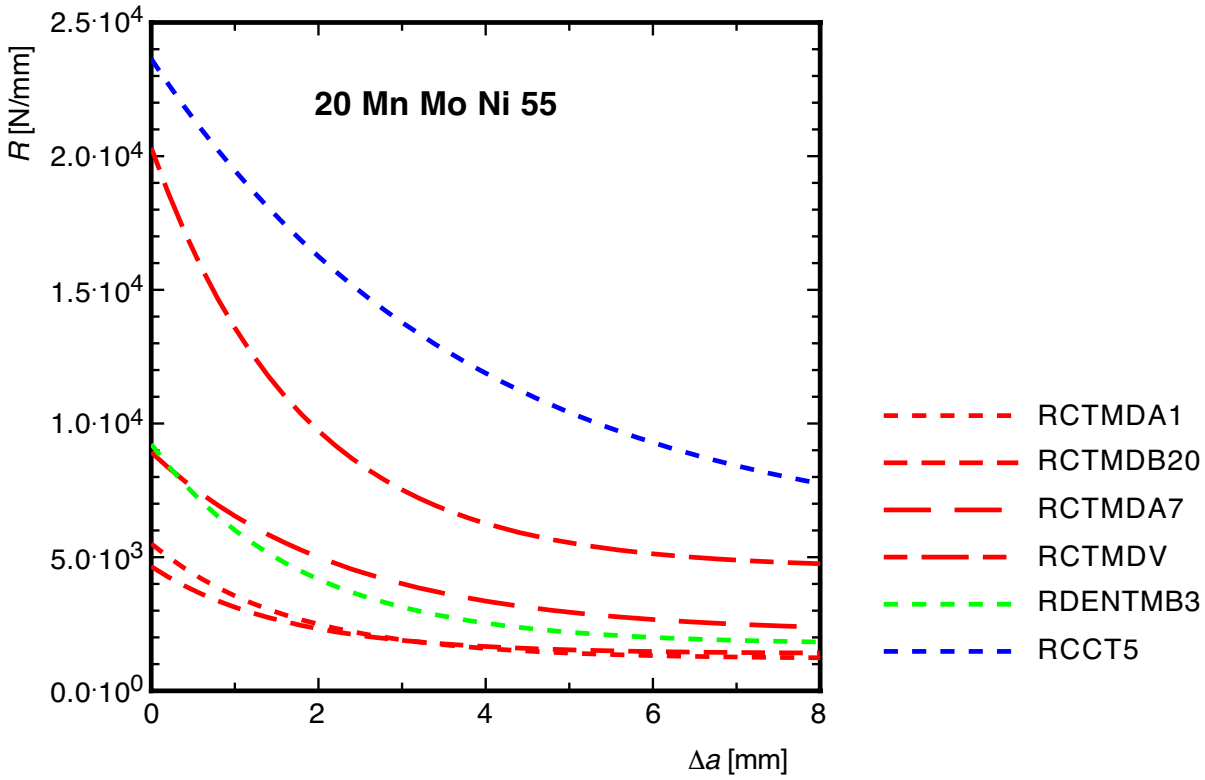

Fig. 3.8: Curve fits of $R(\Delta a)$ for 20 Mn Mi Ni 5 5 (smooth specimens)

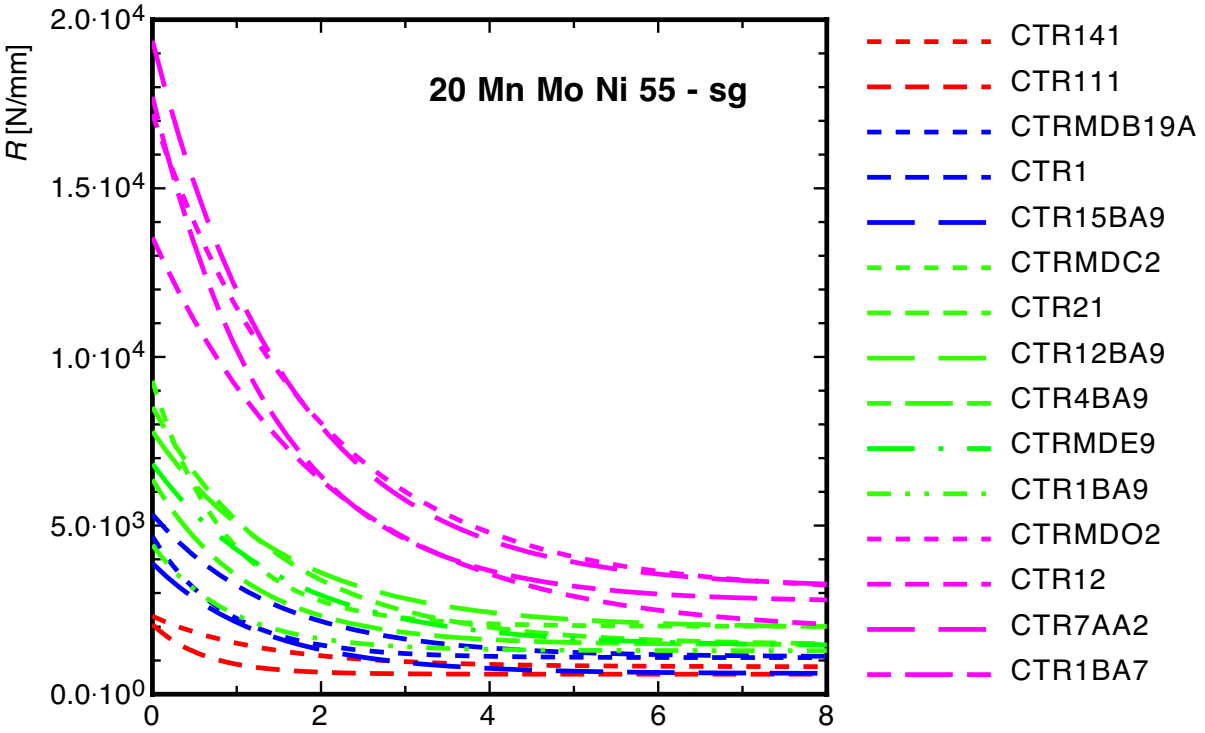

Fig. 3.9: Curve fits of $R(\Delta a)$ for 20 Mn Mi Ni 5 5 (side grooved specimens)

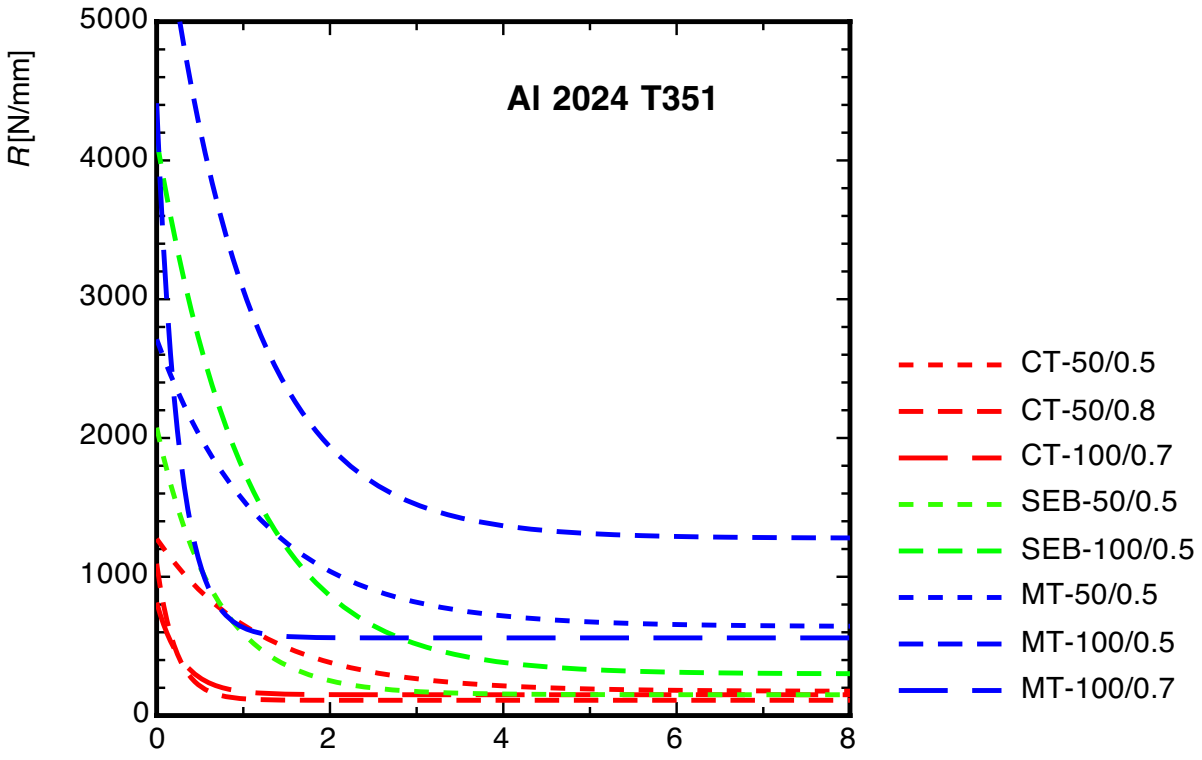

Fig. 3.10: Curve fits of $R(\Delta a)$ for Al 2024 T351

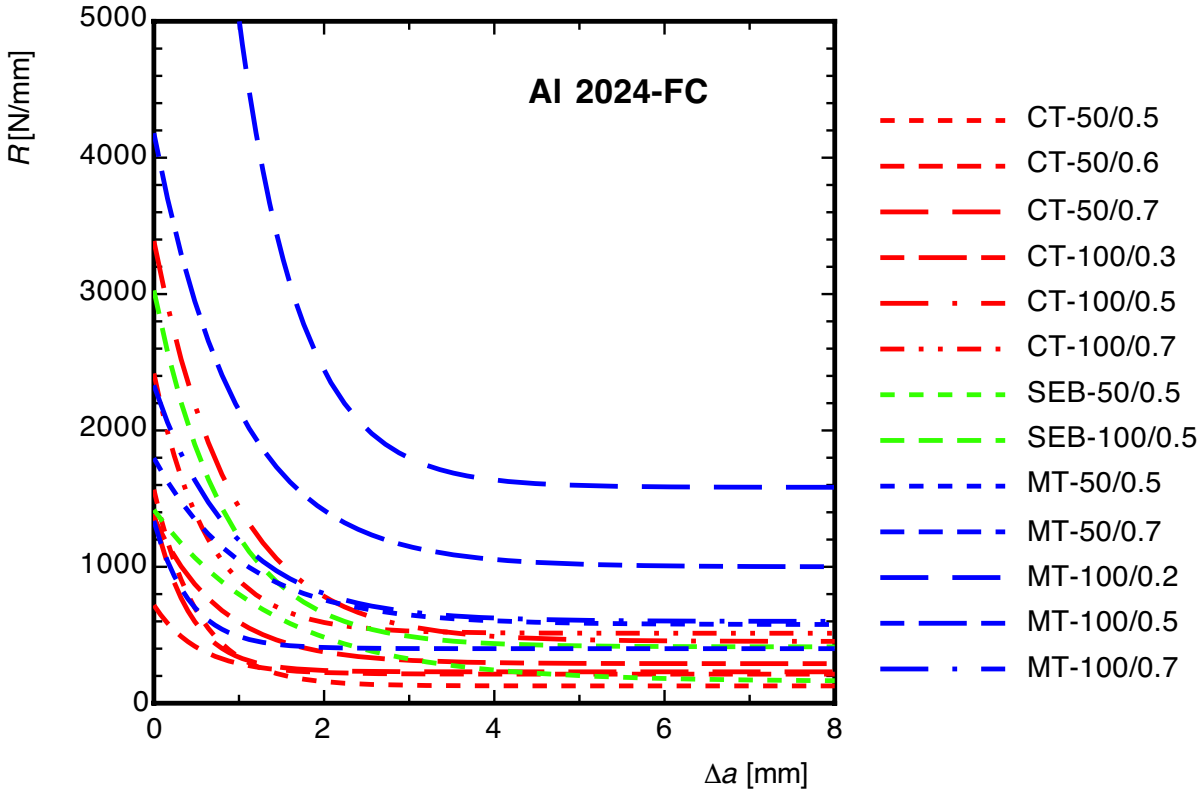

Fig. 3.11: Curve fits of $R(\Delta a)$ for Al 2024 FC

3.2 Effect of specimen geometry

As all crack resistance curves have been fitted by eq. (2-9), the effects of specimen geometry, loading mode and relative crack length can now be discussed in terms of the three fitting parameters, R_∞, α, λ, which have some physical significance, as described in section 2.3. The relations are not very clear, however. Some basic tendencies are observed:

- The crack propagation energy, R_∞, increases with the ligament length, $W - a_0$, see Figs. 3.12, and 3.13, and is significantly higher for tensile type than for bending type specimens. That means that the loading mode affects the dependence on the ligament length. Lower bound values are obtained for square ligaments, $B / (W-a_0) \approx 1.0$, see Fig. 3.12b.
- The ratio of the initial to the final value of the energy dissipation rate, $R_0/R_\infty = \alpha+1$, increases with the ligament length, $W - a_0$, for the side-grooved C(T) specimens of 20 Mn Mo Ni 5 5, - displaying a large scatter, however - and the M(T) of Al 2024 FC, whereas it decreases for the C(T) of Al 2024 T351, see Figs. 3.14, and 3.15. Little effects are recognised for the rest, and no effect of the loading mode can be observed.
- The length of decay, $1/\lambda$, decreases with $W - a_0$ for 20 Mn Mo Ni 5 5, displaying a large scatter for the side-grooved specimens, again, Fig. 3.16, and no effects of the ligament length or the loading mode can be found for both aluminium alloys, Fig. 3.17.

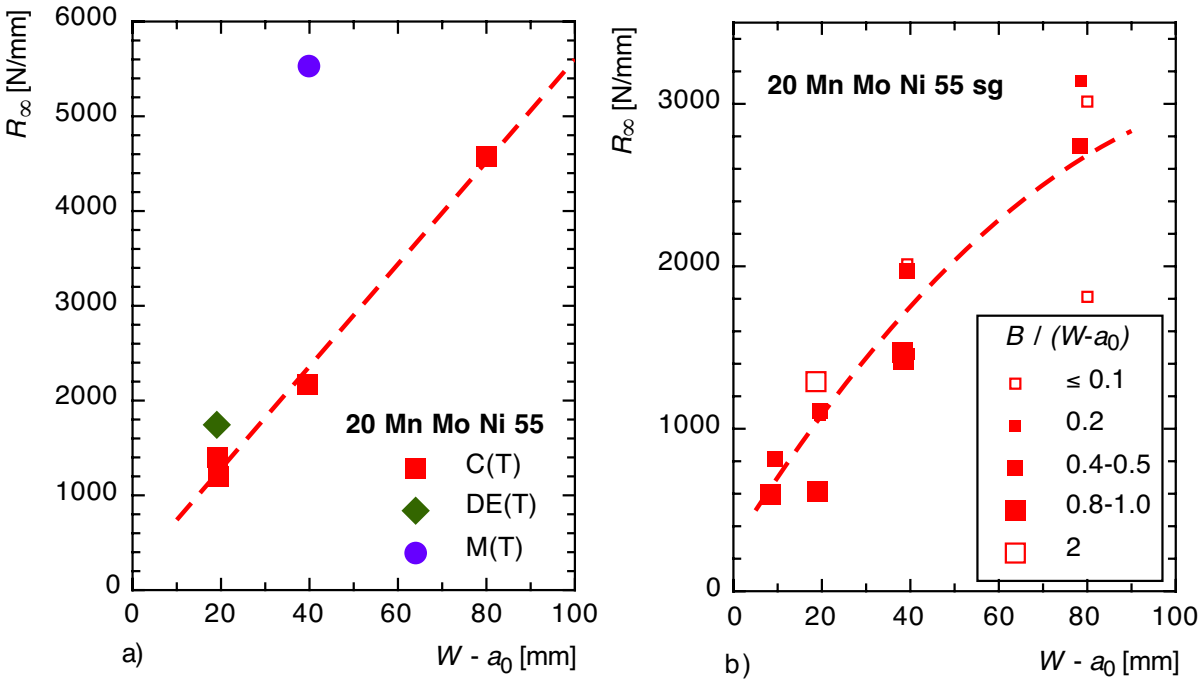

Fig. 3.12: Dependence of crack propagation energy, R_∞, on ligament length for 20 Mn Mi Ni 5 5;
a) smooth specimens, b) side grooved specimens

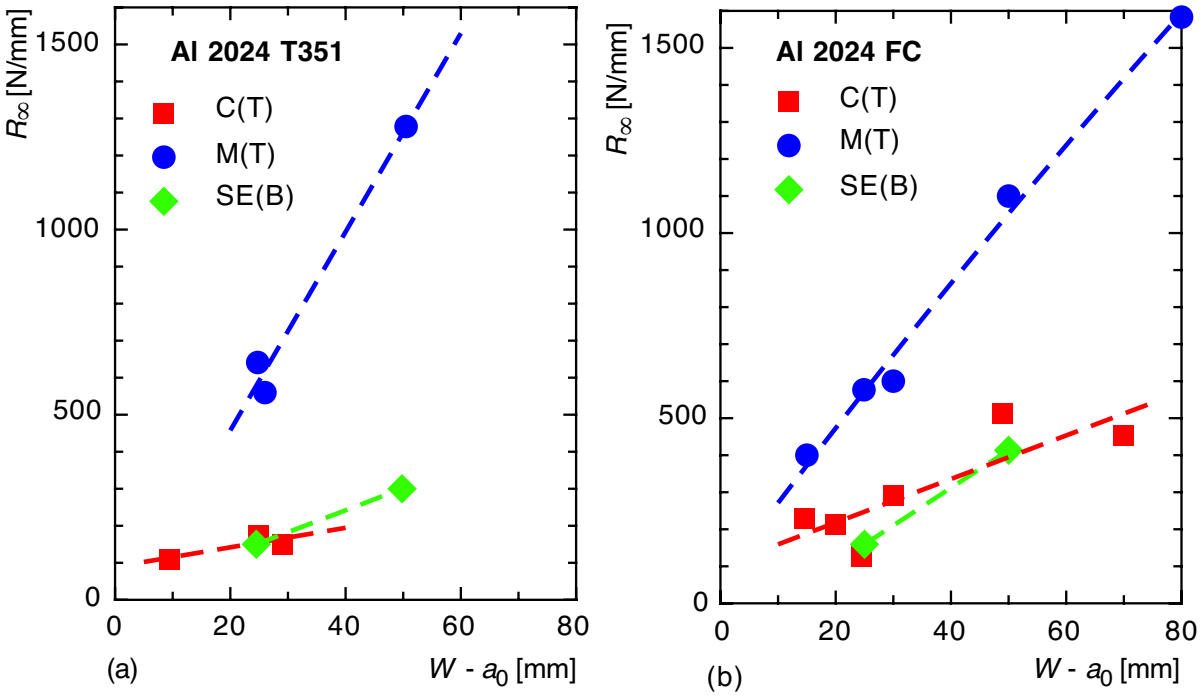

Fig. 3.13: Dependence of crack propagation energy, R_∞, on ligament length;
a) Al 2024 T351, b): Al 2024 FC

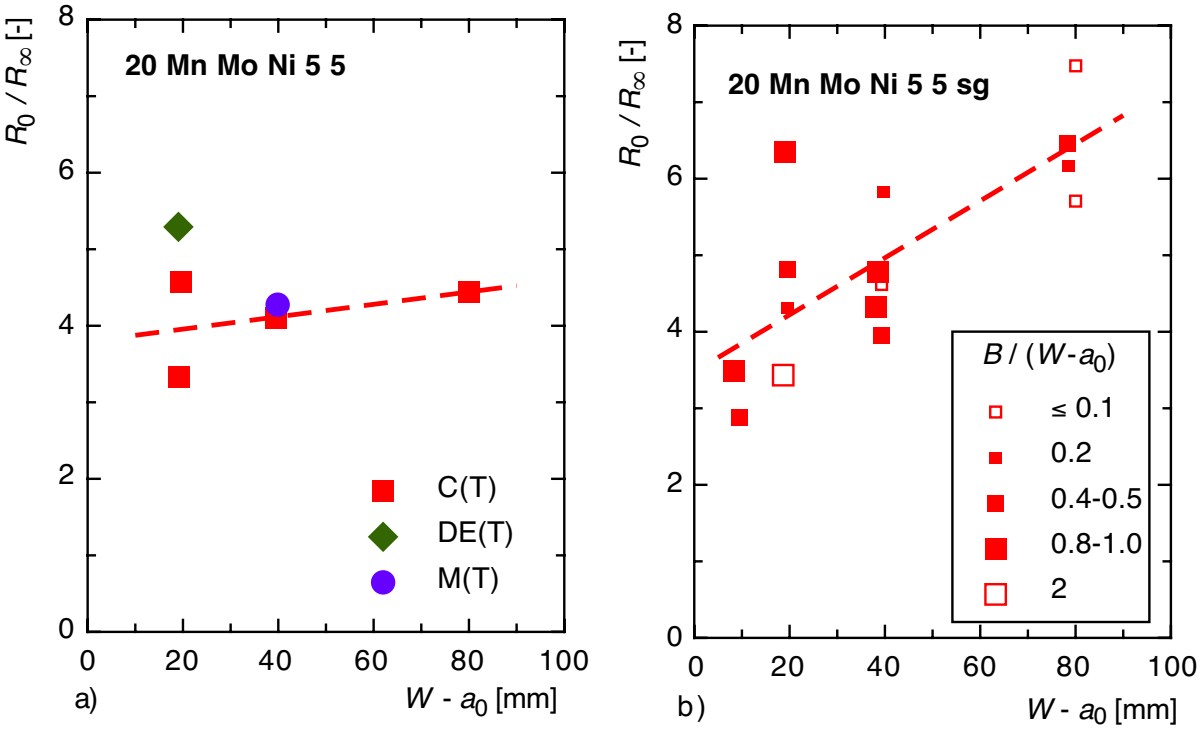

Fig. 3.14: Dependence of R_0 / R_∞ on ligament length for 20 Mn Mi Ni 5 5;
a) smooth specimens, b) side grooved specimens

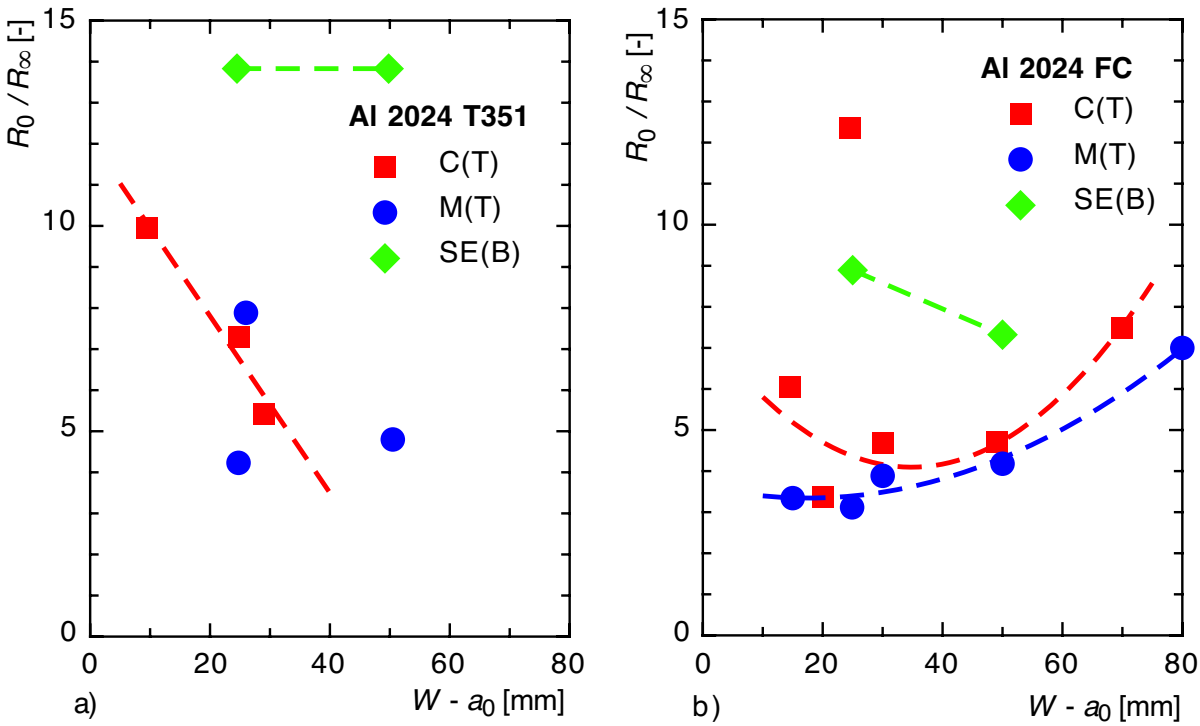

Fig. 3.15: Dependence of R_0 / R_∞ on ligament length,
a) Al 2024 T351, b) Al 2024 FC

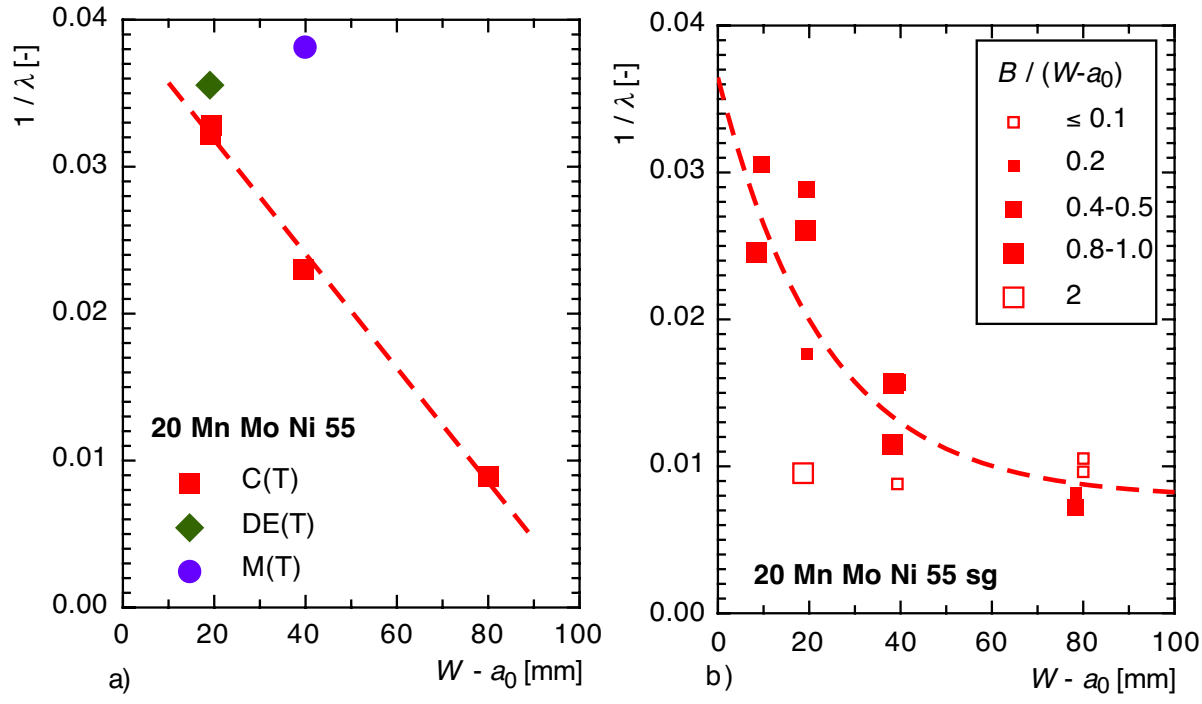

Fig. 3.16: Dependence of 1/λ on ligament length for 20 Mn Mi Ni 5 5;
a) smooth specimens, b) side grooved specimens

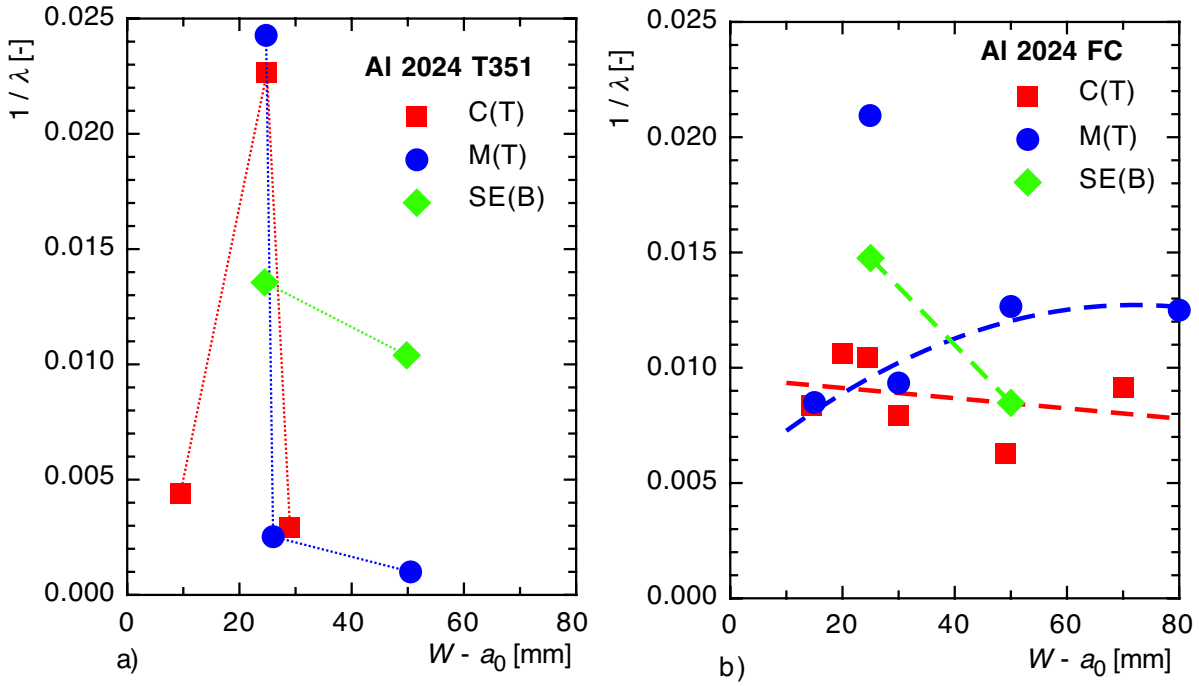

Fig. 3.17: Dependence of $1/\lambda$ on ligament length,
a) Al 2024 T351, b) Al 2024 FC

Several parameters have been proposed to quantify "constraint effects" on crack extension resistance [BRO95], mainly the biaxiality factor β [LEE82], the T stress [RIC74] and the Q stress [ODO91, SHI91]. Neither of them was able to satisfactorily scale the geometry effects on the resistance data in the present case [BRO98]. Fig 3-18 shows the crack propagation energy, R_∞, in dependence on the normalised T-stress, for example, where the T-stress was evaluated according to SHAM [SHA89] and SHERRY et al. [SHE95], see also **Table 3.3**. The T-stress scales with the specimen type, at least for Al 2024 T351, but no constraint effects of the specimen size, ligament length or relative crack length are captured.

The plastic constraint factor, Σ_Y, is defined as the ratio of the plastic limit load of a cracked specimen and a smooth specimen of same net section. For a tensile specimen of cross section Bb, the force in fully plastic condition is simply $F_0 = Bb\sigma_Y$ so that the plastic constraint factor of M(T) specimens is calculated from

$$\Sigma_{Y,MT} = \frac{F_Y}{F_0} = \frac{F_Y}{2\sigma_Y B(W-a_0)} = f_Y \,, \tag{3-1}$$

as in eq. (2-15). The bending moment in the fully plastic state of a bend bar is $M_0 = \frac{1}{4}Bb^2\sigma_Y$. We obtain for a C(T), where $M_Y = \frac{1}{2}F_Y(W+a_0)$,

$$\Sigma_{Y,CT} = \frac{M_Y}{M_0} = \frac{2F_Y(W+a_0)}{\sigma_Y B(W-a_0)^2} = 2\frac{(W+a_0)}{(W-a_0)^2} f_{Y,CT} \,, \tag{3-2}$$

and for a SE(B), where $M_Y = \frac{1}{4}F_Y S = F_Y W$,

$$\Sigma_{Y,SEB} = \frac{M_Y}{M_0} = \frac{F_Y S}{\sigma_Y B\left(W - a_0\right)^2} = \frac{4F_Y W}{\sigma_Y B\left(W - a_0\right)^2} = 4\frac{W}{\left(W - a_0\right)^2} f_{Y,SEB} \ . \qquad (3\text{-}3)$$

The plastic constraint factors of all specimens are summarised in **Table 3.3**. Fig. 3.19 shows the crack propagation energy, R_∞, in dependence on Σ_Y for the two aluminum alloys. R_∞, decreases with increasing plastic constraint, but the large scatter does not really allow for any quantitative relationships. The most important difference between Figs. 3.19 and 3.20 is that the ranking of C(T) and SE(B) changes.

Table 3.3: Constraint factors, T, Σ_y , f_y, and normalisations factor, eq. (2-14),
(a) ferritic steel 20 Mn Mo Ni 5 5

material	**20 Mn Mo Ni 5 5 - smooth specimens**				
designation	T / σ_∞ [-]	$\Sigma_{y\text{-}3D}$ [-]	$f_{y\text{-}3D}$ [-]	R_{ref} [N/mm]	$\overline{R}_\infty = \frac{R_\infty}{R_{ref}}$ [-]
RCTMDA1	8.391	1.177	0.142	2.677	449.42
RCTMDB20	8.519	1.326	0.158	2.938	474.79
RCTMDA7	8.262	1.094	0.134	5.112	424.98
RCTMDV	8.103	1.073	0.134	10.359	441.53
RDENTMB3	-1.383	1.060	1.06	19.489	89.51
RCCT5	-1.352	1.042	1.042	40.080	137.96
material	**20 Mn Mo Ni 5 5 - side grooved specimens**				
CTR141	8.701	1.472	0.172	1.571	517.30
CTR111	9.995	1.445	0.145	1.169	507.46
CRMDB19A	8.328	1.480	0.180	3.410	318.28
CTR1	8.396	1.474	0.178	3.360	329.72
CTR15BA9	8.605	1.474	0.174	3.210	190.64
CTRMDC2	8.301	1.480	0.181	6.862	293.20
CTR21	8.206	1.482	0.183	7.005	208.68
CTR12BA9	8.321	1.480	0.180	6.833	288.50
CTR4BA9	8.627	1.474	0.173	6.388	230.35
CTRMDE9	8.509	1.476	0.176	6.557	217.89
CTR1BA9	(14.77)	1.326	0.068	1.228	**1050.70**
CTRMDO2	8.106	1.484	0.185	14.31	210.52
CTR12	8.102	1.484	0.185	14.33	126.44
CTR7AA2	8.315	1.480	0.180	13.68	229.69
CTR1BA7	8.332	1.480	0.180	13.63	200.96

Table 3.3: Constraint factors, T, Σ_y , f_y, and normalisations factor, eq. (2-14), (b) aluminium alloys Al 2024-T351 and Al 2024-FC, smooth specimens

material	**Al 2024-T351**				
designation	T / σ_∞ [-]	$\Sigma_{y\text{-}3D}$ [-]	$f_{y\text{-}3D}$ [-]	R_{ref} [N/mm]	$\overline{R}_\infty = \frac{R_\infty}{R_{ref}}$ [-]
CT-50/0.5	5.57	1.104	0.183	6.46	27.0
CT-50/0.8	(14.65)[4]	1.065	0.056	0.75	**146.7**
CT-100/0.7	11.36	1.163	0.099	4.01	37.4
SEB-50/0.5	0.19	1.135	0.139	4.78	31.4
SEB-100/0.5	0.16	1.116	0.139	9.40	31.9
MT-50/0.5	-1.23	1.042	1.042	35.25	18.2
MT-100/0.5	-1.22	1.032	1.032	71.09	18,0
MT-100/0.7	(-1.69)	1.060	1.060	38.17	14.7
material	**Al 2024-FC**				
CT-50/0.5	5.74	1.104	0.179	0.328	386.6
CT-50/0.6	8.11	1.102	0.138	0.216	986.6
CT-50/0.7	11.36	1.087	0.092	0.105	**2191.4**
CT-100/0.3	1.27	1.053	0.284	1.538	188.6
CT-100/0.5	5.74	1.076	0.175	0.673	673.1
CT-100/0.7	11.04	1.062	0.094	0.221	**2321.3**
SEB-50/0.5	0.16	1.134	0.142	0.278	573.4
SEB-100/0.5	0.16	1.116	0.139	0.548	754.4
MT-50/0.5	-1.22	1.042	1.042	2.419	238.4
MT-50/0.7	-1.57	1.042	1.042	1.210	330.6
MT-100/0.2	-1.03	1.032	1.032	6.297	251.4
MT-100/0.5	-1.22	1.032	1.032	3.981	276.3
MT-100/0.7	(-1.57)	1.032	1.032	2.391	250.9

[4] outside range of definition

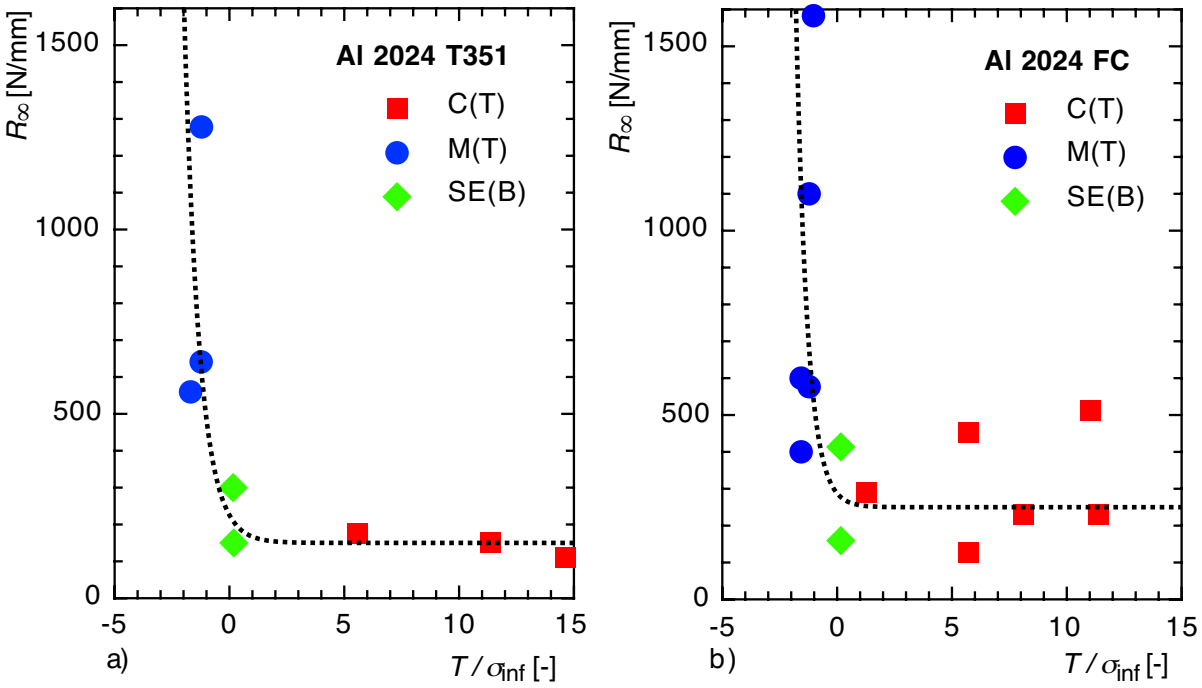

Fig. 3.18: Dependence of crack propagation energy, R_∞, on normalised T-stress;
a) Al 2024 T351, b) Al 2024 FC

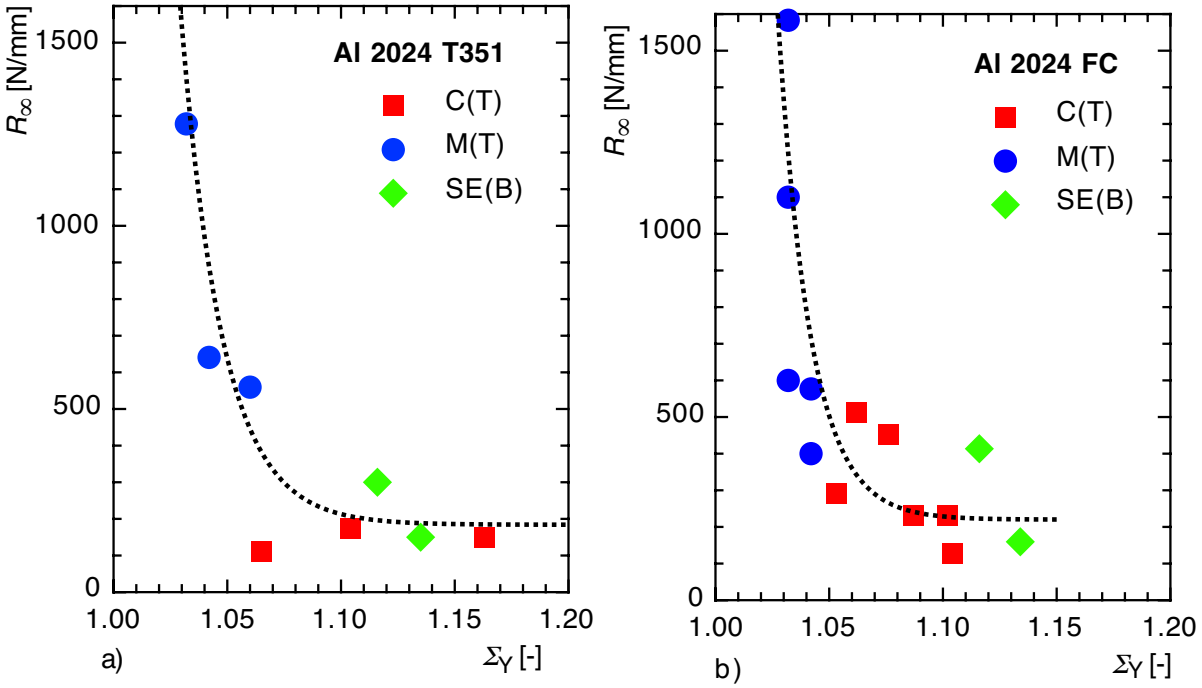

Fig. 3.19: Dependence of crack propagation energy, R_∞, on plastic constraint factor;
a) Al 2024 T351, b) Al 2024 FC

Finally, the normalisation of eqs. (2-13) and (2-14) is applied to all specimens, see Figs. 3.20 to 3.23. It affects the crack propagation energy, R_∞, only. The respective values of R_{ref} and $\overline{R}_\infty$ are also summarised in **Table 3.3**.

Some benefitial effects of this normalisation with respect to geometry independence are observed for the ferritic steel, 20 Mn Mo Ni 5 5, where crack initiation and propagation occurs under conditions of gross yielding, in particular for the larger C(T) specimens, W > 25 mm. Normalisation fails for the DE(T) and M(T) specimens withour side grooves, so that no transfer of J_R-curves from C(T) to other specimen geometries as in Fig. 2.8 is possible. No data of side-grooved M(T) specimens exist for this material. The small side-grroved C(T) specimens of $W = 25$mm (CTR141 and CTR111) and most notably the C(T) with the short ligament, $a_0/W = 0.8$, (CTR1BA9) fall out of the scatterband of the rest, see Fig. 3.21.

In the case of the aluminium alloys, where crack initiation and propagation occurs under conditions of small scale or contained yielding, normalisation appears to be helpful mainly for the M(T) specimens, see Figs. 3.22 and 3.23. Again, the C(T) specimens with a short ligament, $a_0/W = 0.7$, fall significantly out of the scatterband of the rest after normalisation. This indicates that the crack propagation energy does not scale with the plastic limit load for small relative ligament sizes, (W-a_0)/B.

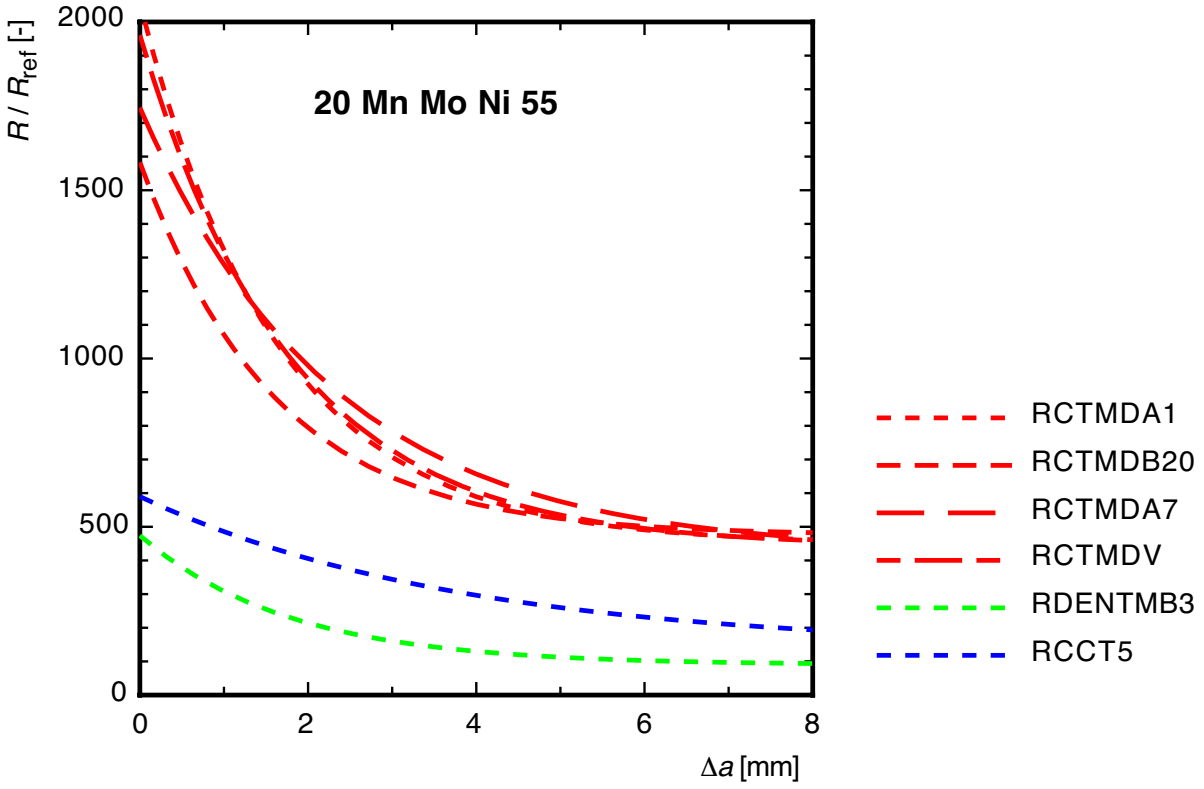

Fig. 3.20: Normalised dissipation rate, $\overline{R}(\Delta a)$, for 20 Mn Mo Ni 5 5, not side grooved

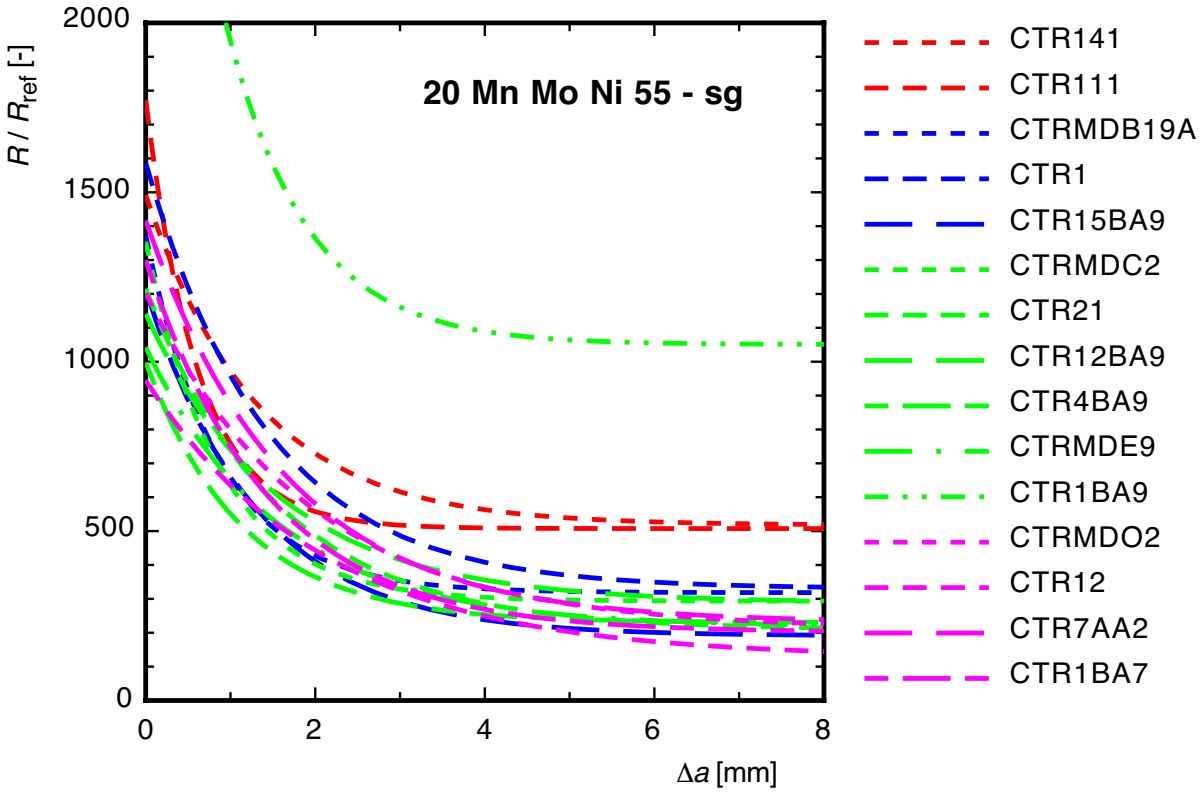

Fig. 3.21: Normalised dissipation rate, $\overline{R}(\Delta a)$, for 20 Mn Mo Ni 5 5, side grooved

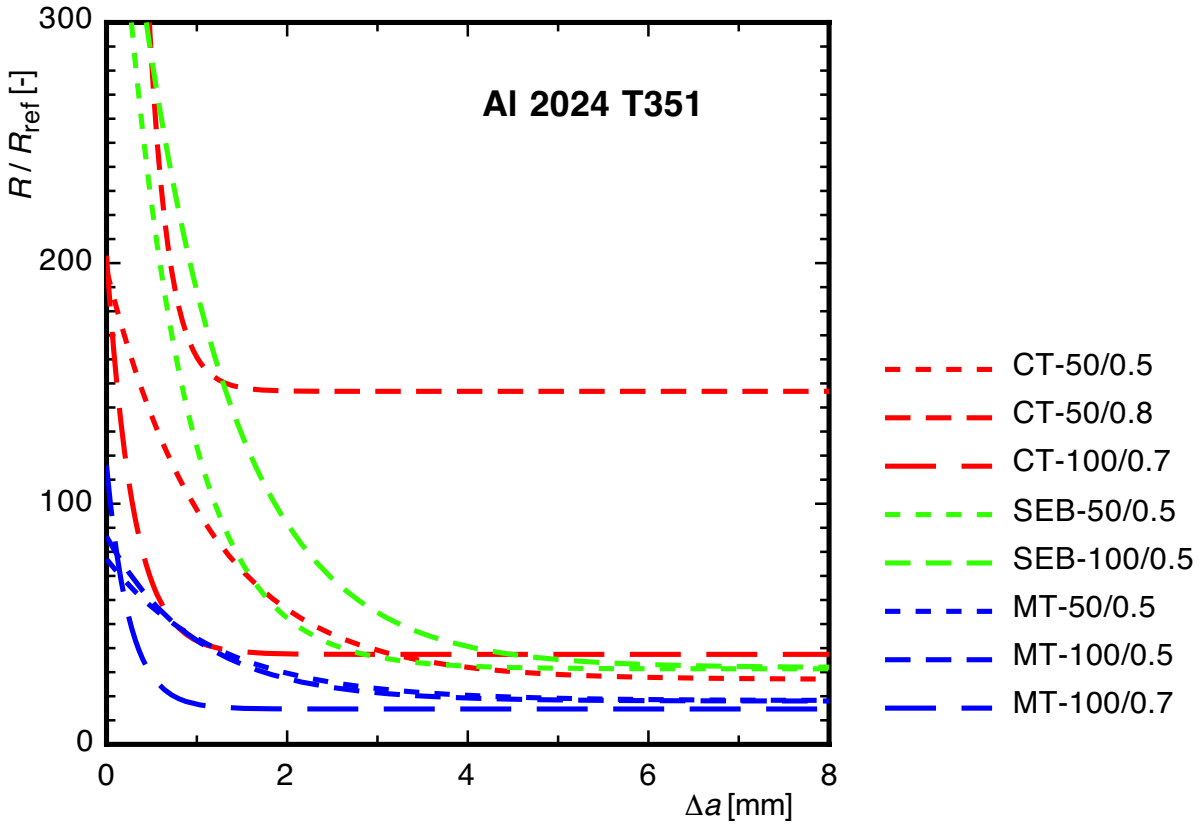

Fig. 3.22: Normalised dissipation rate, $\overline{R}(\Delta a)$, for Al 2024 T351

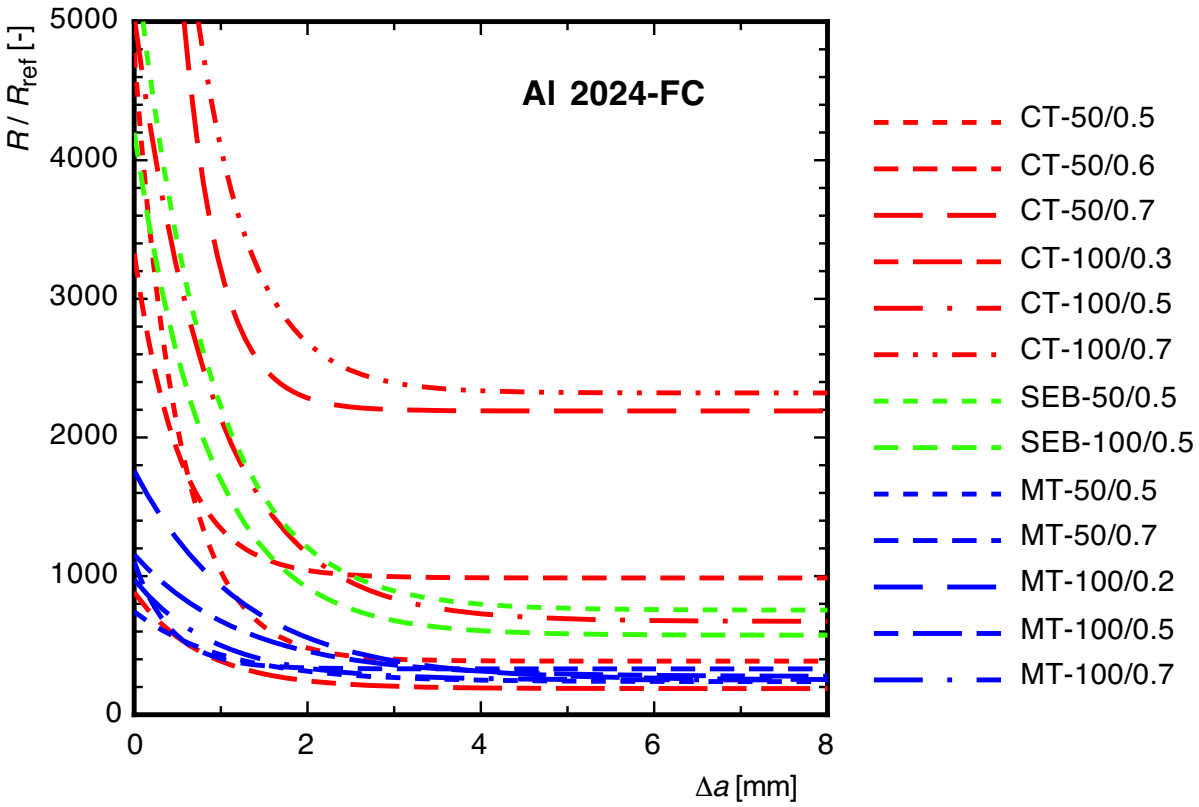

Fig. 3.23: Normalised dissipation rate, $\overline{R}(\Delta a)$, for Al 2024 FC

3.3 Prediction of R-curves

Only a limited number of R-curves are candidates for a successful transfer procedure as described in section 2.6, namely those which result in similar values of $\overline{R}_\infty$, see **Table 3.3** and Figs. 3.20 to 3.23. Two examples for 20 Mn Mo Ni 5 5 and Al 2024 FC are picked out for this study, see **Table 3.4**:

- The J_R-curve of specimen CTR15BA9 (W = 50mm), Fig. 3-24a, is taken to "predict" the R-curves of several larger C(T) specimens of the same relative crack length, a_0 / W. The crack propagation energy, R_∞^{pred}, is calculated according to eq. (2-21), α is taken from the reference specimen, see **Table 3.2a**., and λ is determined in dependence on (W-a_0) from Fig. 3.16b.
- The J_R-curve of specimen CT-100/0.3, Fig. 3-24b, is taken to "predict" the R-curves of several M(T) specimens. The crack propagation energy, R_∞^{pred} is calculated according to eq. (2-21) again, α is either (prediction #1) taken from the reference specimen, $\alpha = 6.5$, or (prediction #2) as an average value over the M(T) specimens, $\alpha = 3.9$, and $\lambda = 109.4$ is taken from the reference specimen, see **Table 3.2b**.

A comparison between R_∞ of the individual specimen and R_∞^{pred} gives a quantitative impression on the quality of the prediction.

Table 3.4: Geometry data and parameter data used for a prediction of R-curves

material	**20 Mn Mo Ni 5 5 - side grooved specimens**						
designation	W [mm]	B_n [mm]	a_0 / W [-]	R_∞ [N/mm]	R_{ref} [N/mm]	λ^{pred} [-]	R_∞^{pred} [N/mm]
CTR15BA9	50.	16.	0.62	612.	3.210	38.3	612.
CTR21	100.	8.	0.61	1462.	7.005	76.3	1336.
CTR4BA9	100.	40.	0.62	1471.	6.388	75.7	1218.
CTRMDE9	100.	40.	0.61	1429.	6.557	76.3	1250.
CTRMDO2	200.	4.	0.60	3014.	14.31	114.9	2728.
CTR7AA2	200.	16.	0.61	3142.	13.68	113.6	2608.
CTR1BA7	200.	40.	0.61	2740.	13.63	113.6	2599.
material	**Al 2024 FC**						
designation	W [mm]	$B = B_n$ [mm]	a_0 / W [-]	R_∞ [N/mm]	R_{ref} [N/mm]	R_∞^{pred} [N/mm]	
CT-100/0.3	100.	5.	0.30	290.1	1.538	290.1	
MT-50/0.5	50.	5.	0.50	400.0	2.419	456.3	
MT-100/0.2	100.	10.	0.20	1583.1	6.297	1187.8	
MT-100/0.5	100.	5.	0.50	1100.0	3.981	750.9	
MT-100/0.7	100.	5.	0.70	600.0	2.391	450.8	

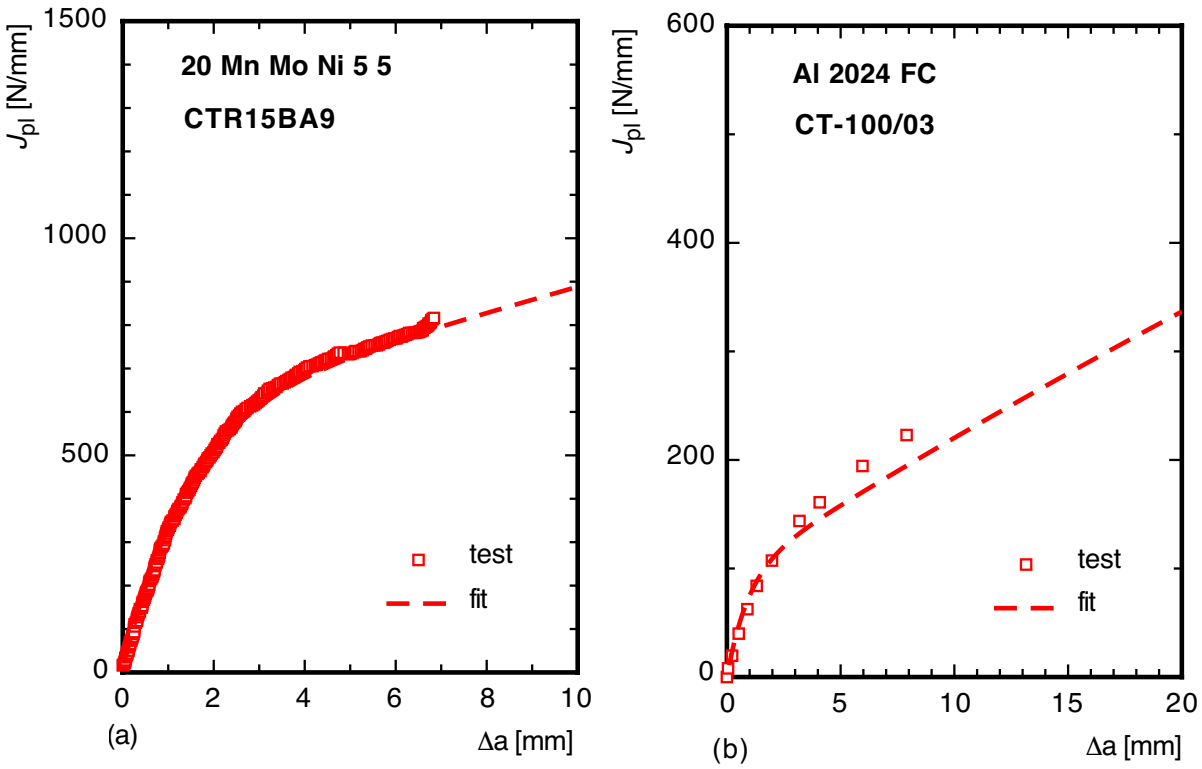

Fig. 3.25: Reference specimens for prediction of J_R-curves
a) 20 Mn Mo Ni 5 5 b) Al 2024 FC

The predicted J_R-curves are displayed in Figs. 3.25 and 3.26.

- The J_R-curves of the thin specimens CTR21 ($W = 100$mm, $B_n = 8$mm), CTRMDO2 ($W = 200$mm, $B_n = 4$mm), CTR7AA2 ($W = 200$mm, $B_n = 16$mm), are slightly underestimated, whereas The J_R-curves of the thicker specimens CTR4BA9 ($W = 100$mm, $B_n = 40$mm), CTRMDE9 ($W = 100$mm, $B_n = 40$mm),, and CTR1BA7 ($W = 200$mm, $B_n = 40$mm) are satisfactorily well predicted. As plane strain conditions have been assumed for all side-grooved specimens, the underestimation of the J_R-curves of the thin specimens could be expected. The respective normalisation has to account for the influence of the specimen thickness, obviously, as it does for the smooth specimens by eq. (2-21) and Fig. 2.6.

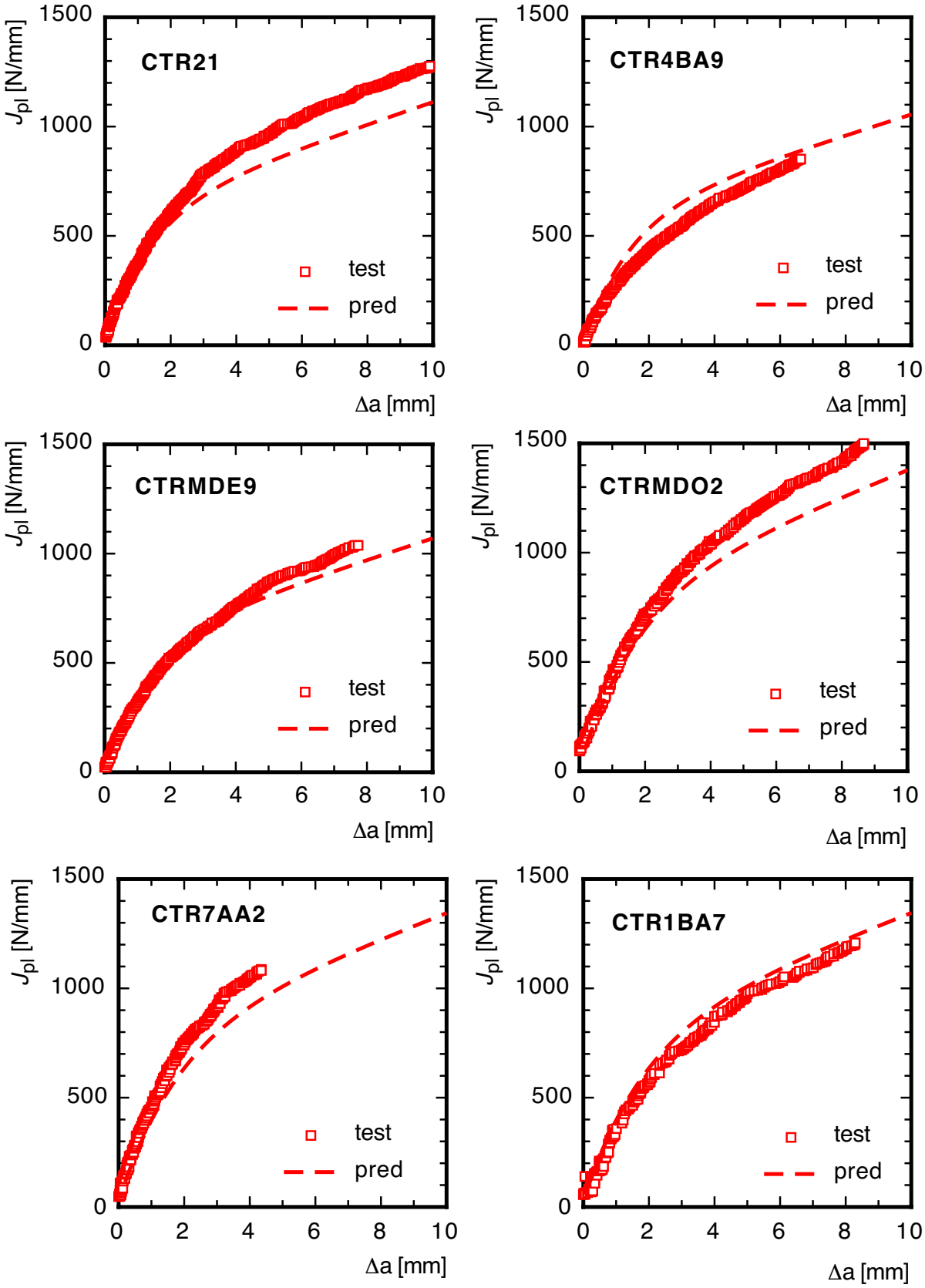

Fig. 3.26: Predicted J_R-curves for various C(T) specimens of material 20 Mn Mo Ni 5 5; $\alpha = 5.35$ from CTR15BA9, $\lambda(W\text{-}a_0)$ from Fig. 3-16b, R_∞^{pred} from eq. (2-21)

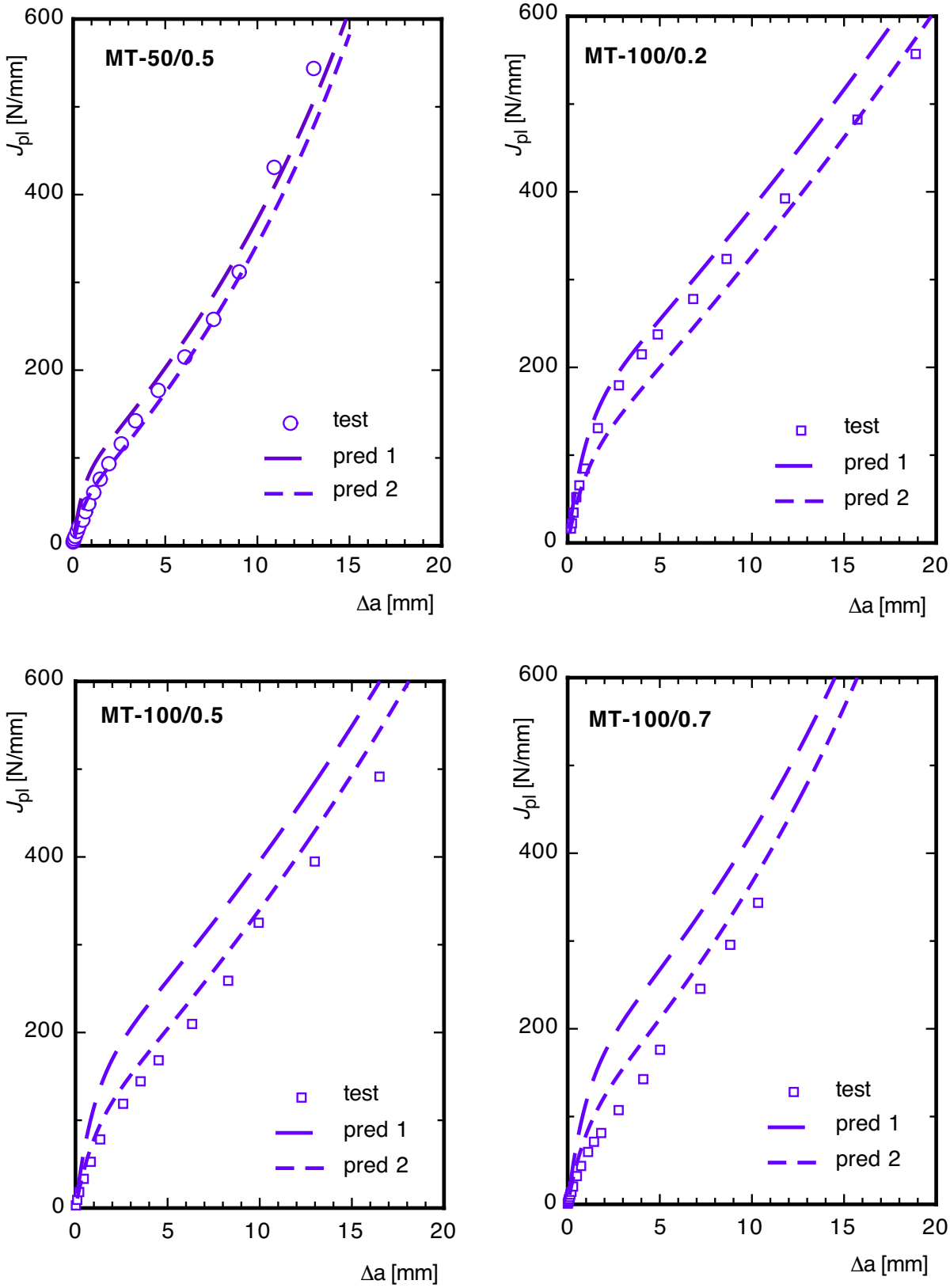

Fig. 3.26: Predicted J_R-curves for various M(T) specimens of material Al 2024 FC; $\alpha = 6.5$ (pred #1) from CT-100/0.3 or $\alpha = 3.9$ (pred #2) average of M(T) specimens, $\lambda = 109.4$ from CT-100/0.3, R_∞^{pred} from eq. (2-21)

- Realising the wide range of J-values, namely
  $J(\Delta a$=10mm) = 220N/mm for the reference C(T) specimen and
  $J(\Delta a$=10mm) = 370N/mm for the M(T)-50/0.5,
  the J_R-curves of the M(T) specimens are satisfactorily predicted. The α-value of the reference specimen CT-100/0.3, which defines the initial slope of the J_R-curves of the M(T) specimens, is rather high however, which results in a general overestimation of the J_R-curves of the M(T) specimens, especially for the MT-100/0.5 and MT-100/0.7. A better prediction is obtained with $\alpha = 3.9$, which is an average value over the M(T) specimens and similar to the respective average value over the C(T) specimens, $\alpha = 4.2$.

The "predictions" given in Figs. 3.25 and 3.26 are true predictions with respect to the stationary value, R_∞, only. Either λ or α , both representing the transition region of ductile tearing, required additional information from the $R(\Delta a)$-curves of other specimens. No phenomenological approach has yet been found to scale the transition behaviour of ductile tearing.

4. Summary and outlook

TURNER [TUR90] proposed the *energy dissipatuion rate*, R, as the "true driving force" for elasto-plastic fracture mechanics alternative to the J-integral, because it is consistent with incremental plasticity. This concept has been applied to a number of experimental J_R-curves, which have been determined at the GKSS research centre for ferritic steels and aluminium alloys.

The analysis of the numerous experimental data revealed, that all $R(\Delta a)$-curves could be characterised by three parameters, namely the initial value, $R_0 = R(\Delta a$=0*)*, the final stationary value or *crack propagation energy*, R_∞, and a characteristic relative transition length, $1/\lambda$. As semi-analytical expressions for $J_R(\Delta a)$-curves can be obtained from $R(\Delta a)$-curves by integration, these three parameters together with an integration constant, the initiation value, J_i, characterise ductile tearing resistance both quantitatively and physically interpretable. The geometry dependence of fracture resistance can hence be characterised quantitatively in terms of these parameters.

$J_R(\Delta a)$-curves obtained by integration of $R(\Delta a)$-curves illustrate, that the shape of cumulative J_R-curves is inherently geometry dependent and a power-law curve fit as, e.g., in [ASTM1820] is not physically based. The crack propagation energy, R_∞, in particular, allows for a physically based extrapolation beyond the measured range of Δa and also beyond the common "validity limits" of J_R-curves.

Geometry functions derived from plastic limit load expressions have been defined for normalisation of $R(\Delta a)$-curves, which covered some of the geometry effects, primarily for

materials of low strength but high toughness. As the dissipation rate includes both, the rate of global plastic strain energy, $\dot{U}_{pl}$, and the rate of local work of separation in the process zone, $\dot{U}_{sep}$, a normalisation by a limit load factor will be most successful, if the plastic work dissipated in the far field of the specimen or component per crack-extension increment is much greater that the local energy release rate at the crack tip. This could be verified by numerical simulations of ductile crack extension with a process zone model based on the concept of BARENBLATT, which allows for a splitting of global and local contributions to the energy dissipation rate.

The normalisation by a limit load factor affects the whole $R(\Delta a)$-curve in the same way and, hence, scales the steady-state value, R_∞, only. No phenomenological approach has yet been found to scale the transition behaviour of ductile tearing characterised by the initial value, R_0, and the transition length, $1/\lambda$..

The problem of geometry dependence of R-curves, which is crucial for fracture mechanics assessments of components, has been discussed intensively since decades, and the number of experimentally determined J_R-curves as well as the number of recognised "constraint effects" has ever increased. A convincing and physically based solution has never been found, however. The concept of the dissipation rate does not give a final answer either, but it provides some approaches to a better physical understanding, what J_R-curves actually are, how they can be characterised and parametrised, which are the reasons for "geometry effects" and how the latter can be quantified under certain conditions. If other existing $J_R(\Delta a)$-data would be re-analysed according to this concept, this might finally lead to a systematic and quantitative treatment of geometry effects resulting in an engineering concept of fracture mechanics assessment for components.

5. References

[ASTM1737] ASTM E 1737-96: "Standard test method for J-integral characterization of fracture toughness", Annual Book of ASTM Standards, Vol. 03.01, American Society for Testing and Materials, West Conshohocken (1998).

[ASTM1820] ASTM E 1820-01: "Standard test method for measurement of fracture toughness", Annual Book of ASTM Standards, Vol. 03.01, American Society for Testing and Materials, West Conshohocken (2002).

[AUR90] AURICH, D. et al.: "Analyse und Weiterentwicklung bruchmechanischer Versagenskonzepte", Forschungsbericht 174, Bundesanstalt für Materialforschung und -prüfung, Berlin, 1990.

[BAR62] BARENBLATT, G.I.: "The mathematical theory of equilibrium cracks in brittle fracture", Advances in Applied Mechanics 7 (1962), 55-129.

[BRO89] BROCKS, W., KÜNECKE, G., NOACK, H.-D., and VEITH, H.: "On the transferability of fracture mechanics parameters to structures unisng FEM", Nucl. Engng. and Design 112 (1989), 1-14.

[BRO92] BROCKS, W.: "Die Dissipationsrate als Rißwiderstand", Materialprüfung 34 (1992), 350-353.

[BRO95] BROCKS, W., and SCHMITT:, W.: "The second parameter in J-R curves: constraint or triaxiality?", 2nd Symp. Constraint Effects, ASTM STP 1224 (M. KIRK und A. BAKKER, edts.), Philadelphia, 1995, 209-231.

[BRO98] Brocks, W.: "Charakterisierung des Rißwiderstandes mit Hilfe der Energiedissipationsrate: Einflüsse von Material, Probenform und -größe", Technical Note GKSS/WMG/98/6, GKSS Research Centre, Geesthacht, 1998.

[BRO00] BROCKS, W., SIEGMUND, TH.: "Effects of geometry and material on the energy dissipation rate", Fracture Mechanics: Application and Challenges, Proc. ECF 13, 6-9 September 2000, San Sebastian.

[EWI72] EWING, D.J.F., and RICHARDS, C.E.: "The yield-point loads of single notched pin-loaded tensile strips, J. Mech. Phys. Solids 22 (1974), 27-36.

[GAR75] GARWOOD, S.J., ROBINSON, J.N. and TURNER, C.E.: "The measurement of crack growth resistance curves using the J-integral", Int. J. of Fracture 11 (1975), 528-530.

[GAR79] GARWOOD, S.J.: "Effect of specimen geometry on crack growth resistance", ASTM STP 677, American Society for Testing and Materials, 1979, 511-532.

[GRI20] GRIFFITH, A.A.: "The phenomena of rupture and flow in solids", Phil. Trans. Roy. Soc. London A211 (1920), 163-198.

[GUR77] GURSON, A. L.: "Continuum theorie of ductile rupture by void nucleation and growth: Part I - yield criteria and flow rules for pourous ductile media", J. Eng. Mater. Tech. 99 (1977), 2-15.

[KAC71] KACHANOV, L.M.: "Fundamentals of the Theory of Plasticity", North-Holland Publication Company (1971).

[KIM96] KIM, Y.-J., MCCLINTOCK, F.A., and PARKS, D.M.: "Yield locus in deep, single face cracked specimens under combined bending and tension, J. Appl. Mech. 63 (1996), 1045-1046.

[KLE86] KLEMM, W., and KALTHOFF, J.F.: "Beschreibung des Werkstoffverhaltens bei schneller Rißausbreitung in Rohrleitungsstählen mit einem neu festgelegten Kennwert", Berichtsband der 18. Vortragsveranstaltung des DVM-Arbeitskreises Bruchvorgänge, Deutscher Verband für Materialforschung and -prüfung, Berlin, 1986, 191-203

[KOL93] KOLEDNIK, O.: "A simple model to explain the geometry dependence of J-Δa-curves", Int. J. Fracture 63 (1993), 263-274.

[KOL97] KOLEDNIK, O., SHAN, G., and FISCHER, F.D.: "The energy dissipation rate - a new tool to interpret geometry and size effects", Fatigue and Fracture Mechanics: 27th Vol, ASTM STP 1296 (R.S. PIASCIK. J.C. NEWMAN, and N.E. DOWLING, Edts.), American Society for Testing and Materials, Philadelphia 1997, 126-151

[LEE82] LEEVERS, P.S., and RADON, J.C.: "Inherent stress biaxiality in various fracture specimen geometries", Int. J. of Fracture 19 (1982), 311-325.

[LIN91] LINK, R.E., LANDES, J.D., HERRERA, R. and ZHOU, Z.: "Something new in size and geometry effects for J-R curves", Defect assessment in Components, Fundamentals and Applications (Edts. J.G. BLAUEL, and K.-H. SCHWALBE), ESIS/EGF 9, Mechanical Engineering Publications, London, 1991, 707-721.

[LIN97] LIN, G., KIM, Y.-J., and CORNEC, A.: "Fracture toughness of a constrained metal layer", Computational Materials Science (1997), 36-47.

[MEM92] MEMHARD, D., and KLEMM, W.: "Zusammenhang zwischen Rißlaufenergie and J-Rißwiderstandskurven", Berichtsband der 24. Sitzung des DVM-Arbeitskreises Bruchvorgänge, Deutscher Verband für Materialforschung and -prüfung, Berlin, 1992, 291-302.

[MEM93] MEMHARD, D., BROCKS, W., and FRICKE, S.: "Characterization of ductile tearing resistance by energy dissipation rate", Fatigue Fract. Engng. Mater. Struct. 16 (1993), 1109-1124.

[MEM94] MEMHARD, D., BROCKS, W., and FRICKE, S.: "Characterization of ductile tearing resistance by energy dissipation rate", Structural Integrity: Experiments - Models - Applications (Hrsg. K.-H. Schwalbe and C. Berger), Vol. I, Proc. ECF 10, Engineering Materials Advisory Services Ltd., Warley, 1994, 149-158.

[MIL88] MILLER, A.G.: "Review of limit loads of structures containing defects", Int. J. Pres. Ves. & Piping 32 (1988), 197-327.

[NEE87] NEEDLEMAN, A., and TVERGAARD, V.: "An analysis of ductile rupture at a crack tip", J. Mech. Phys. Solids 35 (1987), 151-183.

[NEE90] NEEDLEMAN, A.: "An analysis of decohesion along an imperfect interface", Int. J. Fracture 42 (1990), 21-40.

[ODO91] O'DOWD, N.P., and SHIH, C.F.: "Family of crack-tip fields characterized by a triaxiality parameter", J. Mech. Phys. Solids 39 (1991), 989-1015.

[RIC74] RICE, J.R.: "Limitations of small scale yielding approximations for crack tip plasticity", J. Mech. Phys. Solids 22 (1974), 17-26

[SCH84] SCHWALBE, K.-H., and HELLMANN, D.: "Correlation of stable crack growth with the *J*-integral and the crack tip opening displacement, effects of geometry, size, and material", Report GKSS 84/E/37, GKSS Research Centre Geesthacht, 1984.

[SCH98] SCHWALBE, K.-H., et al.: "EFAM ETM 97 - the ETM method for assessing the significance of crack like defects in engineering structures", Report GKSS 98/E/6, GKSS Research Centre Geesthacht, 1998.

[SHA89] SHAM, T.-L.: "The determination of the elastic *T*-term using higher order weight functions", Int. J. Fracture 84 (1989), 81-102.

[SHE95] SHERRY, A.H., FRANCE, C.C., and GOLDTHORPE, M.R.: "Compendium of *T*-stress solutions for two and three dimensional cracked geometries", Fatigue Fract. Engng. Mater. Struct. 18 (1995), 141-155.

[SHI91] SHIH, C.F., O'DOWD, N.P., and KIRK, M.T.: "A framework for quantifying crack tip constraint to surface flaws", ASTM-Symposium on Constraint Effects in Fracture, Indianapolis, 1991, ASTM STP ??.

[SIE98] SIEGMUND, Th., BERNAUER, G., and BROCKS, W.: "Two models of ductile fracture in contest: porous metal plasticity and cohesive elements", Proc. ECF 12, Sheffield, 14.-18. Sept. 1998, Fracture from Defects (Edts. M.W. BROWN, E.R. DE LOS RIOS, K.J. MILLER), Vol. II, Engineering Materials Advisory Services Ltd, 1998, 933-938.

[SIE99] SIEGMUND, TH., and BROCKS, W.: "Prediction of the work of separation and implications to modeling", Int. J. Fracture 99 (1999), 97-116.

[SIE00a] SIEGMUND, TH., and BROCKS, W.: "The role of cohesive strength and separation energy for modeling of ductile fracture", Fatigue and Fracture Mechanics: 30th Vol, ASTM STP 1360 (Edts. K.L. JERINA and P.C. PARIS), American Society for Testing and Materials, 2000, 139-151.

[SIE00b] SIEGMUND, TH., and BROCKS, W.: "A numerical study on the correlation between the work of separation and the dissipation rate in ductile fracture", Engineering Fracture Mechanics 67 (2000), 139-154.

[SIE00c] SIEGMUND, TH., and BROCKS, W.: "Modeling crack growth in thin sheet aluminum alloys", Fatigue and Fracture Mechanics: 31st Vol, ASTM STP 1389 (Edts. G.L. HALFORD and J.P. GALLAGHER), American Society for Testing and Materials, 2000, 475-485.

[SIG83] SIEGELE, D. and SCHMITT, W.: "Determination and simulation of stable crack growth in ADINA", Computers & Structures 17 (1983), 697-703.

[STA00] STAMPFL, J., and KOLEDNIK, O.: "The separation of the fracture energy in metallic materials", Int. J. Fracture 101 (2000), 321-345.

[SUM99] SUMPTER, J.D.G.: "An alternative view of R-curve testing", Engineering Fracture Mechanics 64 (1999), 161-176.

[TUR90] TURNER, C. E.: "A re-assessment of ductile tearing resistance (Part I and II)",. Fracture Behaviour and Design of Materials and Structures (edt. D. FIRRAO), Vol. II, Proc. ECF 8, 1990, 933-949 and 951-968.

[TUR94a] TURNER, C. E., and KOLEDNIK, O.: "Application of energy dissipation rate arguments to stable crack growth", Fatigue and Fracture of Engineering Materials and Structures 20 (1994), 1109-1127.

[TUR94b] TURNER, C. E., and KOLEDNIK, O.: "Simple test method for energy dissipation rate, CTOA and the study of size and transferability effects for large amounts of ductile crack growth", Fatigue and Fracture of Engineering Materials and Structures 20 (1994), 1507-1528.

[TUR97] TURNER, C. E., and KOLEDNIK, O.: "A micro and macro approach to the energy dissipation rate model of stable ductile crack growth", Fatigue and Fracture of Engineering Materials and Structures 17 (1994), 1089-1107.

[TVE82] TVERGAARD, V.: "Ductile fracture by cavity nucleation between larger voids", J. Mech. Phys. Solids 30 (1982).

[WU88] WU, S.X., MAI, Y.W., and COTTERELL, B.: "Slip line field solutions for three-point notch bend specimens", Int. J. Fract. 37 (1988), 13-29.

[XIA95] XIA, L., SHIH, C.F., and HUTCHINSON, J.W.: "A computational approach to ductile crack growth under large scale yielding", J. Mech. Phys. Solids 43 (1995), 389-413.

[YUA96] Yuan, H., Lin, G., and Cornec, A.: "Verification of a cohesive zone model for ductile fracture", J. Mech. Phys. Solids 42 (1994), 1397-1434.

Appendix

A1. Re-evaluation of $R(\Delta a)$ curves from J_R-curves

Resistance curves for the dissipation rate can be re-evaluted from J_R-curves measured on laboratory specimens [MEM92, BRO92]. The respective formula just inverts the procedure of calculating J from test data. If any other than the standard formulas have been applied for the J-evaluation, the re-evaluation of $R(\Delta a)$ has to refer to the respective equation.

A1.1. Bend type specimens, C(T) and SE(B)

The value $J_{(i)}$ at a point corresponding to $a_{(i)}$, $v_{(i)}$, $F_{(i)}$ on the specímen load versus load-line displacement record is calculated from [ASTM1737, ASTM1820]

$$J_{(i)} = J_{\mathrm{el}(i)} + J_{\mathrm{pl}(i)}, \tag{A1-1}$$

where the elastic part, $J_{\mathrm{el}(i)}$, results from the relation to the stress intensity factor

$$J_{\mathrm{el}(i)} = \frac{K_{(i)}^2}{E'} \quad \text{with } K_{(i)} = \frac{F_{(i)}}{\sqrt{\left(BB_{\mathrm{n}}W\right)}} f\left(\frac{a_{(i)}}{W}\right), \tag{A1-2a}$$

and $$E' = \begin{cases} \dfrac{E}{\left(1-\nu^2\right)} & \text{for plane strain} \\ E & \text{for plane stress} \end{cases} .. \tag{A1-2b}$$

B_{n} is the net section thickness for side grooved specimens, with $B_{\mathrm{n}} = B$ for specimens without side grooves. The plastic part, $J_{\mathrm{pl}(i)}$, is determined from the area under the load versus plastic load-line displacement record,

$$J_{\mathrm{pl}(i)} = \left[J_{\mathrm{pl}(i-1)} + \left(\frac{\eta_{(i-1)}}{W - a_{(i-1)}}\right)\frac{A_{\mathrm{pl}(i)} - A_{\mathrm{pl}(i-1)}}{B_{\mathrm{n}}}\right]\left[1 - \gamma_{(i-1)}\frac{a_{(i)} - a_{(i-1)}}{W - a_{(i-1)}}\right]. \tag{A1-3}$$

The geometry factors are

$$\eta = \begin{cases} 2.0 + 0.522\left(1 - a/W\right) & \text{for C(T)} \\ 2.0 & \text{for SE(B)} \end{cases} \tag{A1-4a}$$

$$\gamma = \begin{cases} 1.0 + 0.76\left(1 - a/W\right) & \text{for C(T)} \\ 1.0 & \text{for SE(B)} \end{cases} \tag{A1-4b}$$

The increment of area, $\Delta A_{\mathrm{pl}} = A_{\mathrm{pl}(i)} - A_{\mathrm{pl}(i-1)}$, for a crack growth increment, $\Delta a = a_{(i)} - a_{(i-1)}$, between lines of constant plastic displacement is

$$\Delta A_{\mathrm{pl}} = A_{\mathrm{pl}(i)} - A_{\mathrm{pl}(i-1)} = \tfrac{1}{2}\left(F_{(i)} + F_{(i-1)}\right)\left(v_{\mathrm{pl}(i)} - v_{\mathrm{pl}(i-1)}\right) = \tfrac{1}{2}\left(F_{(i)} + F_{(i-1)}\right)\Delta v_{\mathrm{pl}}\,. \qquad \text{(A1-5)}$$

Rearranging the formula for J_{pl} yields

$$\left(\frac{F_{(i)} + F_{(i-1)}}{2B_N}\right)\left(\frac{\Delta v_{\mathrm{pl}}}{\Delta a}\right)\left(1 - \gamma_{(i-1)}\frac{\Delta a}{W - a_{(i-1)}}\right) = \left(\frac{W - a_{(i-1)}}{\eta_{(i-1)}}\right)\frac{\Delta J_{\mathrm{pl}}}{\Delta a} + J_{\mathrm{pl}(i-1)}\frac{\gamma_{(i-1)}}{\eta_{(i-1)}}, \qquad \text{(A1-6)}$$

from wich the dissipation rate is obtained according to eq. (2-1) for $\Delta a \to 0$, i.e. $(i\text{-}1) \to i$,

$$R = \lim_{\Delta a \to 0}\frac{\Delta U_{\mathrm{dis}}}{B_{\mathrm{n}}\Delta a} = \lim_{\Delta a \to 0}\frac{F\Delta v_{\mathrm{pl}}}{B_{\mathrm{n}}\Delta a}, \qquad \text{(A1-7)}$$

as

$$\boxed{R = \left(\frac{W - a}{\eta}\right)\frac{\mathrm{d}J_{\mathrm{pl}}}{\mathrm{d}a} + J_{\mathrm{pl}}\frac{\gamma}{\eta}}. \qquad \text{(A1-8)}$$

A1.2. Tensile-type specimens, M(T) and DE(T)

The value $J_{(i)}$ at a point corresponding to $a_{(i)}$, $v_{(i)}$, $F_{(i)}$ on the specímen load versus elongation record is calculated from [GAR75, SCH84]

$$J_{(i)} = J_{(i-1)} + \frac{2\Delta U^*}{B_{\mathrm{n}}\left(2W - a_{i-1} - a_i\right)} + \frac{2\left[K_{(i)}^2\left(W - a_i\right) + K_{(i-1)}^2\left(W - a_{i-1}\right)\right]}{E'\left(2W - a_{i-1} - a_i\right)}. \qquad \text{(A1-9)}$$

where the increment ΔU^* for a crack growth increment, $\Delta a = a_{(i)} - a_{(i-1)}$, is determined from the area under the load versus load-line displacement record,

$$\Delta U^* = \int_{v_{(i-1)}}^{v_{(i)}} F\,\mathrm{d}v - \tfrac{1}{2}F_{(i)}\left(v_{(i)} - v_{(i-1)}\right). \qquad \text{(A1-10)}$$

The dissipation rate is again obtained according to eq. (2-1) for $\Delta a \to 0$, i.e. $(i\text{-}1) \to i$,

$$R = \lim_{\Delta a \to 0}\frac{\Delta U_{\mathrm{dis}}}{B_{\mathrm{n}}\Delta a} = \lim_{\Delta a \to 0}\frac{F\Delta v_{\mathrm{pl}}}{B_{\mathrm{n}}\Delta a}, \qquad \text{(A1-11)}$$

with $J_{\mathrm{pl}} = J - J_{\mathrm{el}} = J - \dfrac{K^2}{E'}$ as

$$\boxed{R = \left(W - a\right)\frac{\mathrm{d}J_{\mathrm{pl}}}{\mathrm{d}a}}. \qquad \text{(A1-12)}$$

A2. Numerical differentiation and curve fitting

If the J_R-curves have to be converted into $R(\Delta a)$ curves differentiation is necessary, eqs. (A1-8) and (A1-12). Numerical differentiation is delicate as it is sensitive to oscillations of data, especially, if the data result from experimental records. A specific logarithmic bevelling procedure for precursory smoothing and following differention has been applied for the JR-curves.

As $\ln(x)$ goes to minus infinity for $x \to 0$, a positive constant, c_0, has to be added to the Δa values before taking the logarithm. The logarithmic J_R-curve, $\ln[J(\Delta a+c_0)]$, is then approximated by a linear function, $y = c_1 x + c_2$, by minimising the square of errors. If the the global shape of the curve after re-transformation, i.e. taking $\exp(y)$ and subtracting the added constant, $\Delta a = x - c_0$, coincides satisfactorily with the measured J_R-curve, the fit is proper, see Fig. A2-1a, where the number of test points is ten times larger than displayed in the diagramme. In some cases, the global fit can be improved by changing the value of c_0, which defines the initial point of the osculating curve or bevel used as some kind of carpenter's ruler in the following. The dissipation rate can be calculated according to eq (A1-8) with the derivative of the global fit curve, see Fig. A2-1b.

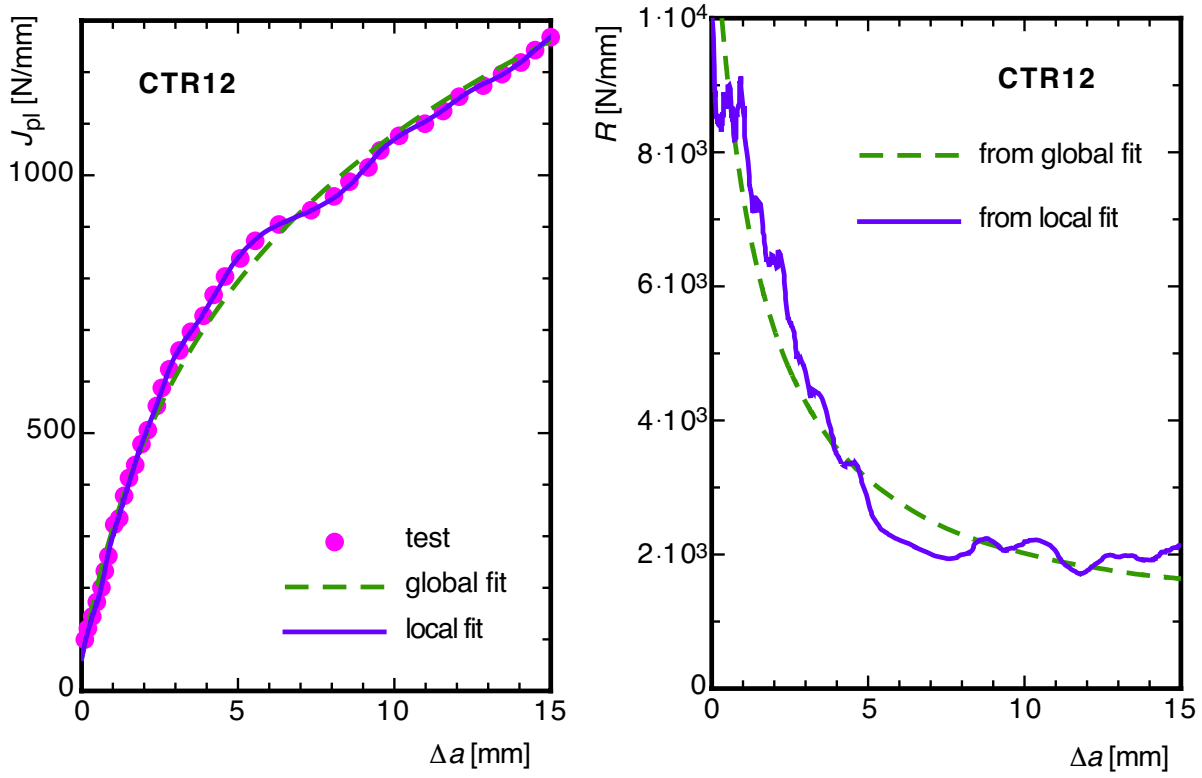

Fig. A2.1: Numerical curve fitting and differentiation (specimen CTR12);
a) J_R-curve b) dissipation rate

Now, a local "n-point bevel" is conducted over the N test points of the J_R-curve by calculating the fit parameters over n data points, $n << N$, starting with the first (global) test point, $j = 1$, and taking the first point, $i = 1$, and the corresponding slope of the local fit as the respective values for the global curve. The bevel is then shifted to the second data point, $j = 2$, and the procedure is repeated until the whole test curve has been passed through, i.e. $j = N - n$, see Fig. A2-1a, The missing data points, $N - n < j \leq N$ can be calculated by starting from the end of the curve. The value n of the "n-point bevel" depends on the specific shape of the curve, the density of data points and their distance, respectively. It is, hence, a second parameter determining the quality of the derivative of the J_R-curve. The dissipation rate is again calculated according to eq (A1-8) with the derivative of the local fit curve, see Fig. A2-1b.

A3. Integration of $R(\Delta a)$ curves

The differential equations (2-2) and. (2-5) for bend- or tensile-type specimens, respectively, can be integrated for a given $R(\Delta a)$ curve to obtain a J_R-curve [MEM93]. By introducing the normalised quantities

$$x = \frac{a}{W} = \frac{a_0}{W} + \frac{\Delta a}{W} = x_0 + \frac{\Delta a}{W} \quad , \quad y = \frac{J_{\mathrm{pl}}}{R_\infty} \quad , \quad r = \frac{R}{R_\infty}, \tag{A3-1}$$

and the abbreviations

$$\left.\begin{aligned} p(x) &= \frac{\gamma(x)}{1-x} \quad , \quad q_{\mathrm{B}}(x) = \frac{\eta(x) r(x)}{1-x} \quad , \quad q_{\mathrm{T}}(x) = \frac{r(x)}{1-x} \\ \eta(x) &= 2 + \eta_1 (1-x) \quad , \quad \gamma(x) = 1 + \gamma_1 (1-x) \end{aligned}\right\}, \tag{A3-2}$$

the differential equations take the simple forms

$$\left.\begin{aligned} y' + p(x) y &= q_{\mathrm{B}}(x) \quad \text{for C(T) and SE(B)} \\ y' &= q_{\mathrm{T}}(x) \quad \text{for M(T) and DE(T)} \end{aligned}\right\} \tag{A3-3}$$

with the general solutions

$$\left.\begin{aligned} y &= \mathrm{e}^{-\int p(x)\mathrm{d}x} \left[\int q_{\mathrm{B}}(x) \mathrm{e}^{\int p(x)\mathrm{d}x}\, \mathrm{d}x + y_0 \right] \quad \text{for C(T) and SE(B)} \\ y &= \int q_{\mathrm{T}}(x) \mathrm{d}x + y_0 \quad \text{for M(T) and DE(T)} \end{aligned}\right\} \tag{A3-4}$$

For arbitrary $r(x)$, the integration has to be performed numerically. The integration constant

$$y_0 = \frac{J_0^{\mathrm{pl}}}{R_\infty} = y(x_0) \tag{A3-5}$$

is determined from the initial condition at physical or technical crack growth initiation, $J_0^{\mathrm{pl}} = J_{\mathrm{i}}^{\mathrm{pl}}$ at $\Delta a = 0$ or $J_0^{\mathrm{pl}} = J_{0.2}^{\mathrm{pl}}$ at $\Delta a = 0.2$ mm, respectively.

The function $J_{pl}(\Delta a)$ now depends on the right hand sides of eqs. (A3-3), i.e. the function *R(Δa)*. The simplest case is **pure stationary crack growth**, i.e. a *constant release rate*,

$$\boxed{r(x) = R/R_\infty = 1}.$$

The respective solutions are

- a logarithmic function for an **M(T)** specimen

$$\boxed{y = y_0 + \int_{x_0}^{x} \frac{r}{1-\xi}\,\mathrm{d}\xi = y_0 + \ln\left(\frac{1-x_0}{1-x}\right)},, \qquad \text{(A3-6)}$$

- a straight line for an **SE(B)** specimen,

$$y = \exp\left(-\int_{x_0}^{x} \frac{\gamma}{1-\xi}\,\mathrm{d}\xi\right)\left[\int_{x_0}^{x} \frac{\eta}{1-\xi}\exp\left(\int_{x_0}^{\xi} \frac{\gamma}{1-\zeta}\,\mathrm{d}\zeta\right)\mathrm{d}\xi + y_0\right]$$

$$= \frac{1-x}{1-x_0}\left[\int_{x_0}^{x} \frac{2(1-x_0)}{(1-\xi)^2}\,\mathrm{d}\xi + y_0\right] = \frac{1-x}{1-x_0}\left(2(1-x_0)\left[\frac{1}{1-\xi}\right]_{x_0}^{x} + y_0\right)$$

$$\boxed{y = y_0\frac{1-x}{1-x_0} + 2\frac{x-x_0}{1-x_0}},, \qquad \text{(A3-7)}$$

- and a sum of exponential functions for a **C(T)** specimen

$$y = \exp\left(-\int_{x_0}^{x} \frac{\gamma(\xi)}{1-\xi}\,\mathrm{d}\xi\right)\left[\int_{x_0}^{x} \frac{\eta(\xi)}{1-\xi}\exp\left(\int_{x_0}^{\xi} \frac{\gamma(\zeta)}{1-\zeta}\,\mathrm{d}\zeta\right)\mathrm{d}\xi + y_0\right]$$

$$\int_{x_0}^{x} \frac{\gamma(\xi)}{1-\xi}\,\mathrm{d}\xi = \ln\left(\frac{1-x_0}{1-x}\right) + \gamma_1(x-x_0)$$

$$\exp\left(-\int_{x_0}^{x} \frac{\gamma(\xi)}{1-\xi}\,\mathrm{d}\xi\right) = \left(\frac{1-x}{1-x_0}\right)\mathrm{e}^{-\gamma_1(x-x_0)}$$

$$\exp\left(\int_{x_0}^{\xi} \frac{\gamma(\zeta)}{1-\zeta}\,\mathrm{d}\zeta\right) = \left(\frac{1-x_0}{1-\xi}\right)\mathrm{e}^{\gamma_1(\xi-x_0)}$$

$$\int_{x_0}^{x} \frac{\eta(\xi)}{1-\xi}\exp\left(\int_{x_0}^{\xi} \frac{\gamma(\zeta)}{1-\zeta}\,\mathrm{d}\zeta\right)\mathrm{d}\xi = 2(1-x_0)\int_{x_0}^{x} \frac{\mathrm{e}^{\gamma_1(\xi-x_0)}}{(1-\xi)^2}\,\mathrm{d}\xi + \eta_1(1-x_0)\int_{x_0}^{x} \frac{\mathrm{e}^{\gamma_1(\xi-x_0)}}{1-\xi}\,\mathrm{d}\xi$$

$$\int_{x_0}^{x} \frac{\mathrm{e}^{\gamma_1(\xi-x_0)}}{(1-\xi)^2}\,\mathrm{d}\xi = \mathrm{e}^{-\gamma_1 x_0}\left\{\left[\frac{\mathrm{e}^{\gamma_1\xi}}{1-\xi}\right]_{x_0}^{x} - \gamma_1\int_{x_0}^{x} \frac{\mathrm{e}^{\gamma_1\xi}}{1-\xi}\,\mathrm{d}\xi\right\} \qquad \text{(by partial integration)}$$

$$\boxed{y = \frac{1-x}{1-x_0}\mathrm{e}^{-\gamma_1(x-x_0)}\left[\left(\frac{2(1-x_0)\,\mathrm{e}^{\gamma_1(x-x_0)}}{1-x} - 2\right) + (1-x_0)(\eta_1 - 2\gamma_1)\mathrm{e}^{-\gamma_1 x_0}\int_{x_0}^{x} \frac{\mathrm{e}^{\gamma_1\xi}}{1-\xi}\,\mathrm{d}\xi + y_0\right]}.. \qquad \text{(A3-8)}$$

The **transient behaviour** of *R(Δa)* curves can be fitted by the exponential function eq. (2-9),

$$\boxed{r(x) = 1 + \alpha\, \mathrm{e}^{-\lambda(x - x_0)}}\,.$$

This function also allows for a closed form integration of eqs. (A3-3), in particular

- for **M(T)** specimens

$$y = \int_{x_0}^{x} \frac{r(\xi)}{1-\xi}\mathrm{d}\xi + y_0 = \int_{x_0}^{x} \frac{1}{1-\xi}\mathrm{d}\xi + \int_{x_0}^{x} \frac{\alpha \mathrm{e}^{-\lambda(\xi - x_0)}}{1-\xi}\mathrm{d}\xi + y_0$$

$$\boxed{y = y_0 + \log\left(\frac{1-x_0}{1-x}\right) + \alpha\, \mathrm{e}^{\lambda x_0} \int_{x_0}^{x} \frac{\mathrm{e}^{-\lambda\xi}}{1-\xi}\,\mathrm{d}\xi}\,, \qquad \text{(A3-9)}$$

- and for **SE(B)**

$$y = \exp\left(-\int_{x_0}^{x} \frac{\gamma(\xi)}{1-\xi} d\xi\right)\left[\int_{x_0}^{x} \frac{\eta(\xi) r(\xi)}{1-\xi} \exp\left(\int_{x_0}^{\xi} \frac{\gamma(\zeta)}{1-\zeta} d\zeta\right) d\xi + y_0\right],$$

$$\int_{x_0}^{x} p(\xi)\mathrm{d}\xi = \int_{x_0}^{x} \frac{\gamma(\xi)}{1-\xi}\mathrm{d}\xi = \int_{x_0}^{x} \frac{\mathrm{d}\xi}{1-\xi} = \log\left(\frac{1-x_0}{1-x}\right),$$

$$\int_{x_0}^{x} \frac{\eta(\xi) r(\xi)}{1-\xi}\left(\frac{1-x_0}{1-\xi}\right)\mathrm{d}\xi = \int_{x_0}^{x} \frac{2(1-x_0)}{(1-\xi)^2}\mathrm{d}\xi + \int_{x_0}^{x} \frac{2\alpha \mathrm{e}^{-\lambda(\xi - x_0)}(1-x_0)}{(1-\xi)^2}\mathrm{d}\xi$$

$$= 2(1-x_0)\left[\frac{1}{1-\xi}\right]_{x_0}^{x} + 2(1-x_0)\alpha \mathrm{e}^{\lambda x_0} \int_{x_0}^{x} \frac{\mathrm{e}^{-\lambda\xi}}{(1-\xi)^2}\mathrm{d}\xi$$

$$= 2\frac{1-x_0}{1-x} - 2 + 2(1-x_0)\alpha \mathrm{e}^{\lambda x_0}\left(\frac{\mathrm{e}^{-\lambda x_0}}{1-x_0} - \frac{\mathrm{e}^{-\lambda x}}{1-x} + \lambda \int_{x_0}^{x} \frac{\mathrm{e}^{-\lambda\xi}}{1-\xi}\mathrm{d}\xi\right)$$

$$\boxed{y = y_0 \frac{1-x}{1-x_0} + 2\frac{x-x_0}{1-x_0} + 2(1-x_0)\alpha\left(\frac{\mathrm{e}^{-\lambda(x-x_0)}}{1-x} - \frac{1}{1-x_0} + \lambda \int_{x_0}^{x} \frac{\mathrm{e}^{-\lambda\xi}}{1-\xi}\mathrm{d}\xi\right)}. \qquad \text{(A3-10)}$$

The integrals $\int_{x_0}^{x} \frac{\mathrm{e}^{c\xi}}{1-\xi}\,\mathrm{d}\xi$ in eqs. (A3-8) to (A3-10) can be solved through substitution $\zeta = 1 - \xi$ by an infinite series

$$\int_{x_0}^{x} \frac{\mathrm{e}^{c\xi}}{1-\xi}\,\mathrm{d}\xi = -\mathrm{e}^{c} \int_{1-x_0}^{1-x} \frac{\mathrm{e}^{-c\zeta}}{\zeta}\,\mathrm{d}\zeta = -\mathrm{e}^{c}\left[\log\zeta - \frac{c\zeta}{1\cdot 1!} + \frac{(c\zeta)^2}{2\cdot 2!} - \frac{(c\zeta)^3}{3\cdot 3!} + -\ldots\right]_{1-x_0}^{1-x} \qquad \text{(A3-10)}$$

Due to the geometry functions $\gamma(x)$ and $\eta(x)$, the integrals are even more complicated for a **C(T)** specimen so that numerical integration is advisable.